치의과학 박사학위논문

Effects of nanofibrous engineered matrix on osteoblast and odontoblast differentiation

나노섬유상 지지체가 골모세포와 상아모세포 분화에 미치는 영향

2017년 8월

서울대학교 대학원

치의과학과 분자유전학 전공

오 정 환

Effects of nanofibrous engineered matrix on osteoblast and odontoblast differentiation

나노섬유상 지지체가 골모세포와 상아모세포 분화에 미치는 영향

지도교수 우 경 미

이 논문을 치의과학 박사학위논문으로 제출함

2017년 4월

서울대학교 대학원

치의과학과 분자유전학 전공

오 정 환

오정환의 박사학위논문을 인준함

2017년 6월

위 원 장 _____ (인)

부 위 원 장 _____ (인)

위 원 _____ (인)

위 원 _____ (인)

위 원 _____ (인)

Abstract

Effects of nanofibrous engineered matrix on osteoblast and odontoblast differentiation

Joung-hwan Oh
Molecular Genetics Major
Department of Dental Science
The Graduate School of Seoul National University
(Directed by Prof. Kyung Mi Woo, D.D.S., Ph.D.)

This study intended to investigate the effect of the morphological features of the extracellular matrix (ECM) and its nanofibrous structure, on the differentiation of osteoblasts and odontoblasts, and the applicability of a nanofibrous engineered matrix, to support bone and dentin regeneration. Collagen, a fibrous protein that accounts for most of the ECM proteins of hard tissues, plays a key role in osteoblast differentiation and hard tissue regeneration. Moreover, the fibrous structure of collagen, can enhance the stability of the Runx2 protein, which is known to promote osteoblast differentiation. In this context, polystyrene, a common tissue culture dish

material, was chosen as a synthetic polymer to simulate the morphological characteristics of collagen for *in-vitro* tests. For *in-vivo* animal experiments, poly-ε-caprolactone, a highly biocompatible polymer, was tested. Each polymer was independently fabricated to a nanofibrous engineered matrix, with morphology similar to collagen, through electrospinning. As a natural polymer, autologous fibrin was used to prepare the fibrous engineered matrix and evaluated for its effect on osteoblastic differentiation and bone regeneration. In the *in-vitro* tests, electrospun polystyrene suppressed the degradation of the Runx2 protein, in a manner comparable to that of collagen. This was confirmed in both, MC3T3-E1 osteoblasts and Runx2 gene transfected C2C12 myoblasts. In the pulp capping model using beagle dogs, the fiber structured poly-ε-caprolactone membrane, promoted the formation of excellent dentin bridges and maintenance of healthy pulp. Through in-vitro tests, using MDPC-23 preodontoblasts, the electrospun poly-ε-caprolactone membrane, not only provided a fibrous ECM but also had the effect of blocking the cytotoxicity that occurs in the hydration stage of the mineral trioxide aggregate, one of the cement materials, used in the pulp capping procedure. The fibrin could be made to be morphologically similar to the collagen, and the selective adsorption of fibronectin, which is known to promote bone regeneration, was confirmed to be superior to collagen. In addition, MC3T3-E1 osteoblasts showed a higher proliferation rate on the fibrin than collagen, and fibrin was more favorable for bone differentiation and regeneration, at the level of the Runx2 protein, transcription activity, and alkaline phosphatase activity. It was verified that this property of fibrin could be controlled by the thrombin concentration treatment, used in the preparation of fibrin from fibrinogen. The selective adsorption of fibronectin, increased with the concentration of treated thrombin. In the in-vitro MC3T3-E1 osteoblast tests, the level of Runx2 protein increased, as the selective adsorption of fibronectin increased

and the activity of integrins β_1 and β_3, reported to be associated with osteoblast differentiation, were jointly increased. These results suggest that the natural and synthetic polymer materials can stimulate differentiation of osteoblasts and odontoblasts by mimicking the fibrous morphological features of the ECM. Furthermore, the findings imply that a better performance may be expected, when suitable materials are selected, according to the medical purpose and applied as a nanofibrous engineered ECM which mimicks the morphological features of the hard tissue, required for regeneration.

Key words: nano fiber, tissue engineering, electrospinning, osteoblast, odontoblast
Student number: 2010-22022

CONTENTS

LIST OF FIGURES

PART-I

PART-II

PART-III

PART-IV

I. INTRODUCTION

Effective anti-aging medical interventions are likely to increase the average human lifespan by several decades. If the challenge of conventional medicine was to fight against some kind of exceptional condition, called disease, the current medical paradigm is focused on coping with the extremely natural phenomenon of aging. Thus, the need for regenerative medicine/tissue engineering is increasing [Lucke et al. 2010; McConnel and Turner 2005]. In the field of dentistry, it is acknowledged that the lifespan of a tooth cannot keep up with the increasing average human lifespan. Indeed, it is impossible to maintain a lifespan with exclusively natural healthy teeth, considering the present average lifespan. Consequently, most of the population will experience dental restoration or substitution (implant) at least once during their life. However, existing tooth replacements have a shorter lifespan than natural teeth, hence, the possibility of requiring a secondary or tertiary replacement is high. In terms of function, however, artificial alternatives are inferior to natural teeth. Accordingly, proposals have been made for tissue engineering to regenerate damaged or worn natural teeth [Black et al. 2015].

All cell types constituting each tissue are in contact with the extracellular matrix (ECM). The primary role of the ECM is to act as a cell scaffold and maintain the physical strength of the tissues. However, besides its structural function, the ECM also regulates cell growth, differentiation and behavior. The cells also have a dynamic relationship with the ECM which is constantly reconstructed by each differentiation step. Therefore, in clinical applications, not only is the focus on the proliferation and differentiation of stem cells crucial but, in the context of tissue regeneration, it also necessary to secure the physical stiffness and space which can

profoundly influence stem cell behavior [Kim et al. 2016]. Thus, the characteristics and functions of the ECM are attracting increasing attention in tissue engineering. The aim of tissue engineering is to construct biological replicates that imitate the complexity and function of living human tissues [Asghari et al. 2017; Cui et al. 2010]. From a tissue engineering perspective, it is necessary to secure space, by providing scaffolds or an artificial ECM, which must also recruit the cells to be differentiated or induce differentiation of transplanted stem cells for regeneration. However, the interest in the dynamics of the ECM is relatively short in the history of cell biology. The ECM of each tissue not only has various selective ligands but also various factors, such as characteristic morphology, stiffness, and elasticity, which are influenced by cell differentiation and function. The complicated relationship and communication between the ECM and the cells are not well known [Fernandes et al. 2009]. In addition, the ECM topography is nano-scaled, presenting very different physical phenomenon than the macro- and microscale dimensions. Completely simulating nano-level structures has technically challenging barriers. In the future, tissue engineering will likely require a technological accumulation to understand the cellular/molecular biomechanical roles between cells and the ECM, and the nano-level phenomenon of the ECM to mimic its structure.

Collagen type I is the main component of the ECM in hard tissues. Several researchers investigating bone regeneration via tissue engineering, have focused on collagen type I or collagen type I mimics [Li et al. 2002; Wnek et al. 2003; Yoshimoto et al. 2003; Luo et al. 2008; Beniash et al. 2005; Chen and Ma 2004; Woo et al. 2007]. Consequently, several independent studies have shown that collagen or its mimics promotes osteoblast differentiation and bone regeneration.

Runx2, a bone-specific transcription factor, is crucial to turning on osteoblast or

odontoblast differentiation [Bruderer et al. 2014]. Run2 knock-out mice showed incomplete bone maturation [Komori et al. 1997]. Osteocalcin, type I collagen, osteopontin, alkaline phosphatase, and osterix, known as osteoblast-specific markers, are induced by Runx2 [Shahi et al. 2017; Nakashima et al. 2002; Prince et al. 2000; Otto et al. 1997]. In addition, bone morphogenetic proteins (BMPs) upregulate Runx2 expression [Wang et al. 2017b; Xiao et al. 2002; Tamura et al. 2001]. Based on these findings, there have been several attempts to regenerate bone by gene therapies with Runx2 [Fliefel et al. 2017; Phillips et al. 2006; Zhao et al. 2005]. The protein levels of Runx2 are regulated by the ubiquitin-proteasome pathway. Previously, an investigation into the mechanism of inducing osteoblast differentiation by collagen [서지혜. 2007], demonstrated that the osteoblastic MC3T3-E1 cells did not display an increase in Runx2 transcription level in the collagen matrix but the Runx2 protein level increased, due to a reduction in Runx2 protein degradation associated with ubiquitination. Also, the suppression of Runx2 protein degradation was reduced when the collagen fibrous structure was destroyed by collagenase. This result confirmed that the morphological properties of collagen are pivotal to induce hard tissue regeneration by reducing degradation of the Runx2 protein.

The dental pulp is a soft tissue occupying the core of the tooth that supports the dentinal response to noxious stimuli and the regeneration of dentin. The pulp can be exposed by cavities or cracks in the dentin, causing serious pain and clinical harm. A pulp capping material should not only protect pulp from the oral environment but also be attached to the remaining dentin tissue to stabilize and support dentinogenesis. Various capping materials have been used to cure pulp exposure but calcium hydroxide remains the most common. Nonetheless, mineral trioxide aggregate (MTA)

appears to be a potential calcium hydroxide replacer, supporting better dentin-bridge generation and showing low irritation. According to the literature, MTA upregulates the levels of the matrix adhesion proteins and the transcription factors that induce odontoblast differentiation [Song et al. 2017; Accorinte et al. 2008; Paranjpe et al. 2010; Balto 2004]. Yet, the virulence of high pH in the initial setting phase of the cement materials, remains unsolved regarding the use of MTA [Agrafioti et al. 2016; Baraba et al. 2016; Okiji and Yoshiba 2009; Balto 2004]. Hence, it is necessary to develop a new material to block the cytotoxicity but still allow the positive effects of MTA.

Fibrin, an abundant natural biopolymer, is a cost-effective, representative natural material in regenerative medicine research. Moreover, autologous fibrin has great potential as clinical approaches. Fibrin is produced from fibrinogen in blood clotting for hemostasis during wound healing and because it can be harvested from the patient, is immunocompatible. Fibrin matrices are capable of expressing matrix proteins and growth factors [Chiti et al. 2017; Ahmed et al. 2008; Laurens et al. 2006; Mosesson 2005], including fibronectin which is known to induce osteoblast differentiation and bone regeneration [Chiti et al. 2017; Marie 2013; Breen et al. 2009; Wilson et al. 2005]. Although fibrin shows good performance in bone regeneration [Ma 2008; Woo et al. 2007; Li et al. 2002], a comparative biological effectiveness of fibrin and collagen has not yet been evaluated.

Integrins are well-known as typical cell adhesion proteins. Integrins have αß heterodimer forms and more than 20 different types have been identified. Integrin $\alpha_v\beta_3$ binds to fibrinogen which, as above-mentioned, is the precursor of fibrin [Laurens et al. 2006; Mosesson 2005; Savage et al. 1995]. Integrins $\alpha_4\beta_1$, $\alpha_5\beta_1$, $\alpha_{IIb}\beta_3$, $\alpha_V\beta_3$, $\alpha_V\beta_6$, and $\alpha_V\beta_8$, bind to fibronectin which adsorbs to ECM components such as f

i

b

r

C. F.</author><author>Cheng, S. L.</author></authors></contributors><titles><title>αvβ integrins play an essential Blocking the α_1 integrin subunit leads to a decrease in osteoblast differentiation [Gronthos et al. 2001]. Also, the $\alpha_1ß_1$ and $\alpha_2ß_1$ complexes have been shown to regulate early osteoblast differentiation, induced by BMP-2 [Xiao et al. 2002]. Collectively, therefore, it can be considered that the activity of integrins, is important to understand the mechanism of osteoblast differentiation and bone regeneration, by a nanofibrous engineered fibrin matrix.

II. LITERATURE REVIEW

II.1. Collagen Type I

Collagens are most abundant extracellular matrix (ECM) protein in hard tissues. About 30% of the total proteins in mammals are collagens [Ricard-Blum 2011]. In the ECM of all connective tissues, collagens are most structural elements. Especially, about 80% of the total proteins are collagens in bone and around 95% of them is collagen type I [Viguet-Carrin et al. 2006].

There are 28 subtypes of collagen have been identified [Heino 2007], but over 90% of them is type I in human body (all fibrous tissues except cartilage [Shoulders and Raines 2009]) Most of them constructed by three alpha chained polypeptide strands which forms a unique triple-helical structure (in collagen type I, two α_1(I)-chains and one α_2(I)-chain) [Exposito et al. 2010]. An individual heterotrimeric form of type I collagen is 1~2 nm in diameter and ~300nm in length. [Shoulders and Raines 2009] This molecules are self-assembled to form fibrils up to 1 cm in length (in tendon [Craig et al. 1989]), and up to 20 ~ 500 nm in diameter [Shoulders and Raines 2009; Tzaphlidou 2005]

The fibril structure of the collagen is the most characteristic feature of ECM morphology. Tissues are made up with cells and ECM proteins. Between cells and cells, the extracellular space is filled up ECM proteins. The cells adhere to the ECM and regenerate the ECM. The ECM is constructed by glycoproteins, proteoglycans, carbohydrates and collagens that make a microenvironment around the cells [Huber and O'Day 2017]. In most cases, the collagen is the major structural matrix protein in mammals. In tissue engineering, so many researchers have tried to mimic the

collagen fibrous structure in natural ECM, and to report the positive results for regenerative medicine. [Moll et al. 2017; Sionkowska et al. 2017; Ma 2008; Woo et al. 2007; Li et al. 2002]

The other hands, the collagen molecules have specific binding motifs [Addi et al. 2016]. The integrin family which is transmembrane receptor is known to bind to RGD sequences and to be involved in typical cell adhesion. Of these, $\alpha_1\beta_1$, $\alpha_2\beta_1$, $\alpha_{10}\beta_1$, $\alpha_{11}\beta_1$ integrins bind directly to collagen. Other subtypes indirectly bind via the other constitutive proteins of ECM such as fibronectin ($\alpha_4\beta_1$, $\alpha_5\beta_1$, $\alpha_{IIb}\beta_3$, $\alpha_V\beta_3$, $\alpha_V\beta_6$, $\alpha_V\beta_8$) and vitronectin ($\alpha_V\beta_1$, $\alpha_V\beta_3$, $\alpha_V\beta_5$). [Zeltz and Gullberg 2016; Hamidi and Ivaska 2017; Wang et al. 2017a; Kapp et al. 2017; Knight et al. 2000] Integrin is a molecule located in the cell membrane that activates and initiates signaling into the cell when bound to a ligand and each subtype performs a different function. Collagen has a binding motif that these integrins can bind directly, or that can bind to a protein that the integrin can bind [Addi et al. 2016]. In other words, the difference in the type and arrangement of the binding motifs due to differences in the structure of the collagen constituting the different ECM results in the difference of the activated integrin. It means a difference in the signal transmitted to the inside of the cell.

Especially in bone biology, collagen type I is abundant ECM protein and have been reported to be important for osteoblast differentiation and bone regeneration. Collagen type I gel induced osteoblast differentiation and maintenance the phenotype in osteoblast, bone marrow stromal cells, and periodontal ligament fibroblasts [Alves et al. 2015; Mizuno et al. 2000; Lynch et al. 1995]. Clinical osteogenesis imperfecta was mostly caused by mutation of collagen type I [Marini et al. 2007], Wallace *et al.* reported in 2011 that the fibrous structure of collagen type I was incompletely produced in the mouse osteogenesis imperfecta model [Wallace

et al. 2011]. These are saying the importance of the fibrous structure of the collagen as ECM for bone generation. So, in tissue engineering, there are so many efforts to make fibrous engineered matrix mimicking the morphology of collagen [Sionkowska et al. 2017; Ma 2008; Woo et al. 2007; Li et al. 2002].

II.2. Fibrin

Fibrin is a natural polymer that can be easily obtained from the patient's own body. There have been many attempts for medical applications including bone regeneration, such as collagen. Because of its origin, there are great advantages of avoiding immunity rejection along with cost. [Chiti et al. 2017]

Generally, fibrin is formed by the enzymatic action of thrombin from the soluble precursor fibrinogen in the course blood clotting. Fibrinopeptide A and B are cut out from fibrinogen by thrombin. And then, Fibrin monomer which produced by thrombin cleavage is aggregated to each other and polymerized into the fibrous form. This construct a fibrin clot with platelets, which serves not only for homeostasis but also works as a scaffold for wound healing. [Hsieh et al. 2017] In other words, one of the role of the fibrin clot is very similar to the concept of tissue engineering for wound regeneration.

Fibrin has been noted early for application in regenerative medicine for the following reasons and has been applied clinically. Basically, the fibrin matrix that is created for hemostasis stores and delivers the matrix proteins and growth factors needed for wound healing, and acts as an ECM to support wound healing [Chiti et al. 2017; Ahmed et al. 2008; Laurens et al. 2006; Mosesson 2005]. Thrombin, which is essential for making fibrinogen into fibrin, has been reported to help proliferation

of osteoblasts and inhibit apoptosis in the early period of bone regeneration [Song et al. 2005a; Song et al. 2005b; Pagel et al. 2003]. Fibrin has a binding capacity to fibronectin, which is known to help osteoblast differentiation. Fibrin treatment has been reported to be beneficial for bone regeneration [Chiti et al. 2017; Marie 2013; Breen et al. 2009; Osathanon et al. 2008; Wilson et al. 2005; Karp et al. 2004; Bensaïd et al. 2003]. These advantages for bone regeneration are shared with collagen as mentioned above.

II.3. Electrospinning

Electrospinning was a technique to produce fibers have diameter commonly ranging from a few micro to sub-micron level by using electrostatic forces. [Reneker and Yarin 2008] Academically, nano-scale means less than 100 nm at least one dimension of some substance or structure [MacDiarmid et al. 2001]. But in the fibril commercial fields, allow including the sub-micron diameter ranging fibers as nano-fiber. In later views, the electrospinning is one of the techniques for nano-fibrous technology [Ramakrishna 2005]. In addition, the development of the electrospinning technique became to be able to make ultrafine fiber ranging from < 3 nm [Norman and Desai 2006; Ramakrishna 2005; Frenot and Chronakis 2003].

Basically, electrospinning is including put electric charge a drooping solution or melt of polymer. When the electric field is applied, the polymer suspended at the tip of the nozzle is formed jet to the air toward to collector. In this process, the jet forming polymer solution or melt is solidified by drying or cooling and stacked onto the collector. [Norman and Desai 2006]

Effective fiber formation condition, the diameter of the fiber and the other things

of electrospun product features are determined by several factors. And they are related to each other. To explain briefly, first, viscosity (related with concentration and molecular weight of polymer), electronic conductivity, surface tension, and dielectric effect of polymer solution/melt are main factors. In this progress, fiber formation means a kind of elongation from a small amount of liquid form by electric power, and solidification by drying or cooling before roll back by the repulsive force of elasticity, surface tension, cohesion, etc. So the factors of a liquid formed material prepared for electrospinning become to be very important. Secondly, the electric charge loaded on the nozzle, the feeding speed, the diameter of the nozzle, and the kind of materials of the collector are important parameters. These are related to the amount of electric charge being loaded on per unit area of the end of the nozzle, and the discharging rate after polymer jet. Temperature and distance between nozzle-collector are also important because they are interconnected directly the volatilization rate of the solvent or cooling time of the melt. Environmental elements like air, humidity, atmospheric pressure, etc. can effect on the structure of the product. The morphology of fibers can be controlled freely by considering and control them within some restricted area. [Babitha et al. 2017; Reneker and Yarin 2008; Thompson et al. 2007; Ramakrishna 2005; Subbiah et al. 2005]

Comparing the other methods for engineering ECM production, electrospinning has some traits and advantages like to the followings. At first, electrospinning is easy to make a 2D plane or 3D spatial structure by the organization of the equipment and construction progress. Especially two-dimensional plane surface design is useful for cell biological *in-vitro* study comparing previous cell culture system like called as 'Tissue culture dish' And three-dimensional structures are closer to the natural tissue system. Electrospinning methods is useful for both of them. Researchers have been

developed the methods to form several kinds of fibrous assemblies using electrospinning technique, from randomly arranged or parallel aligned fibrous mesh to fibrous bundle, membrane, scaffold, composite with more than two materials, core-shell structure, etc. [Cui et al. 2010] Second, it is required related simple facilities and low cost. This system needs an only small area to install, very fit a lab scale research. [Ramakrishna et al. 2006; Subbiah et al. 2005; Li and Xia 2004]

Above of all, electrospinning is suitable for most of the polymers, not only synthetic like polyglycolic acid (PGA), polylactic acid (PLA), poly-ε-caprolactone (PCL), poly(*N*-isopropylacrylamide), etc. but also natural like chitin, chitosan, alginate, collagen, gelatin, and fibrin. [Asghari et al. 2017] This signifies electrospinning is considerable for the development of drug delivery system using wide biocompatible/biodegradable synthetic and natural materials too. [Cui et al. 2010] Because of this various applicability, studies and tries to evolve applications using electrospinning are increasing in the field of biomaterials and tissue engineering. [Aruna et al. 2017; Ramakrishna et al. 2006; Norman and Desai 2006; Subbiah et al. 2005; Li and Xia 2004]

III. PURPSOSE OF STUDY

This study aimed to explore the possibility of hard tissue regeneration by providing an artificial substrate that mimics the structure of collagen, which accounts for most of the ECM of bone tissues. Two main strategies were implemented. First, nanofibrous engineered matrices were developed to mimic the fibrous structure of collagen, by electrospinning synthetic polymers. As an in-vitro model, polystyrene, a material of tissue culture dishes, was used to investigate how the structural characteristics of the nanofibrous matrix promoted bone differentiation. As a simulated clinical approach model, the nanofibrous engineered matrix was applied to a beagle tooth pulp capping procedure, using electrospun poly-ε-caprolactone, a reportedly biocompatible and biodegradable, synthetic material [Asghari et al. 2017].

In the second approach, fibrin was investigated as a natural polymer material to mimic collagen. The biological properties of fibrin and collagen on osteoblast differentiation were compared. Then, the fibronectin capacity of fibrin was examined, according to the difference in fibrin structure depending on the thrombin concentration used in preparing fibrin, to provide evidence which is necessary for fibrin application.

IV. PART I.

Suppression of Runx2 protein degradation by fibrous engineered matrix

This part was already published in Biomaterials 32, no. 25 (2011): 5826-36. doi: 10.1016/j.biomaterials.2011.04.074

IV.1. Introduction

As an artificial extracellular matrix (ECM), a scaffold should support cells structurally and also should provide cells with suitable micro-environments for regenerating tissue. It is often beneficial for scaffolds to mimic certain advantageous characteristics of a natural ECM or developmental and wound healing processes [Ma 2008].

Natural ECMs in bone tissues are mainly composed of type I collagen. Collagen, by definition, is characterized by a unique triple-helix formation that extends over a large portion of its structure. A predominant morphologic feature of type I collagen molecules is its long, stiff, triple-stranded helical structure, in which three collagen polypeptide chains are wound around one another in a rope-like super-helix. After being secreted into extracellular space, collagen molecules assemble into higher-order polymers called collagen fibrils. The fibrils then assemble into collagen fibers with diameters ranging from 50 to 500 nm. Fibrous collagen influences the development and maintenance of the osteoblast phenotype [Lynch et al. 1995] and induces differentiation of bone marrow stromal cells along the osteoblast pathway [Mizuno et al. 2000]. Therefore, the development of nano-fibrous materials that mimic the morphology of fibrous collagen as advanced scaffolds for bone tissue engineering has previously been proposed. Diverse natural or synthetic polymers have been utilized to make nano-fibers, and various techniques, including electrospinning, self-assembly and phase separation, have been explored to fabricate nano-fibrous materials [Li et al. 2002; Wnek et al. 2003; Yoshimoto et al. 2003; Luo et al. 2008; Beniash et al. 2005; Chen and Ma 2004; Woo et al. 2007]. Consistently, fibrous scaffolds have shown good biological performance for bone regeneration. However, the mechanisms by which morphological-mimicking synthetic nano-fibers

mimic the function of collagen remain largely unknown.

Runx2 has been widely accepted as a master transcriptional factor that can turn on osteoblast differentiation based on the findings that Runx2-knockout mice display complete bone loss due to arrested osteoblast maturation [Komori et al. 1997], and it plays a critical role in osteoblast marker gene expression including osteocalcin, type I collagen, osteopontin, and alkaline phosphatase [Otto et al. 1997; Prince et al. 2000]. A zinc finger-containing transcription factor, Osterix (Osx), also necessary for osteoblast differentiation, has been shown to act downstream of Runx2 [Nakashima et al. 2002]. Most osteogenic factors, such as Bone morphogenetic proteins (BMPs), can induce expression of Runx2, and various extracellular signals can affect the transcriptional activity of Runx2 [Xiao et al. 2002; Tamura et al. 2001]. Therefore, Runx2 is mostly used in gene therapy for bone regeneration [Zhao et al. 2005; Phillips et al. 2006]. It has been shown that osteoblast differentiation and bone formation in vitro and in vivo are inhibited by Smad ubiquitin regulatory factor 1 (Smurf1) through direct interaction with Runx2 [Zhao et al. 2004; Yamashita et al. 2005]. Ubiquitination and subsequent proteasome-dependent protein degradation is an important regulatory mechanism for control of numerous cellular processes. Runx2 is also selectively targeted for ubiquitination of lysine residues and subsequent proteasomal degradation by specific ubiquitin E3 ligases such as Smurf1. The degradation of Runx2 can be regulated by growth factors such as BMP2 and FGF2 [Jeon et al. 2006; Jun et al. 2010; Park et al. 2010]. BMP2 has been shown to stimulate Runx2 acetylation, which inhibits the Smurf1-mediated degradation of Runx2 [Jeon et al. 2006; Jun et al. 2010]. FGF2-activated Erk mitogen-activated protein kinase has been shown to enhance Runx2 acetylation and stabilization [Park et al. 2010]. Given these results, Runx2 has been shown to be a key regulatory factor

suitable for evaluating biomaterials that support bone regeneration. Understanding the mechanisms of the control of Runx2 proteins by a fibrous engineered matrix could lead to an improvement in therapies used for bone regeneration.

In the previous study, it was investigated that the regulatory mechanisms of Runx2 using a fibrous collagen matrix. MC3T3-E1 pre-osteoblasts grown on the collagen fiber matrix were compared with the cultures grown on conventional tissue culture dishes or on a degraded, non-fibrous collagen matrix. [서지혜, 2007] At 7 days, osteocalcin and bone sialoprotein (BSP), markers of late-stage osteoblast differentiation, were profoundly expressed in the cells on collagen fibers. In addition, mineralization was determined by assaying the amount of calcium. As early as 1 days, although the level of Runx2 transcription in the cells on collagen was not different from that in the cells on tissue culture dish, the level of the Runx2 protein in the cells on collagen was clearly greater than that in the cells on tissue culture dish. The cells on collagen fibers exhibited obviously higher levels of Runx2 activity in a reporter assay. Because a discrepancy between the levels of the transcript and the protein of Runx2 was observed, the degradation of Runx2 was examined. E3 ubiquitin ligase Smurf1 is known to be responsible for the degradation of the Runx2 protein. Therefore, the ubiquitination of Runx2 was checked in the absence and presence of proteasome inhibitor MG132. Ladders of ubiquitinated Runx2 were clearly detected in cells on the tissue culture dish in the presence and absence of MG132. The results indicate that the Runx2 protein in cells on the t was substantially degraded in a proteasome- and ubiquitin-dependent manner. On the contrary, ubiquitinated Runx2 in cells grown on fibrous collagen were not detected. These results demonstrate that the inhibition of Runx2 degradation in cells grown on a collagen fiber matrix contributes to collagen-induced osteoblast differentiation. Next,

to determine the role of the fibrous structure of collagen in osteoblast differentiation, collagenase-treated collagen matrix was prepared. The amount of Runx2 protein in a collagenase-treated (non-fibrous) matrix was significantly reduced. This result indicated that the collagen-induced stabilization of Runx2 involves, at least in part, the fibrous structure of collagen and provides initial evidence that the fibrous structure plays a role in collagen-mediated osteoblast differentiation.

In this study, a polystyrene fiber matrix was prepared, and we confirmed the fiber matrix-mediated control of Runx2 in MC3T3-E1. Next, we genetically modified C2C12 myoblasts with Runx2, cultured the cells on a polystyrene fiber matrix, and examined the regulation of exogenous Runx2 by an engineered fiber matrix.

IV.2. Materials and methods

IV.2.1. Materials and reagents

Foetal bovine serum (FBS), HEPES buffer solution, penicillin–streptomycin solution, and collagenase came from GibcoBRL (Carlsbad, CA). L-Ascorbic acid, glycerol 2-phosphate, phosphatase inhibitor cocktails, MG132 (N-CBZ-Leu-Leu-Leu-AL), Dimethylformamide (DMF). Ascorbic acid-free α-MEM came from WelGene (Daegu, Korea). Easy-BLUE™ RNA Extraction Reagent and West-Zol™ came from Intron Biotechnology (Seoul, Korea). AccuPower RT-Premix was from Bioneer (Daejeon, Korea). Protease inhibitor cocktail tablets complete was from Roche (Basel, Switzerland). Anti-Runx2, anti-actin and HRP-conjugated IgG antibodies were purchased from Santa Cruz Biotechnology.. Mouse monoclonal antibody to ubiquitinylated protein came from BIOMOL (Plymouth, PA). Tissue culture plate of polystyrene (PS) purchased from BD Falcon was shattered in order to obtain PS.

IV.2.2. Preparation of matrix

A polystyrene (PS) fiber matrix was prepared by electrospinning. The PS tissue culture plate was dissolved in dimethylforamide (DMF), and an 8% (weight/volume) PS solution was added into a 10-mm syringe with a stainless steel syringe needle (30 G). The electric potential and the distance to the collector were 30 kV and 20 cm, respectively. After electrospinning, a very small amount of DMF was spread on the bottom of a petri dish and a PS sheet was placed over it. Then, a PS sheet fixed onto a petri dish was dried in a vacuum oven at ambient temperature for a day.

Subsequently, the PS sheet on a petri dish was immersed in 70% ethanol for a day and then distilled water for 8 h to remove any residual DMF. Afterwards, it was dried again in a vacuum oven.

IV.2.3. Cell culture

MC3T3-E1 pre-osteoblasts and C2C12 myoblasts were seeded at a density of 5.25×10^5 per 60-mm dish. Approximately 12 h after cell seeding, the cells were cultured in α-MEM supplemented with 10% FBS, 50 μg/ml ascorbic acid, and 10 mm β-glycerophosphate (differentiation medium) for up to seven days. To force the expression of Runx2 in C2C12 myoblasts, the cells were transiently transfected with a Runx2 expression vector [Lee et al. 2003] using a Lipofectamine Plus reagent. After overnight stabilization in the maintenance medium, the cells were cultured in the differentiation medium for one or three days.

IV.2.4. Scanning electron microscopy (SEM)

The PS fiber matrices were sputter-coated with gold–paladium and observed under an SEM at 12 kV (FE-SEM Hitachi S-4700, Japan).

IV.2.5. Extraction of total RNAs and RT-PCR

Quantitative real-time RT-PCR (reverse transcription polymerase chain reaction) were used to evaluate mRNA expression. Total RNAs were isolated using the Easy-Blue™ RNA extraction reagent. The concentration and purity of the RNA preparations were determined by measuring the absorbance of RNA at 230, 260 and 280 nm. RNA integrity was analyzed on a 1% native agarose gel to determine the

18S and 28S bands, and cDNAs were synthesized using the AccuPower RT-Premix according to the manufacturer's instructions. A 20-μl of first-strand cDNA was synthesized from 1 μg of the total RNAs, and 2 μl of cDNA was used for PCR amplification. Table I-1 lists the mouse primer sequences that were used. The relative levels of the target gene mRNAs were normalized to those of glyceraldehyde-3-phosphate dehydrogenase (GAPDH) using a quantitative real-time PCR. The relative intensity of gene expression was calculated by comparison with cells grown on TCDs without any treatment. Each experiment was duplicated at least three times.

IV.2.6. Western blot analysis

Cell lysates were prepared using a buffer of 10 mM Tris-Cl (pH 7.5), 150 mM NaCl, 1 mm EDTA (pH 8.0), 1% Triton X-100, 1 mM phenylmethylsulfonyl fluoride, 50 mM NaF, 0.2 mM Na3VO4, a phosphatase inhibitor and a complete protease inhibitor cocktail tablet. The samples were subjected to 8–10% SDS-PAGE and then they were transferred onto a polyvinylidene difluoride membrane. The amount of lysates loaded was adjusted based on DNA content and confirmed by β-actin using a western blot analysis. The membrane was blocked by 3% bovine serum albumin and incubated with each primary antibody. This procedure was followed by incubation with an HRP-conjugated secondary antibody. Luminescence was detected by Fujifilm LAS-1000 (Fuji, Tokyo, Japan). The intensities of specific bands were measured using the NIH Image/ImageJ program and normalized by β-actin. The relative intensity was calculated by comparison with cells grown on TCDs without any treatment.

IV.2.7. Alkaline phosphatase assay

ALP activity was measured using spectrophotometry with *p*-nitrophenyl phosphate (*p*-NPP) as a substrate. After 7 days of culture, cells were collected and homogenized in 0.5 ml of distilled water using a sonicator. Cell homogenate aliquots were incubated with 15 mM *p*-NPP in 0.1 M glycine–NaOH (pH 10.3) at 37 °C for 30 min. The reaction was stopped using 0.25 M NaOH and the absorbance was measured at 410 nm. The ALP activity was calculated and presented as the amount of *p*-NP converted from *p*-NPP per milligram of total protein in an hour (μmol mg^{-1} h^{-1}). Each experiment was repeated three times (n = 3).

IV.2.8. Statistical analysis

All data are` presented as average ± standard deviation (SD). A statistical analysis was performed using Student's t-test or two-way ANOVA. Differences between groups were considered significant if the p value was less than 0.05.

Table I-1. Sequences of Primers used in RT-PCRs

Molecules	Primer sequences used in quantitative PCR	Accession No. (Gene bank)
Runx2	5′-TTCTCCAACCCACGAATGCAC-3′ 5′-CAGGTACGTGTGGTAGTGAGT-3′	NM_001146038.1
GAPDH	5′-CATGTTCCAGTATGACTCCACTC-3′ 5′-GGCCTCACCCCATTTGATGT-3′	NM_008084.2

IV.3. Results

IV.3.1. Effects of polystyrene fiber on degradation of Runx2 protein

The chemical nature of the scaffolding materials can affect the biological performance of the scaffolds. To provide additional evidence that the fiber structure exhibits certain properties comparable to natural collagen fibers, a PS fiber matrix was fabricated by electrospinning since tissue culture dishes are essentially composed of PS. The morphology of electrospun PS fibers is presented in Fig. I-1. The thickness of PS fibers mostly ranged from 100 to 300 nm (193 ± 54 nm). We cultured MC3T3-E1 cells on a TCD and on a PS fiber. ALP activity was two times higher in cells grown on PS fibers than in those on TCD, which indicates that the PS fiber matrix also supported osteoblast differentiation (data not shown). We then examined whether a PS fibrous matrix could regulate Runx2. Both matrices supported the expression of Runx2 transcripts at similar levels, which was confirmed by quantitative real-time PCR and ANOVA analysis (Fig. I-2A). However, the level of the Runx2 protein was obviously enhanced in cells that were grown on PS fibers as shown in Fig. I-7B ($p < 0.05$). Upon treatment with MG132, the level of Runx2 on the TCD was high and comparable to that on PS fiber ($p < 0.05$). These results show that the Runx2 protein was profoundly degraded in cells grown on TCD, whereas the PS fibers suppressed the degradation of Runx2 (Fig. I-2B). The results from the cultures on the PS fiber were consistent with those from the fibrous collagen matrix, which indicated that the fibrous structure of the engineered matrix stabilized the Runx2 protein, which consequently contributed to osteoblast differentiation.

IV.3.2. Effects of polystyrene fiber on degradation of exogenous Runx2

protein

Considering that Runx2 is a molecule frequently used in gene therapy for bone regeneration, we examined whether the PS fiber matrix could inhibit the degradation of the exogenous (forced expressed) Runx2 protein using Runx2-transfected C2C12 cells (Runx2_C2C12). We transfected a Runx2 expression construct into C2C12 myoblasts and observed that the transfected cells expressed Runx2 (Fig. I-3A), whereas the parental C2C12 cells expressed little of Runx2 as reported previously [Lee et al. 2003]. The Runx2_C2C12 cells induced the differentiation of myoblasts into osteoblasts, which was assessed by ALP activity (Fig. I-3B). The Runx2_C2C12 cells were then cultured on TCD and PS fibers. As shown in Fig. I-4A, higher ALP activity was observed in cells grown on the PS fibers than those on the TCD. We then checked the levels of exogenous Runx2 proteins were to examine effects of MG132 treatment on the cultures on the different surfaces (Fig. I-4B). The ANOVA test indicates that the exogenous Runx2 protein in the Runx2_C2C12 cells on the PS fibers was significantly higher than that on the TCD ($p < 0.05$). An inhibitor of proteosomal degradation, MG132 treatment revealed that the exogenous Runx2 in cells on the TCD was profoundly degraded ($p < 0.05$). These results consistently indicated that exogenous Runx2 was also protected from degradation by the fibrous matrix and emphasized the importance of the scaffolding structure in gene therapeutic approaches involving Runx2.

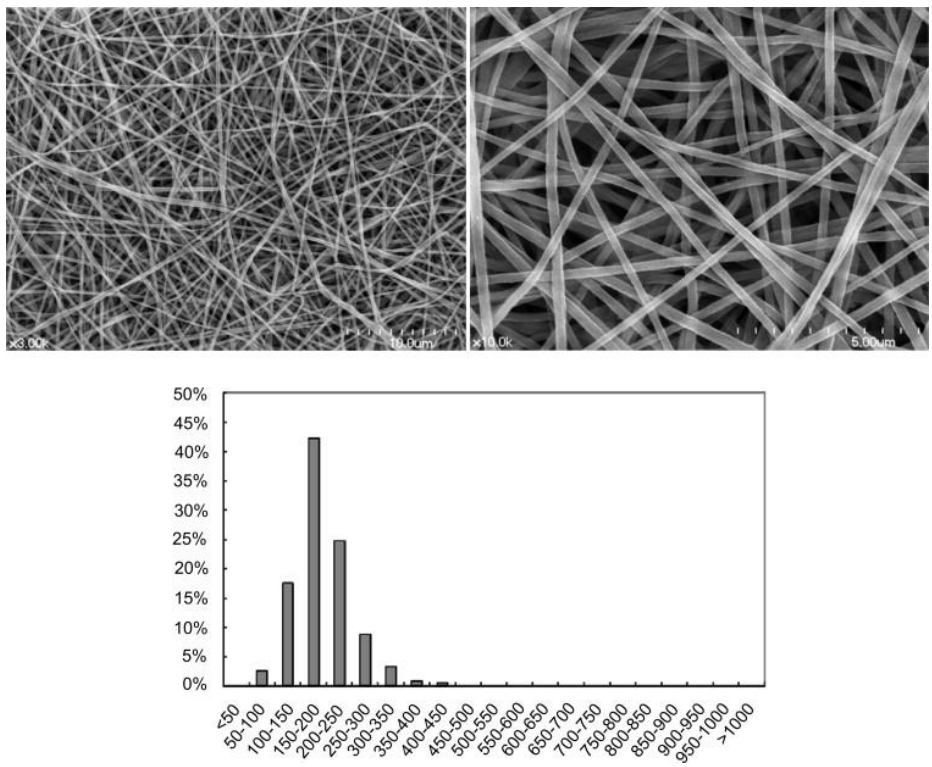

Figure I-1. Scanning electron microscopic views of an electrospun polystyrene (PS) fiber matrix. Magnifications were 3,000× (left) and 10,000× (right). Fiber thickness was measured on scanning electron microscopic images with a magnification of 10,000× (n = 436).

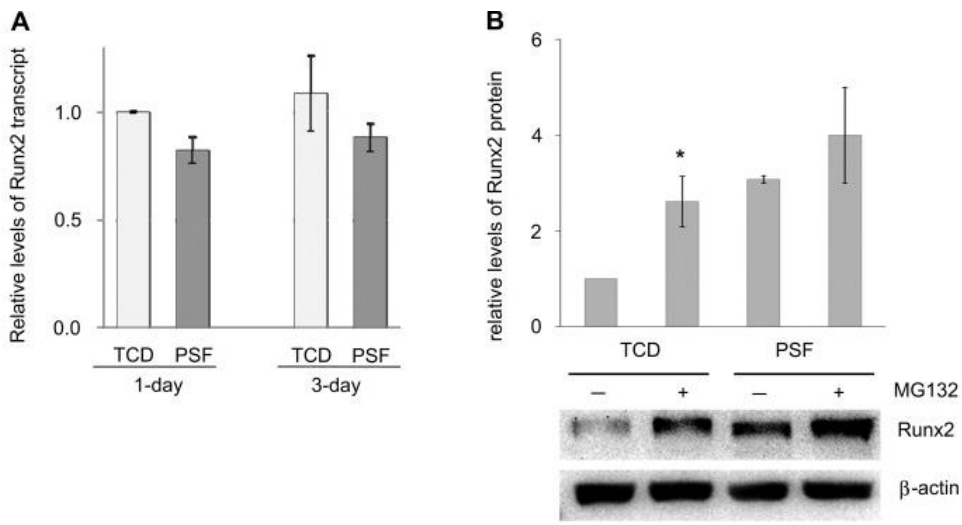

Figure I-2. Polystyrene fiber matrix stabilises the Runx2 protein. (A) Real-time PCR. MC3T3-E1 cells were grown on TCD and on PSF for one or three days in an osteogenic differentiation medium. Data are presented as averages ± SDs (n = 3). (B) Western blot analysis for Runx2. The cells were cultured in an osteogenic differentiation medium for 12 h and then treated with 5 μM MG132 for 24 h. Total cell lysate was subjected to western blotting for Runx2. The intensities of Runx2 protein were measured and normalized by β-actin. Shown are the relative expression intensities in cells cultured on PSF to TCD. Data are presented as averages ± SDs (n = 3). ∗ Significant difference between MG132-treated and non-treated cells grown on TCD (ANOVA, $p < 0.05$).

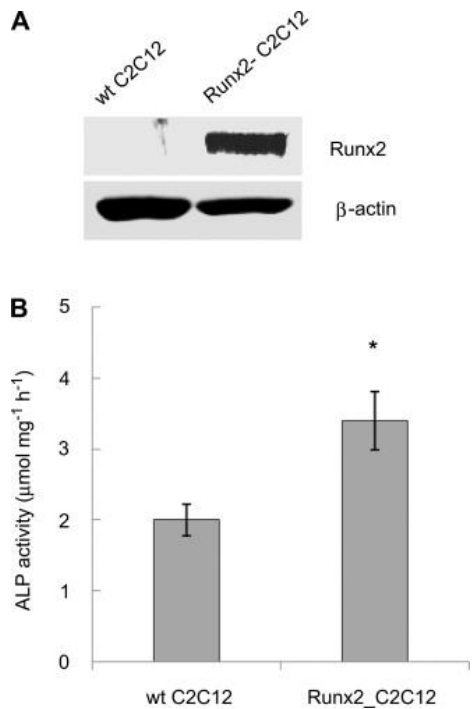

Figure I-3. Transfection of the Runx2 expression construct into C2C12 myoblasts. The parental C2C12 (wtC2C12) and Runx2-transfected C2C12 (Runx2_C2C12) were cultured on a TCD. A western blot for Runx2 protein (A) and ALP activities (B) was performed for wtC2C12 and Runx2_C2C12 cells. Data are presented as averages ± SDs (n = 3). ∗ Significantly different from wtC2C12 (Student's t-test, $p < 0.05$).

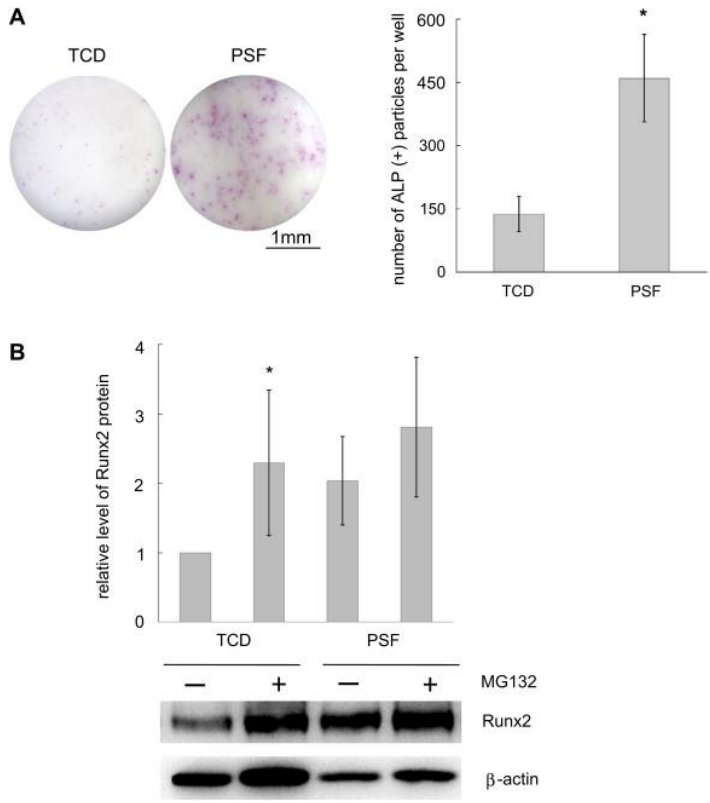

Figure I-4. Polystyrene fiber matrix stabilises the exogenous Runx2 protein and promotes osteoblast differentiation in the Runx2-transfected C2C12 cells. (A) Stereomicroscopic views of ALP staining. Magnification was 20×. Numbers of ALP-stained particles were counted. Data are presented as averages ± SDs (n = 3). ∗ Significantly different from TCD (Student's t-test, $p < 0.05$). (B) Effect of proteosomal degradation inhibitor MG132 on the Runx2 protein in Runx2_C2C12 cells grown on TCD and PSF. The intensities of Runx2 protein were measured and normalized by β-actin. Shown are the relative expression intensities in cells cultured on PSF to TCD. Data are presented as averages ± SDs (n = 3). ∗ Significant difference between MG132-treated and non-treated cells grown on TCD (ANOVA, $p < 0.05$).

IV.4. Discussion

This study demonstrated a mechanism indicating that a fibrous engineered matrix promotes osteoblast differentiation. Polystyrene matrices protected the Runx2 protein from proteosomal degradation in osteoblasts, whereas the cells grown on amorphous, non-fibrous, tissue culture dishes obviously showed degradation of the Runx2 protein. This was a more definitive proof of the hypothesis of the previous study comparing fibrous collagen and non-fibrous collagen matrix [서지혜, 2007]. Furthermore, in the genetically modified C2C12 myoblasts with Runx2, the polystyrene fiber matrix stabilized and sustained exogenous Runx2, which promoted osteoblast differentiation.

The fibrous structure of collagen has been noted in bone regenerative approaches. A previous in vivo study showed that the implantation of BSP with fibrillar collagen into calvarial defects induced early mineral deposition, whereas implantation with gelatin lacking the fibrillar structure did not induce matrix mineralization [Xu et al. 2007]. In this study, the authors concluded that the fibrillar microstructure of reconstituted collagen was essential for retaining BSP at a higher concentration within the defects, which enhances BSP-mediated matrix mineralization and osteoblast differentiation during the repair of rat calvarial defects. Notably, they stated that, even without BSP-loading, the expression of osteoblast markers and new bone formation was significantly greater in the collagen-treated defects than in the gelatin-BSP treated defects, which may suggest that the fibrillar structure of collagen plays a role in osteoblast differentiation and bone formation. Another study showed that the mineralization capacity of Runx2-engineered fibroblasts is scaffold-dependent and fibrous collagen foams exhibit a ten-fold higher mineral volume

compared with poly-ε-caprolactone and polylactide-co-glycolide matrices [Phillips et al. 2006]. In that study, the authors concluded that the osteogenic potential of Runx2-expressing fibroblasts was highly dependent on the architecture and surface properties of polymeric scaffolds. The role of collagen fiber on normal bone development was discussed in studies on osteogenesis imperfecta (OI) [Marini et al. 2007; Wallace et al. 2011]. OI is a generalized disorder of the connective tissue characterized by fragile bones and high susceptibility to fracture. Most cases of OI are caused by mutations in type I collagen. The OI functional mutations involving type I collagen showed 78.6% (much higher than expected on the basis of random occurrence) substitution of glycine, which is an amino acid residue responsible for collagen's helical (fiber) structure. Among the substitution mutations of glycine, regions in lethal mutations were aligned with collagen binding sites for integrins and fibronectin [Marini et al. 2007]. Recently, in a mouse model of OI, it was shown that the nanoscale morphology of type I collagen was altered [Wallace et al. 2011]. The above-mentioned studies suggest the importance of the collagen fiber structure and its nanoscale features in cell–matrix interaction and bone development. In this study, by using fibrous matrices made of natural collagen and synthetic polystyrene polymers, we provided evidence that both of these fibrous matrices greatly promoted osteoblast differentiation compared with the matrices lacking fibrous structures. Because we prepared the two-dimensional matrices on tissue culture dishes, we can rule out the influence of the scaffold architecture (porosity, pore size and the interconnectivity of the pores) on the cells and focus on effects of the fibrous surface topology of matrices on osteoblast differentiation.

Runx2 has been shown to be the earliest and most powerful molecular determinant of osteoblast differentiation [Karsenty 2008]. Given the critical

functions of Runx2 in osteoblast differentiation and bone formation, its expression and activity should be tightly regulated. When Runx2 is overexpressed in the osteoblasts of transgenic mice, osteopenia and multiple fractures develop in spite of an increased number of osteoblasts. It has been proposed that multiple signaling pathways converge on Runx2 to regulate osteoblast differentiation [Franceschi et al. 2003]. Growth factors involved in osteoblast differentiation and bone formation, such as BMP2 and FGF2, were reported to induce the post-translational modifications of Runx2 and regulate the degradation of the Runx2 protein [Jun et al. 2010; Park et al. 2010]. Following the previous study[서지혜, 2007], we revealed that a fibrous engineered matrix can also regulate the degradation of Runx2 in this study. Interestingly, the stabilization of the exogenous Runx2 protein, such as that expressed in the Runx2-transfected myoblasts, also depended greatly on the fibrous structure of the engineered matrix, which proposed a practical guideline for determining the surface topology of scaffolds in bone regenerative approaches involving gene therapies of Runx2. Although the detailed mechanisms underlying how a fibrous engineered matrix leads to the suppression of the degradation of the Runx2 protein need further study, two possibilities can be proposed. First, integrin-mediated signaling may play an important role in suppressing the degradation of Runx2 protein. Several studies have shown that fibrous collagen contributed to osteoblast differentiation through its own motif, which can bind directly to integrin receptors [Moursi et al. 1997] and through its fibronectin-binding motif [Knight et al. 2000]. Compared with gelatin or collagenase-treated collagen, which lack a fibrous structure, fibrous collagen enhanced alpha2β1 integrin-mediated cell adhesion [Knight et al. 2000], which suggests the importance of the fibrous structure of collagen for recognition by its integrins. In addition, the large surface area provided by a nano-fibrous architecture allows for greater adsorption of serum

proteins, including fibronectin and vitronectin, which could contribute to osteoblast differentiation and bone formation [Woo et al. 2007; Woo et al. 2003; Woo et al. 2009]. Second, one can consider the geometric control of a fibrous matrix influencing osteoblast differentiation [Guilak et al. 2009; McBeath et al. 2004; Arnold et al. 2004]. A study using micropatterned substrates that contained extracellular matrix-coated adhesive islands has revealed that the cell shape in response to the geometry of underlying artificial ECM controls the lineage commitment of mesenchymal stem cells into an adipogenic or osteoblastic phenotype and these effects can be regulated by modulating endogenous RhoA activity [McBeath et al. 2004]. It was also demonstrated that the spacing between the cell-adhesive nanodots regulated formations of focal adhesion and actin stress fibers in MC3T3-E1 and these cell responses were attributed to the clustering of integrin [Arnold et al. 2004]. These studies suggest that nanotopologic cues of the fibrous matrix may influence osteoblast differentiation in which the changes in cytoskeletal organization and structure be involved.

IV.5. Conclusion

In this study, we demonstrated that the fibrous structure of an engineered matrix inhibited the degradation of Runx2, a master transcription factor that can switch on osteoblast differentiation. In the previous study, MC3T3-E1 pre-osteoblasts grown on a fibrous collagen matrix sustained a high level of Runx2 protein compared with those on a degraded non-fibrous collagen matrix. The ubiquitin-dependent degradation of Runx2 was profoundly lower in the cells on the fibrous collagen matrix. The forced expression of Smurf1, an ubiquitin ligase responsible for Runx2 degradation, abrogated the collagen fiber-induced increase of Runx2 [서지혜, 2007]. In this study, we also prepared a polystyrene fiber matrix and confirmed that this matrix stabilized the Runx2 protein. Furthermore, exogenous Runx2 in C2C12 transfected with Runx2 on a polystyrene fiber matrix suppressed degradation and was sustained at higher levels, which led to the further promotion of osteoblast differentiation. Our results provide evidence that the fibrous structure of an engineered matrix contributes to osteoblast differentiation through the stabilization of the Runx2 protein.

V. PART-II.

Performance of electrospun poly-ε-caprolactone fiber meshes used with mineral trioxide aggregates in a pulp capping procedure

This part was already published in Acta Biomater 8, no. 8 (Aug 2012): 2986-95. doi: 10.1016/j.actbio.2012.04.032.

V.1. Introduction

Dental pulp is the soft connective tissue that occupies the central portion of the tooth. As a vital tissue, it is highly vascularized, innervated, and connected to periodontal tissues. It supports the dentin, responds to various stimuli, and is involved in reparative processes. Living dental pulp tissue that is exposed to the oral environment by caries, trauma, and/or mechanical injury should be protected with an appropriate pulp capping material to sustain its vitality and function. The pulp capping material needs to prevent the noxious stimuli of the oral environment from entering the pulp and must support the dentinogenesis potential of the pulp cells to form a dentin-bridge [Schröder 1985; Goldberg and Smith 2004]. Various materials have been used in pulp capping and pulpotomy procedures. For instance, calcium hydroxide is commonly used in dental clinics. However, due to several disadvantages of calcium hydroxide, including the irritation to the pulp tissue, its poor sealing properties, and the presence of porosity in the dentin barrier that it produces, there have been attempts to develop more effective and reliable pulp capping materials [Schröder 1985; Goldberg and Smith 2004; Murray and García-Godoy 2006; Goldberg et al. 1984]. Recently, mineral trioxide aggregate (MTA) has been demonstrated to induce significantly greater dentin-bridge formation with less pulp inflammation than does calcium hydroxide [Pitt Ford et al. 1996; Aeinehchi et al. 2003; Accorinte et al. 2008]. Therefore, MTA has become the material of choice for pulpotomies or direct pulp capping procedures. MTA has been shown to up-regulate the levels of the transcription factors and matrix adhesion proteins that regulate the differentiation of stem cells into preodontoblasts and odontoblasts [Okiji and Yoshiba 2009; Paranjpe et al. 2010; D'Antò et al. 2010]. This process contributes to the formation of the dentine bridge. However, the cytotoxicity of MTA during the

initial setting phase [Okiji and Yoshiba 2009; Balto 2004; Haglund et al. 2003; Dominguez et al. 2003] requires the use of a new material that can act as a barrier to direct MTA contact but permits the favorable effects of MTA.

Previous studies have shown that a fibrous engineered matrix mimicking the architecture of the natural extracellular matrix can modulate the cell responses leading to tissue regeneration [Ma 2008]. Numerous studies have shown the potential of fibrous scaffolds in tissue engineering for bone [Yoshimoto et al. 2003; Shin et al. 2004], cartilage [Li et al. 2003], skin [Chong et al. 2007], blood vessel [Pektok et al. 2008], and nerve [Schnell et al. 2007]. Previously, we investigated synthetic nanofibrous matrices for bone regeneration and reported that nanofibrous scaffolding architecture selectively enhances protein adsorption, including that of fibronectin and vitronectin adhesion proteins [Woo et al. 2003]. It also promotes osteoblast differentiation and biomineralization in vitro and in vivo and suppresses the degradation of Runx2 protein [Woo et al. 2007; Woo et al. 2009; Oh et al. 2011]. Considering that the nature of odontoblasts appears similar to that of osteoblasts, we hypothesized that a fibrous engineered matrix could be used to support the regeneration of dentin–pulp complex by not only acting as a physical barrier to unset MTA but also promoting the differentiation of pulp cells into odontoblast-like cells when the fiber meshes are used with MTA. This potential application is also supported by recent reports indicating that dental pulp stem cells are differentiated into odontoblast phenotypes by nanofibrous scaffolds [Yang et al. 2010; Wang et al. 2011].

This study examined the feasibility of using electrospun poly-ε-caprolactone (PCL) fiber meshes for its use in the MTA-based pulp capping procedures. Experimental pulp cappings were performed on the premolars of beagle dogs, and

we evaluated the efficacy of the PCL fiber meshes covering MTA (PCL-F/MTA) in terms of dentin-bridge formation. Furthermore, the responses of dental pulp cells to PCL-F/MTA were compared with their responses to MTA in an in vitro culture.

V.2. Materials and methods

V.2.1. Materials and reagents

The poly-ε-caprolactone (PCL), dimethylformamide (DMF), dichloromethane (MC), L-ascorbic acid, a calcium assay kit, glutaraldehyde, Weigert's iron hematoxylin solution, and Eosin Y solution were purchased from Sigma (St Louis, MO). The MTA (OrthoMTA) used in this study was purchased from BioMTA (Seoul, Korea). The fetal bovine serum (FBS), Dulbecco's modified Eagle's medium (DMEM), and penicillin–streptomycin solution were purchased from Hyclone (Logan, UT). The hexamethyldisilazane (HMDS) was obtained from Merck (Darmstadt, Germany). The Plank–Rychlo solution was obtained from T&I (Seoul, Korea). The β-glycerophosphate was obtained from Calbiochem (La Jolla, CA). The RNAiso Plus RNA extraction reagent, the PrimeScript™ RT reagent kit, and the SYBR Premix Ex Taq real-PCR reagent were obtained from Takara (Shiga, Japan). The Mg^{2+} Lysis/Wash buffer and bovine serum albumin (BSA) were purchased from Millipore (Kankakee, IL). The Sytox® Green reagent and Qunat-iT™ PicoGreen® dsDNA-assay kit were obtained from Invitrogen (Eugene, OR). The protein assay kit was purchased from Bio-Rad (Hercules, CA). The anti-DSP antibodies were purchased from Santa Cruz Biotechnology (Santa Cruz, CA). Biotinylated anti-rabbit IgG antibodies and the ABC Reagent kit were obtained from Vectastain (Burlingame, CA). The diaminobenzidine tetrahydrochloride (DAB) solution was purchased from Thermo (Fremont, CA). The 10 ml disposable syringes were obtained from Henke Sass Wolf (Tuttlingen, Germany). The 27G blunt needles for electrospinning were purchased from NanoNC (Seoul, Korea). The 7.9 mm and 6.4 mm styrene tubings were obtained from Plastruct (Industry, CA).

V.2.2. Preparation of PCL fiber matrices

A PCL fiber (PCL-F) matrix was prepared by electrospinning with 10% (w/v) PCL solution in MC and DMF (4:6). PCL was dissolved in MC by gentle rocking. After the PCL had dissolved completely in MC, the DMF was added to the PCL-MC solution and mixed gently on a rocker. The PCL solution was poured into a 10 mL syringe with a blunt stainless steel syringe needle (27G), and electrospun to a drum collector (drum diameter 10 cm, 25 rpm rotation). The electric potential and the distance to the collector were 15 kV and 10 cm, respectively. The morphology of electrospun fibers was observed under scanning electron microscopy (SEM) (Fig. II-1). The fiber thickness was measured from SEM images by using ImageJ (NIH) software. For use in the experiments, the PCL-F mesh was cut, kept for one day in a desiccator, and sterilized using ethylene oxide according to the manufacturer's instructions (GreenCross, Seoul, Korea).

V.2.3. Animals and surgical procedures

All procedures were approved by the Institute of Laboratory Animal Resources at Seoul National University (authorization number SNU-101025-2). Three healthy 18-month-old male beagles were used in the present study. They were caged individually with regulated light and temperature and fed Dog Chow and water. The dogs were anesthetized with an intravenous injection of ketamine at a dose of 1 mg kg^{-1}. General anesthesia was induced with an intramuscular injection of thiopental sodium. The maxillary second and third premolar teeth were randomly divided. Each tooth was trephinated through a 10 mm diameter class V cavity to generate a standardized pulp exposure (1.5 mm in diameter) by using a #4 round bur in a high-speed handpiece with copious water spray, and hemostasis was achieved via saline

irrigation and cotton pellets. The pulp capping procedure was conducted with either MTA or PCL-F/MTA (n = 6). MTA was placed on the exposed pulp area in the MTA group. In the PCL-F/MTA group, the PCL-F mesh was folded twice (four layers in total) and placed over the exposed pulp, and then filled with MTA (Fig. II-2). The MTA was mixed using a water–powder ratio of 3:1 (v/v) and applied to the exposure site using an MTA applicator. After applying the MTA filling, the cavities were restored with a light-cure resin.

V.2.4. Micro-computed tomography (CT)

The beagles were sacrificed by an intravenous injection of KCl under anesthesia, 8 weeks after surgery. The upper jawbone was excised, trimmed, and fixed in 4% paraformaldehyde for 24 h at 4 °C. The specimens were scanned using Micro-CT (Skyscan 1172, Skyscan, Aartselaar, Belgium). The scanning conditions were a source voltage of 100 kV, a source current of 100 μA, a 0.400° rotation step, and an image pixel size of 17.69 μm. The data images were reconstructed using NRecon software (Skyscan).

V.2.5. Histology

After the Micro-CT measurements, the specimens were decalcified in Plank–Rychlo solution for 3 months at room temperature, dehydrated with an ascending graded alcohol series, embedded in paraffin, sectioned at 6 μm, and stained with hematoxylin and eosin (H-E). For immunohistochemistry (IHC), the section slides were immersed in 0.3% H_2O_2 for 30 min and blocked in 1% BSA in PBS for 1 h. The sections were then incubated with anti-DSP antibodies for 60 min and secondary antibodies for 30 min. Next, the slides were placed in DAB solution for 1 min. The

H-E and IHC images were observed using a Leica DM2500 microscope. To measure the relative thickness of dentin-bridge and area of newly formed dentin in PCL-F/MTA group to those in MTA group, the thickness of dentin-bridge and the area of newly formed dentin were measured from three mid-sections per tooth and six teeth per group (18 sections per group) by using ImageJ software.

V.2.6. Preparation of the MTA and PCL-F mesh unit for cell culture

A 6.4 mm polystyrene tube (outer diameter 6.4 mm, inner diameter 4.9 mm) was cut into 1 mm thick rings (6.4⌀ ring), and a length of 7.9 mm tubing (outer diameter 7.9 mm, inner diameter 6.5 mm) was cut into 1.5 cm thick cylinders (7.9⌀ cylinder). The PCL-F meshes were cut into 1 × 1 cm squares and sterilized. OrthoMTA and DW (600 μl DW per 1 g MTA) were mixed and transferred to the 6.4⌀ rings on a thick, heavy glass plate, which was then covered with the other glass plate. After 1 h of mixing, the cover was taken off. The MTA-filled 6.4⌀ rings were turned upside down. For the MTA group, the MTA-filled 6.4⌀ rings were inserted into a 7.9⌀ cylinder. For the PCL-F/MTA group, a 1 × 1 cm PCL-F piece was laid over an MTA-filled 6.4⌀ ring, and then it was inserted into a 7.9⌀ cylinder. The cells were seeded onto the units for the experiments after 2 h of mixing.

V.2.7. Cell culture

The MDPC23 cell line derived from mouse fetal molar dental pulp papillae [Hanks et al. 1998] was maintained in DMEM supplemented with 10% FBS. The MDPC23 cells were seeded at densities of 1×10^5 cells per well of 12-well plate and

1.5×10^4 cells per MTA or PCL-F/MTA unit. Approximately 1 day after cell seeding, the cells were cultured in DMEM supplemented with 5% FBS, 50 μg ml^{-1} ascorbic acid, and 10 mM β-glycerophosphate.

V.2.8. Preparation of MTA extraction media

A mixture of 200 mg MTA powder and 120 μl DW was kept in a conical tube for 24 h. Then, 50 ml of DMEM was added, and the resulting mixture was gently rocked for a day. To collect the MTA-extracted media, the tube was centrifuged. Fresh DMEM was poured into the tube and kept there for one additional day. After centrifugation, the first and second MTA extracts were pooled and filtered with a 0.2 μm filter.

V.2.9. Scanning electron microscopy (SEM)

The cells that were cultured on MTA or PCL-F/MTA were fixed using 2.5% glutaraldehyde. After fixation, each specimen was dehydrated by dipping it in ethanol and then critical point drying with HMDS. After drying, the specimens were sputter-coated with gold–palladium and observed under an SEM at 15 kV (FE-SEM Hitachi S-4700, Japan).

V.2.10. Cell toxicity and proliferation

To test the cytotoxicity of MTA and PCL-F/MTA, the cells were seeded on MTA and PCL-F/MTA and cultured for 2 h, and Sytox® Green reagent, permeable to the dead cells, was added to 10 μl of each sample following the manufacturer's

instructions. For the proliferation tests, after 1 and 5 days of culture, 100 µl of Mg^{2+} Lysis/Wash buffer was added and then 10 µl of PicoGreen® reagent was added to each sample according to the manufacturer's instructions. After the incubation, the fluorescence was measured using FLUOstar OPTIMA (BMG Labtech Gmbh, Ortenberg, Germany).

V.2.11. Extraction of total RNAs and reverse transcription polymerase chain reaction (RT-PCR)

Quantitative real-time RT-PCR was performed to evaluate the expression of transcripts. The total RNAs were isolated using the RNAiso Plus RNA extraction reagent. The concentration and purity of the RNA preparations were determined by measuring the absorbance of RNA at 230, 260 and 280 nm. Then, 10 µl of first-strand cDNA was synthesized from 500 ng of the total RNAs using a PrimeScript™ RT reagent kit according to the manufacturer's instructions. One microliter of cDNA was used for PCR amplification. All reactions were performed with SYBR Premix Ex Taq real-PCR reagent according to the manufacturer's instructions by using 7500 Real-Time PCR System thermal cycler (Applied Biosystems, Carlsbad, CA). The denaturation was performed at 95 °C for 5 s, and the annealing/extension was done at 60 °C for 34 s. Table 1 lists the mouse primer sequences that were used. The level of the target gene transcripts was normalized to that of glyceraldehyde-3-phosphate dehydrogenase (GAPDH) ($-\Delta C_T$). The relative levels of expression in the experimental group were calculated by ΔΔCT ($\Delta C_{T\ Control} - \Delta C_{T\ Experiment}$).

V.2.12. Determination of calcium contents

Calcium deposition was examined in 7 day cultures using a calcium assay kit. The cultures were placed in 0.5 N HCl and incubated for 24 h. Then, the calcium reagent working solution was added to each sample according to the manufacturer's instructions. The absorbance was measured at 575 nm.

V.2.13. Statistical analysis

The data are presented as the mean and standard deviation. Statistical analyses were performed using an analysis of variance (ANOVA). The differences were considered significant if the p value was <0.05.

Table II-1. Sequences of Primers used in real-time PCRs

Molecules	Primer sequences	Accession No. (Gene bank)
Dspp	5′-AACACATCCAGGAACTGCAGC-3′ 5′-TGACTCGGAGCCATTCCCATC-3′	NM_010080.2
Alkaline phosphatase	5′- CAGAGCGCACGCGATGCAAC-3′ 5′- GCACTGGGTGTGGCGTGGTT-3′ 5′-GTAGCTGTATTCGTCCTCAT-3′	NM_007431.2
Gapdh	5′- GTGAACCACGAGAAATATGACAAC-3′ 5′- CATGAGCCCTTCCACAATGCC-3′	NM_008084.2

V.3. Results

V.3.1. Experimental pulpotomy in premolars of beagle dogs

We prepared a PCL-F mesh from a 10% PCL solution by electrospinning (Fig. II-1). The average of the fiber diameters was ～600 nm (n = 238). Experimental pulpotomies were conducted in the beagle dogs with either MTA or PCL-F/MTA (Fig. II-2). The Micro-CT images after 8 weeks of pulp treatment showed the evident formation of the dentin-bridge in the PCL-F/MTA group (Fig. II-3). In the MTA group, the dentin-bridge could not be distinguished from the radio-opaque MTA material. However, the invasion of radio-opaque material into the root canals was frequently observed in the MTA group.

The histology demonstrated the thicker formation of the dentin-bridge and more integrated pulp tissue in the PCL-F/MTA group compared with the MTA group (Fig. II-4A). Columnar polarized odontoblast-like cells with long processes and tubular dentin-like matrices were observed beneath the dentin-bridge in the PCL-F/MTA group. It was also notable that the dentin-bridge in the PCL-F/MTA group continuously closed the opening of the pulp chamber. In contrast, MTA tended to produce narrow dentin-bridges under the large step, which is most likely the space where the MTA was. A considerable amount of tertiary dentin was formed in the MTA adjacent to the dentin on the wall of the pulp chamber, with clear demarcation lines between the pre-existing and newly formed dentin, which led to a narrower pulp chamber and root canal. The dentin formed in the MTA appeared as an amorphous matrix with barely observable dentinal tubules. Immunostaining for dentin sialoprotein (DSP) supported the differentiation of the pulp cells into

odontoblast-like cells in the PCL-F/MTA; the cells beneath the dentin-bridge were intensely immunostained for DSP (Fig. II-4B).

The thickness of the dentin-bridge in the PCL-F/MTA group was approximately four times that in the MTA group (Fig. II-5A). Interestingly, the total area of the newly formed dentin in the PCL-F/MTA group was only approximately three times that in the MTA group (Fig. II-5B), suggesting that a substantial amount of tertiary dentin was formed on the wall of the pulp chamber in the MTA group. The differences in the thickness of the dentin-bridge and the area of the reparative dentin were statistically significant (ANOVA, $p < 0.05$).

V.3.2. Cell toxicity and proliferation in an *in-vitro* culture

We fabricated a cell culture unit to compare the responses of MDPC23 cells to PCL-F/MTA with those to MTA (Fig. II-6). As the unit itself without MTA or PCL-F did not show any cell toxicity, the unit provided the substrates of MTA or PCL-F/MTA for the cells. SEM images indicated that the MDPC23 cells seeded on PCL-F/MTA appeared to adhere to the matrix and to grow well, even when the cells were seeded after 1 h of MTA hydration (Fig. II-7). By contrast, most of the cells on MTA were dead, and only the cell debris could be observed, especially when the cells were seeded after 1 h of MTA hydration. However, cells seeded on MTA after 24 h of MTA hydration appeared to recover to some extent in 4 day cultures. As shown in Fig. 8, PCL-F/MTA significantly reduced cell death to 7.9% of that in the MTA group. The differences were statistically significant (ANOVA, $p < 0.05$). Furthermore, the proliferation of the cells cultured on PCL-F/MTA was much greater than that of the cells cultured on MTA. The cells were seeded at the same density on both substrates after 24 h of MTA hydration. The amounts of DNA on PCL-F/MTA were ～35-fold

greater than those on MTA after 4 days of culture, whereas they were ～2.4-fold greater after one day of culture (Fig. II-9). The differences were statistically significant (ANOVA, $p < 0.05$).

V.3.3. Cell differentiation in an *in-vitro* culture

The effects of PCL-F/MTA on the differentiation of MDPC23 to odontoblast-like cells were examined. Real-time RT-PCR demonstrated that the MDPC23 cells grown on PCL-F/MTA exhibited higher expression levels of alkaline phosphatase (ALP) and dentin sialophosphoprotein (DSPP) than those grown on MTA (approximately two- and threefold, respectively; Fig. 10A). ALP is a characteristic molecule in hard-tissue-forming cells such as osteoblasts and odontoblasts. DSPP is the major non-collagen matrix protein in dentin and plays an important role in dentin formation and biomineralization [Qin et al. 2004]. In repeated experiments, the difference between the expressions was confirmed to be significant (ANOVA, $p < 0.05$). In addition, the effect of PCL-F covering to MTA on biomineralization was assessed using a calcium deposition assay. Because MTA elutes substantial calcium ions [Okiji and Yoshiba 2009], we could not evaluate the cultures in which the cells were directly seeded onto MTA. Instead, the MTA-extracted DMEM was prepared, and the cells were cultured on a tissue culture dish (TCD) and the PCL-F mesh. The amounts of calcium deposited by the cultures were significantly different; the cultures prepared on PCL-F exhibited approximately twofold greater calcium deposition than the cultures prepared on TCD (Fig. II-10B). Regarding effects of the extracts from the MTA and PCL-F/MTA, both extracts enhanced the expression of DSPP compared to the original DMEM, and the relevant levels were not significantly different from each other (Fig. II-10C). These results indicate that PCL-F/MTA promoted the

differentiation of MDPC23 cells to odontoblast-like cells and biomineralization.

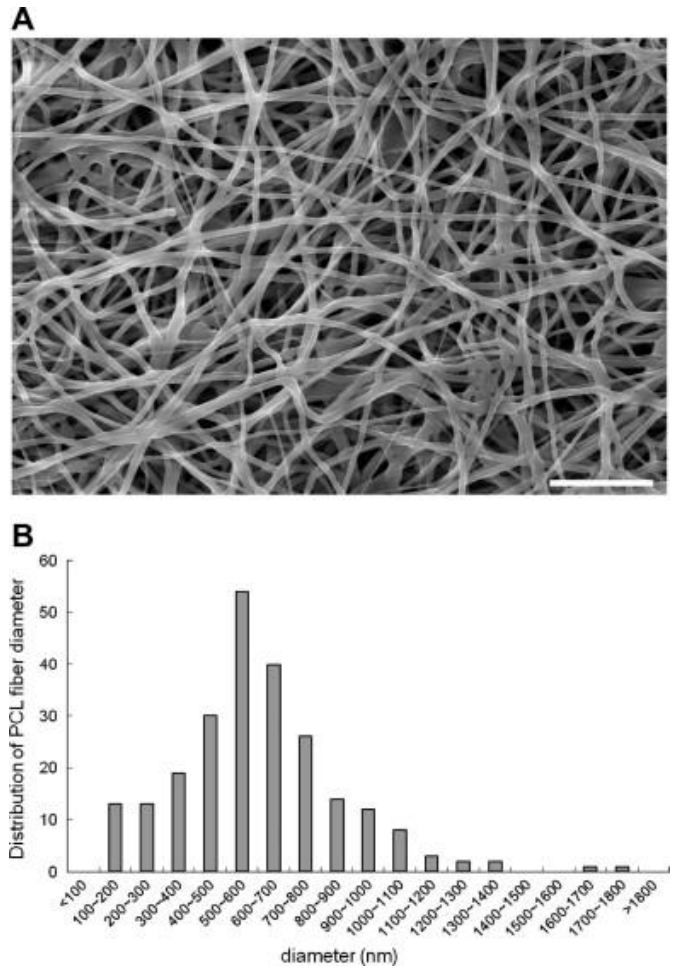

Figure II-1. (A) Scanning electron microscopic views of PCL-F. The PCL-F mesh was made of 10% (w/v) PCL solution in MC and DMF (4:6). Bar length: 10 μm. (B) Distribution of the fiber diameter. The diameter was measured in scanning electron microscopic images with a magnification of 20,000× using software (n = 238).

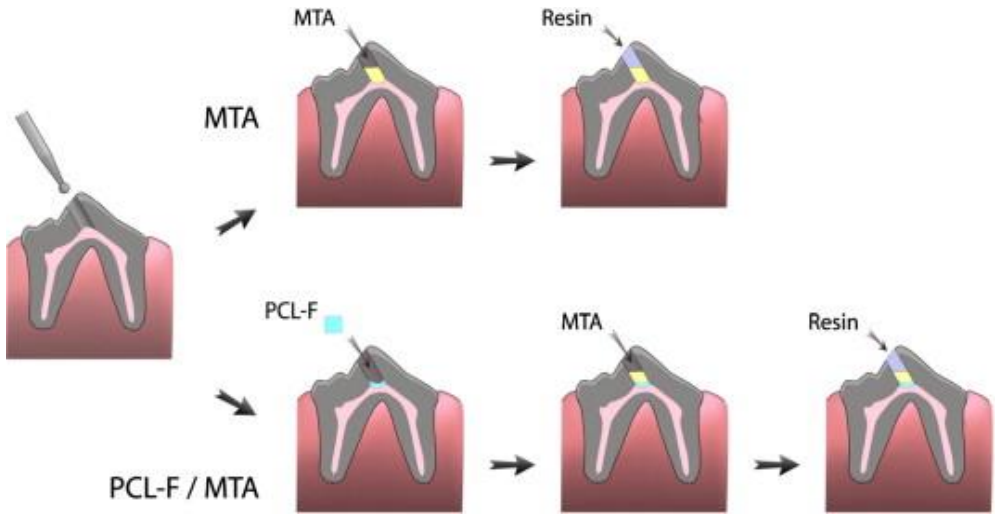

Figure II-2. Diagram of an experimental pulp capping performed in the premolars of beagle dogs. The pulp was exposed by drilling with a 1.5 mm diameter round bur. In the control MTA group, the defect was filled with MTA and light-curing resin (upper). In the experimental PCL-F/MTA group, it was filled with the PCL-F mesh applied over the MTA and then with the resin (lower).

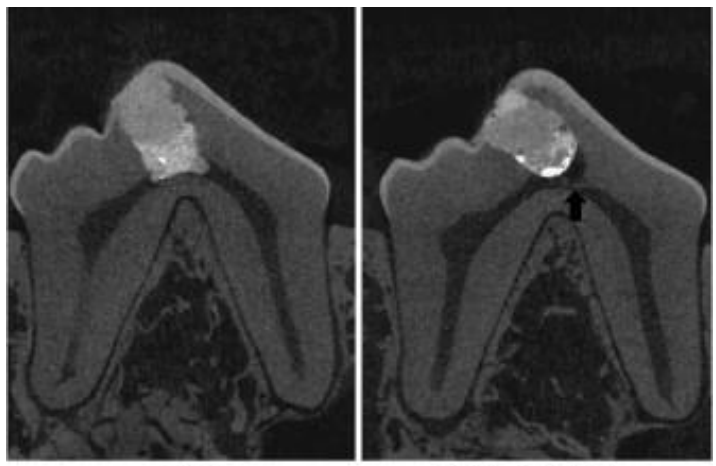

Figure II-3. Micro-CT images. The premolars after 8 weeks of pulp capping treatment were scanned and the data images were reconstructed. A reconstructed image of mesio-distal plane (lateral view) including the cusp tip is presented for each group. The arrow indicates the dentin-bridge.

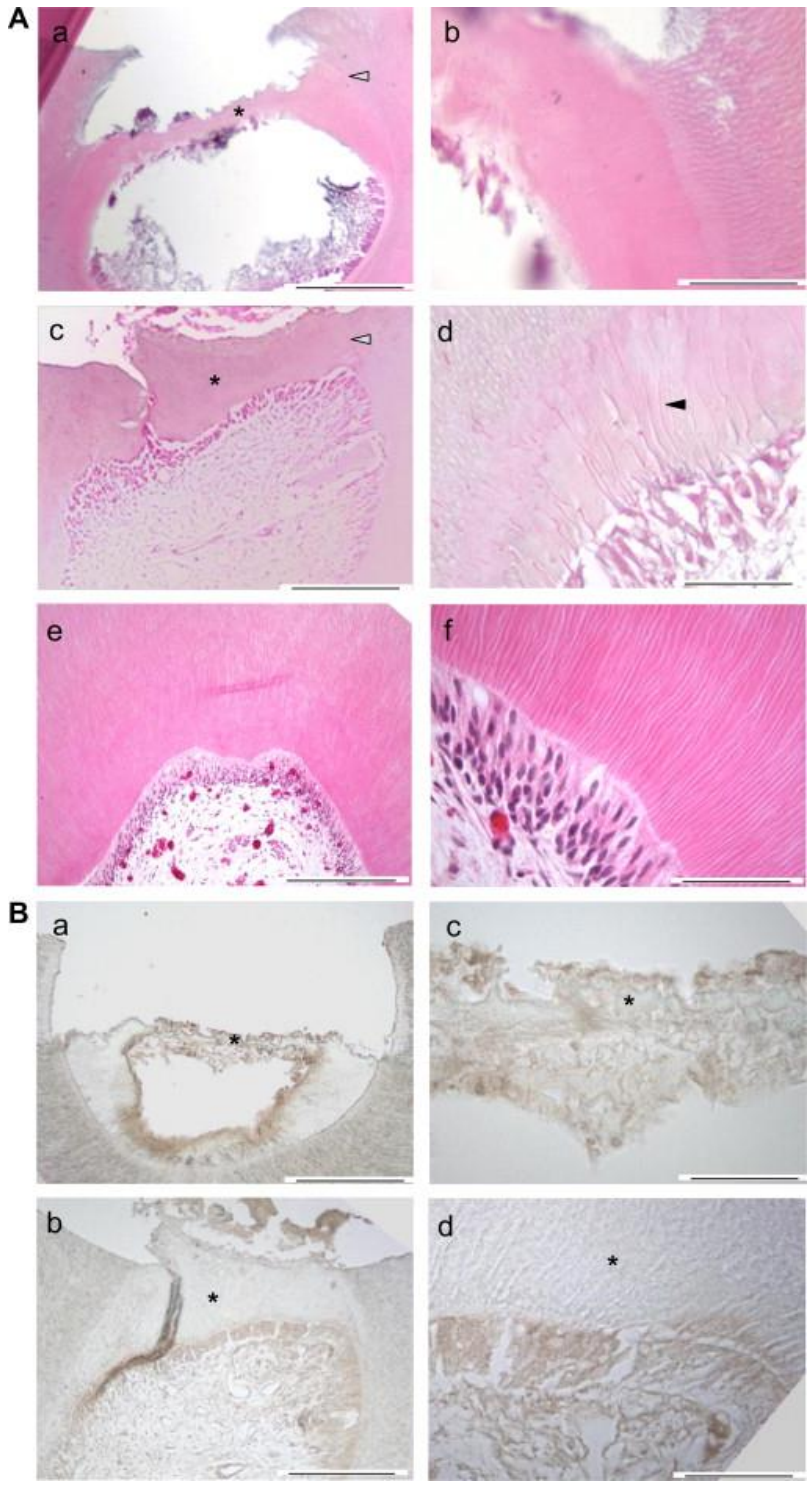
A
a
b
c
d
e
f
B
a
c
b
d

Figure II-4. (A) H-E staining showing microscopic views of a pulp capping-treated tooth filled with MTA (a, b) or PCL-F/MTA (c, d) and an untreated healthy tooth (e, f). ∗ indicates the dentin-bridge, ∗∗ indicates the remnants of PCL-F, the grey arrow indicates the demarcation line between the pre-existing and newly formed dentin, and the black arrow indicates the odontoblast process. Bar length: (a, c, e), 200 μm; (b, d, f), 50 μm. (B) DSP-immunostaining showing microscopic views of a pulpotomy-treated tooth filled with MTA (a, b) or PCL-F/MTA (c, d).

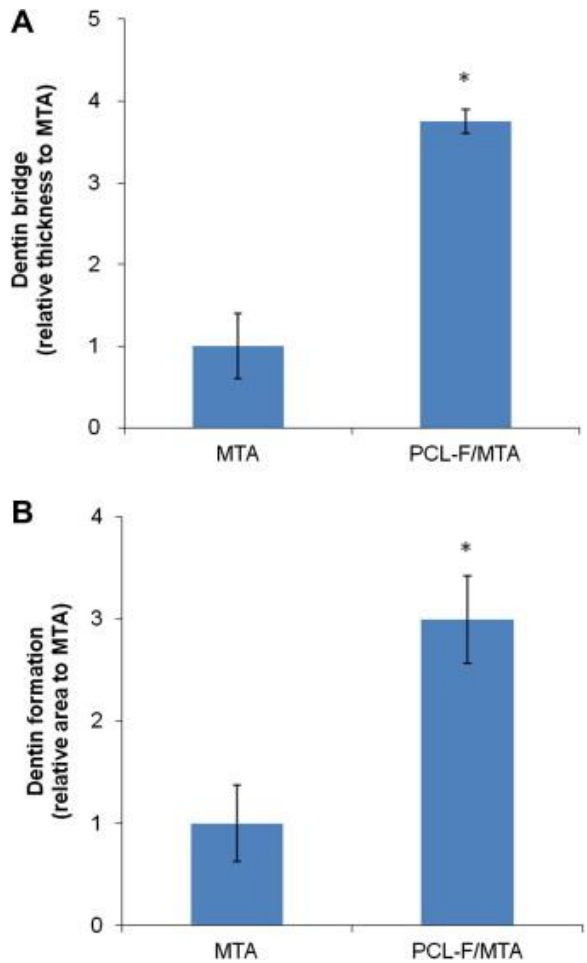

Figure II-5. (A) Thickness of the dentin-bridge formed after pulp capping treatment. The thickness was measured using microscopic images with a magnification of 100× (n = 18). (B) Area of newly formed dentin measured using microscopic images with a magnification of 100× (n = 18). ∗ indicates significant differences from MTA ($p < 0.05$, ANOVA).

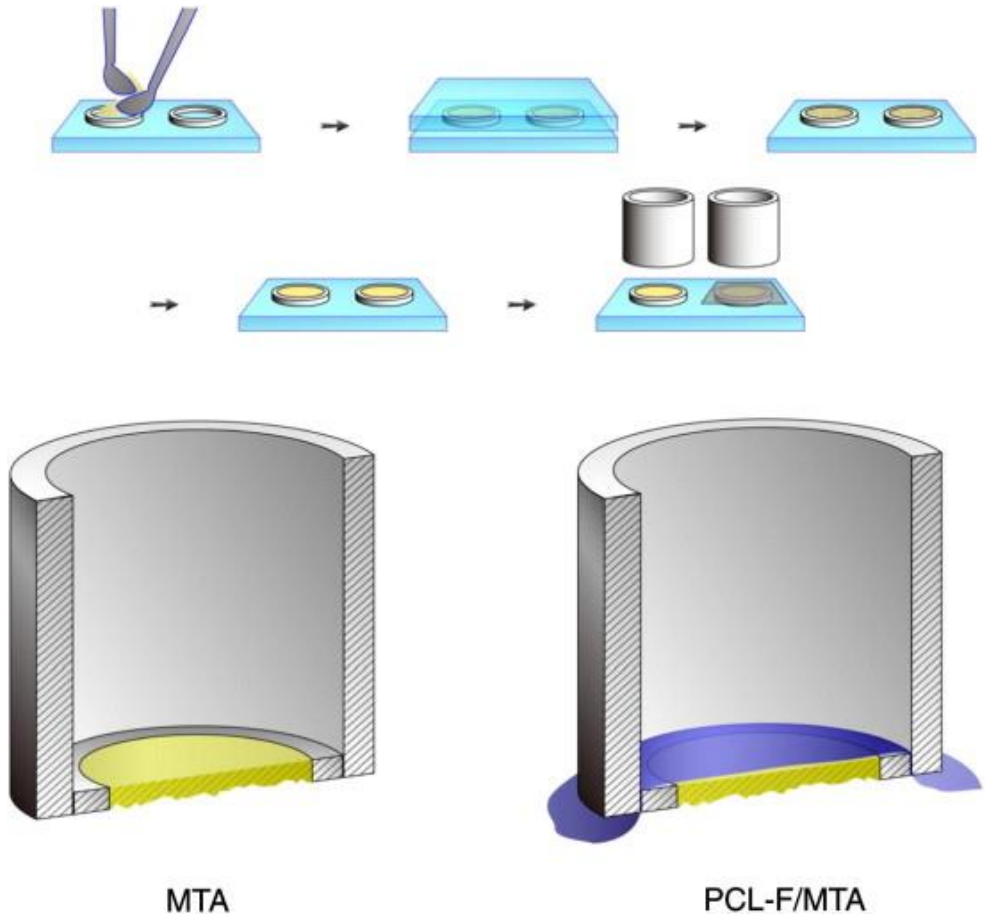

Figure II-6. Illustration on the fabrication of MTA and PCL-F/MTA culture unit. Inner rings were placed on a mixing slab and filled with the MTA mixture. The other mixing slab was placed over the rings for 1 h. Outer cylinders were assembled over the rings with or without the insertion of a PCL-F mesh.

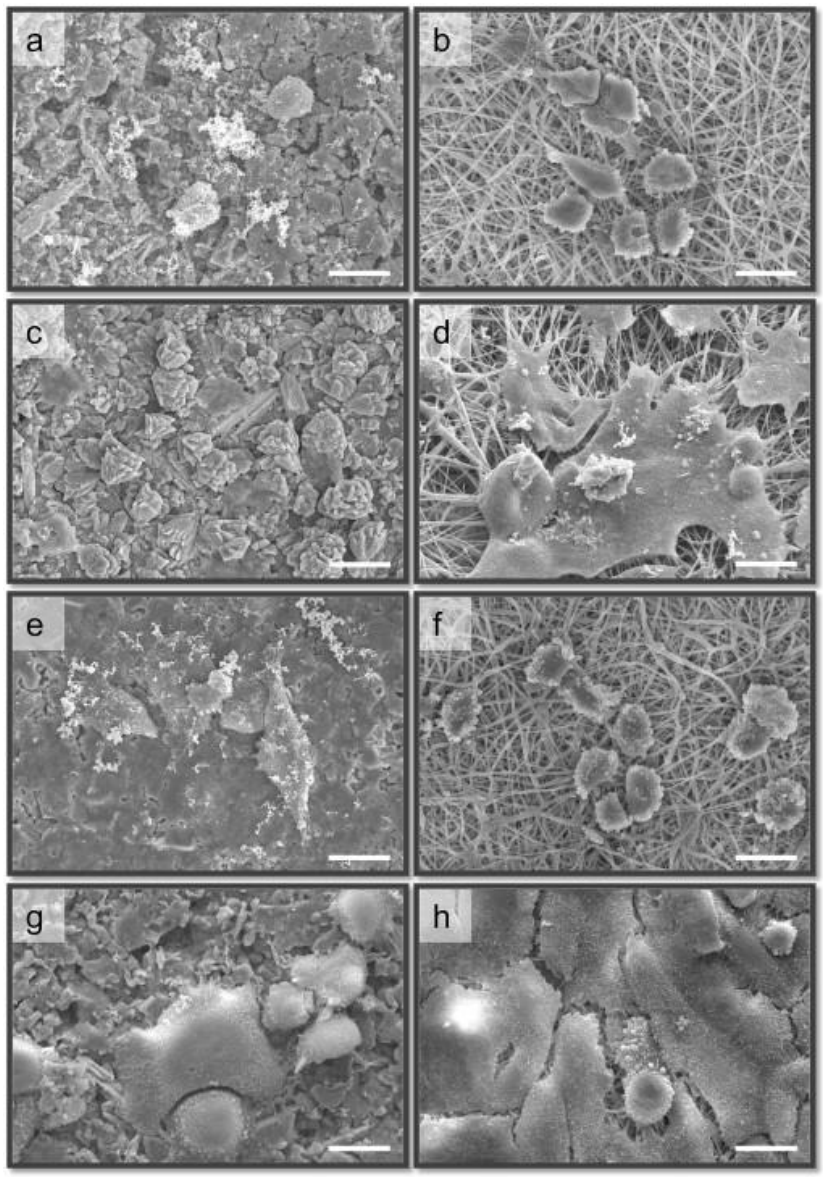

Figure II-7. Scanning electron microscopic images of MDPC23 cells cultured on MTA (a, c, e, g) **and PCL-F/MTA** (b, d, f, h)**.** The cells were seeded after 1 h (a–d) or 24 h (e–h) of MTA hydration and cultured for 1 day (a, b, e, f) or 4 days (c, d, g, h). Bar length: 20 μm.

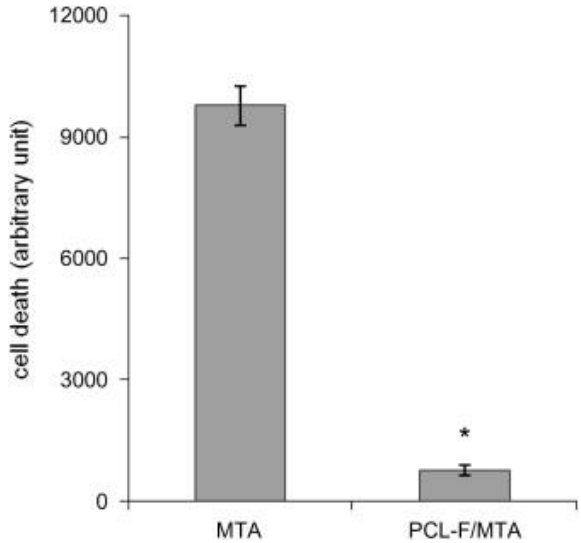

Figure II-8. Cell toxicity. The cells were seeded after 1 h of MTA hydration and cultured for 2 h on MTA or PCL-F/MTA. The cell toxicity was examined using Sytox® Green reagent (n = 5). ∗ indicates a significant difference from the MTA ($p < 0.05$, ANOVA).

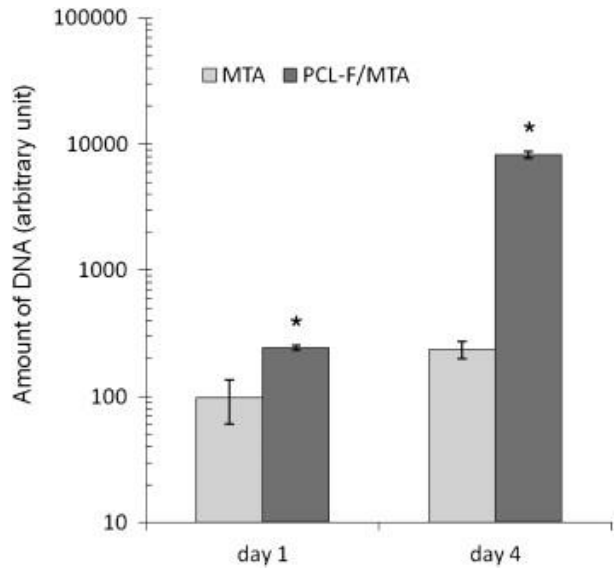

Figure II-9. Cell proliferation. The cells were seeded after 24 h of MTA hydration and cultured for 1 or 4 days on the MTA or PCL-F/MTA. The cell proliferation was examined using PicoGreen® reagent (n = 5). ∗ indicates significant differences from the MTA ($p < 0.05$, ANOVA).

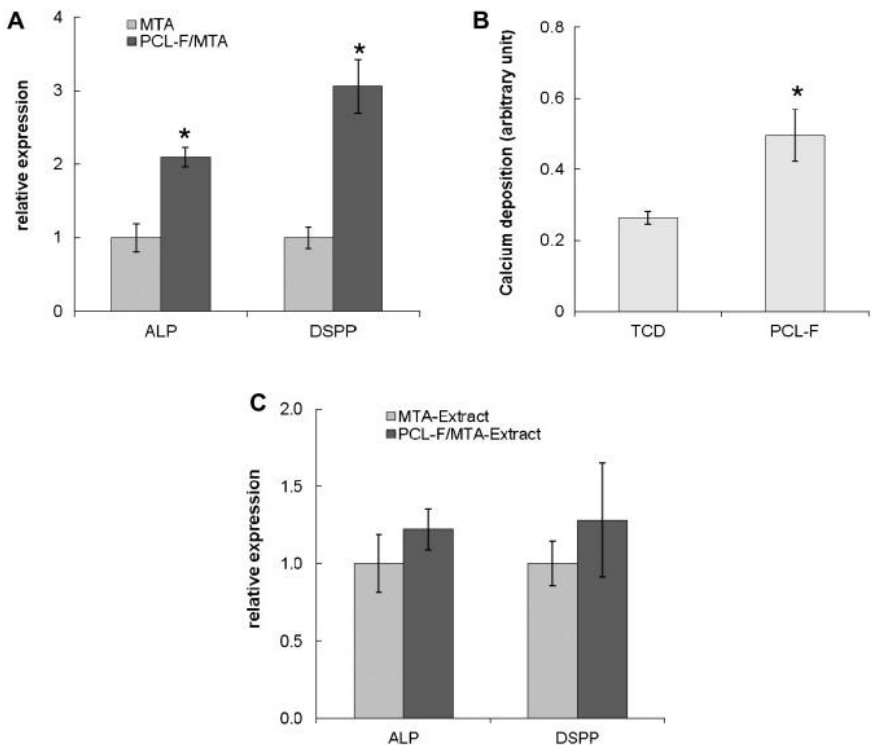

Figure II-10. Cell differentiation. (A) Expression levels of ALP and DSPP. MDPC23 cells were seeded after 24 h of MTA hydration and cultured for 7 days on MTA or PCL-F/MTA in DMEM supplemented with 5% FBS, 50 μg ml^{-1} ascorbic acid, and 10 mM β-glycerophosphate (differentiation media). The expression of ALP and DSPP was examined using real-time RT-PCR and normalized with GAPDH. ∗ indicates significant differences from MTA ($p < 0.05$, ANOVA). (B) Calcium deposition on the cultures. The cells were cultured on tissue culture dishes (TCD) or PCL-F meshes for 7 days in MTA-extracted differentiation media. ∗ indicates significant differences from the TCD ($p < 0.05$, ANOVA). (C) Effect of the MTA and PCL-F/MTA extracts on expression levels of ALP and DSPP. MDPC23 cells were seeded on TCD and cultured for 7 days in MTA- or PCL-F/MTA-extracted differentiation media.

V.4. Discussion

This study sought to determine whether a synthetic nanofiber mesh PCL-F might be suitable for use in vital pulp therapies by acting as a barrier to direct MTA while permitting the favorable effects of MTA. We also intended to determine whether the PCL-F/MTA was capable of promoting the differentiation to odontoblast-like cells. The results demonstrated that the PCL-F/MTA substantially enhances the formation of the dentin-bridge while preserving the integrity of the pulp tissues, protects the pulp cells from the deterimental effects of MTA during an early period of its hydration, supports cell proliferation, and promotes the expression of the odontoblast phenotype and the extent of mineralization. These results suggest that the use of PCL-F may be beneficial for the regeneration of the dentin–pulp complex when used with MTA in pulp capping procedures.

Dental pulp tissue is considered to possess regenerative potential. A portion of the dental pulp cells has been demonstrated as pluripotent stem cells. Dental pulp stem cells (DPSCs) from permanent [Gronthos et al. 2000] and deciduous [Miura et al. 2003] teeth showed rapid proliferation and multiple differentiation potentials, suggesting their vast potential therapeutic implications. Given the regenerative potential of dental pulp, the method described here implies a feasibility of the conservative and effective regimen for pulp cells to regenerate the dentin–pulp complex if the pulp tissue remains vital. Currently, MTA is the material of choice in vital pulp therapeutic procedures. Set MTA is known to be biocompatible and have negligible cytotoxicity [Pelliccioni et al. 2004; Bonson et al. 2004]. However, MTA in its freshly mixed state exhibits high cytotoxicity [Balto 2004; Haglund et al. 2003]. Animal studies also showed that MTA caused limited pulp tissue necrosis shortly after application [Okiji and Yoshiba 2009; Dominguez et al. 2003; De Souza Costa

et al. 2008]. In this study, consistent with previous reports, the longer time that passed after MTA mixing, the lower the cell toxicity (Fig. II-7). In practice, MTA is applied in the unset state. Thus, we hypothesized that it would be more advantageous to protect the pulp from direct contact with unset MTA to regenerate the dentin–pulp complex. The PCL-F mesh in this study appears to be an efficient temporal barrier for MTA to be set. Both the SEM observation and the cytotoxicity test showed that the substantial amount of cells in the PCL-F/MTA protected MDPC23 cells from the noxious effect of unset MTA (Fig. II-7; Fig. II-8). The PCL-F/MTA supported cell proliferation as well (Fig. II-9). On the other aspect, the PCL-F seems to permit the favorable effects of MTA. The extracts from the MTA and PCL-F/MTA both enhanced the expression of DSPP, and the relevant levels were not significantly different from each other (Fig. II-10C). Furthermore, the cells grown on PCL-F/MTA significantly enhanced DSPP expression, compared with those grown on MTA (Fig. II-10A). The MTA extracts increased calcium deposition to a greater extent in the cells grown on PCL-F than did those grown on TCD (Fig. II-10B). These features indicate that PCL-F/MTA not only permits the favorable effects of MTA but also promotes the differentiation to odontoblast-like cells.

The experimental pulp capping conducted in this study showed that PCL-F/MTA formed a dentin-bridge that was approximately fourfold thicker than that formed by the MTA (Fig. II-4; Fig. II-5). The cells beneath the dentin-bridge in the PCL-F/MTA group appeared to have odontoblast-like features including columnar polarized cell morphology with a long process embedded in (pre)dentin and its expression of DSPP (Fig. II-4). These observations confirmed that the PCL-F mesh was definitively beneficial to the regeneration of the dentin–pulp complex in the MTA-based pulp capping treatment. Interestingly, there was also a notable difference in the pattern of

reparative dentin formation. In the MTA group, the reparative dentin was formed along the pulp chamber wall and the root canal walls with a distinct line between the pre-existing and newly formed dentins (Fig. II-4; Fig. 5). This pattern can also be found in previous reports [Okiji and Yoshiba 2009; Bortoluzzi et al. 2008]. In contrast, in the PCL-F/MTA group, minimal dentin formation was observed in areas other than the dentin-bridges between the exposed pulp tissue and the restorative material. The pulp chamber and root canal in the PCL-F/MTA group were better sustained than in the MTA group. These features suggest that the mechanism of formation of reparative dentin in PCL-F/MTA is somewhat different from that that in MTA alone.

The setting reaction of MTA involves the hydration of anhydrous mineral oxide compounds via the dissolution of the compounds followed by the crystallization of the hydrates. During the hydration process, calcium silicate hydrate is produced together with calcium hydroxide crystals which can be dissolved [Okiji and Yoshiba 2009]. Most of the cytotoxicity of unset MTA is considered to be due to the high pH value in aqueous solution of calcium hydroxide. Set MTA is mainly composed by an insoluble matrix of silica which maintains its integrity in contact with water or tissue fluid. However, it was able to release its soluble fraction in a decreasing rate during the long period of time [Fridland and Rosado 2005]. It was confirmed that this soluble fraction was mainly composed by calcium hydroxide and that the calcium ion was attributed to the dentin-bridge formation underneath the MTA pulp capping [Fridland and Rosado 2003]. PCL is aliphatic polyester and considered as a hydrophobic polymer [Woodruff and Hutmacher 2010]. It is presumed that PCL-F used in this study could act as a temporal barrier to the hydroxyl ion during the early periods of MTA hydration due to the hydrophobic nature of PCL. Later on, as the

PCL-F became wet, it might permit the passage for the soluble fraction of set MTA such as calcium ion, which could contribute to form the dentin-bridge.

PCL is degraded by hydrolysis of its ester linkages in physiological conditions, and the degradation of PCL produces the acidic products which can diffuse out. The degradation of PCL compared to other degradable polymers is slow, making it much more suitable for long-term degradation applications [Woodruff and Hutmacher 2010]. It has been reported that PCL scaffolds in simulated physiological conditions lost ～18% of the mass after 60 months [Lam et al. 2008]. It was speculated that the PCL-F in this study might be maintained for a substantial period. However, it should be pointed out that the hydroxyl ion released from the MTA could speed up the degradation of PCL [Lam et al. 2008]. Since the degradation of PCL-F might affect the sealing ability of PCL-F/MTA, further long-term studies should be performed to confirm the efficacy of PCL-F in the MTA-based pulp therapies for its use in practice.

Recently, nanofibrous scaffolds have been studied for their possible applications in dental tissue engineering. The previous in vitro and in vivo studies have demonstrated that nanofibrous scaffoldings supported the expression of odontoblast phenotypes and biomineralization in rat and human DPSCs, and they have confirmed the potential applications of nanofibrous scaffolds in dentin regeneration [Yang et al. 2010; Wang et al. 2011]. In this study, we provide evidence that the nanofiber meshes can be used in the MTA-based pulp therapeutic procedures, presenting the performance of PCL-F/MTA in supporting the formation of a dentin–pulp complex-like structure. Considering that nanofibers are capable of delivering drugs and recombinant proteins [Yoo et al. 2009], the applications of nanofiber meshes can be further extended to complicated pulp diseases to control bacterial infections in the pulp and to modulate the regenerative potential of individuals.

V.5. Conclusion

In this study, the feasibility of using electrospun PCL fiber meshes in the MTA-based pulp capping procedures was verified. Experimental pulp cappings were performed in the premolars of beagle dogs and the efficacy of the PCL-F meshes was evaluated after 8 weeks. PCL-F/MTA allowed for the formation of a dentin-bridge that was approximately four times thicker than that formed in the MTA group. Columnar polarized odontoblast-like cells with long processes and tubular dentin-like matrices could be observed beneath the dentin-bridge in the PCL-F/MTA group. The cells were also intensely immunostained for dentin sialoprotein. In the cell cultures, PCL-F/MTA significantly reduced cell death to ~8% of that in the MTA. The proliferation of the cells grown on PCL-F/MTA was much greater than that of the cells grown on MTA. Furthermore, PCL-F/MTA promoted the differentiation into odontoblast-like cells and biomineralization, as confirmed by the expression of ALP and DSPP and by the degree of calcium deposition. Based on these results, PCL-F may be used efficiently in the MTA-based dental pulp therapy.

VI. PART III.

Comparative evaluation of the biological properties of fibrin for bone regeneration

This part was already published in BMB Reports 47, no. 2 (Feb 2014): 110-4. doi: 10.5483/BMBRep.2014.47.2.156

VI.1. Introduction

Natural biopolymers such as collagen and fibrin have been frequently utilized as biomaterials for bone regeneration. The extracellular matrix in bone tissues is mainly composed of type I collagen. Collagen is characterized by a unique triple-helix formation that extends over a large portion of its structure. Fibrous collagen influences the development and maintenance of the osteoblast phenotype and induces the differentiation of bone marrow stromal cells along the osteoblast pathway [Lynch et al. 1995; Mizuno et al. 2000]. In addition to the specific motifs of collagen that bind cellular integrin receptors [Moursi et al. 1997; Knight et al. 2000], the fibrous structure of collagen contributes to osteoblast differentiation by stabilizing Runx2 proteins [Oh et al. 2011]. Mimicking the fibrous morphology of collagen, fibrous engineered matrices have been developed and have shown good biological performance for bone regeneration [Li et al. 2002; Woo et al. 2007; Ma 2008].

Fibrin, a fibrous biopolymer, forms naturally during blood clotting. Hemostasis is the primary role of fibrin, but fibrin also functions as a provisional matrix during wound healing. Fibrin possesses suitable properties for use in regenerative medicine. For instance, fibrin is capable of conveying matrix proteins and growth factors [Ahmed et al. 2008; Laurens et al. 2006; Mosesson 2005]. During the early stages of bone repair, thrombin contributes to the proliferation of osteoblasts [Song et al. 2005a]. Fibrin supports osteoblast differentiation and bone healing, in which thrombin engaged in fibrin modulates the fibronectin binding capacity of fibrin [Bensaïd et al. 2003; Osathanon et al. 2008; Oh et al. 2012; Karp et al. 2004]

Based on their biological properties, collagen and fibrin have been widely

examined in biomedical research due to their ability to repair tissue. Collagen and fibrin can be used as scaffolding materials, coating agents for synthetic polymers, and carriers for the delivery of genes, drugs, or bioactive agents [Breen et al. 2009]. Despite the frequent use of collagen and fibrin in bone regenerative approaches, their comparative efficacies have not yet been evaluated. In the present study, we evidenced the superiority of fibrin to collagen in the adsorption of serum fibronectin, osteoblast proliferation, and osteoblast differentiation. Collagen and fibrin matrices were prepared using the same concentrations of fibrinogen and type I collagen, and serum protein adsorption to the matrices was evaluated. MC3T3-E1 pre-osteoblasts were cultured on the matrices, and cell proliferation, Runx2 expression and transcriptional activity, alkaline phosphatase (ALP) activity, and calcium deposition were determined.

VI.2. Materials and methods

VI.2.1. Reagents

Bovine fibrinogen, thrombin, aminocaproic acid, L-Ascorbic acid and glycerol 2-phosphate were purchased from Sigma (St. Louis, MO). Rat tail type I collagen was purchased from BD Bioscience (San Jose, CA). Fetal bovine serum (FBS), HEPES buffer solution, and penicillin-streptomycin solution were from GibcoBRL (Carlsbad, CA), and ascorbic acid-free α-MEM was from WelGene (Daegu, Korea). The MicroBCA™ assay kit was from Pierce-Thermo (Rockford, IL). Qunat-iT™ PicoGreen® dsDNA-assay kit was from Invitrogen (Eugene, OR). West-Zol™ was from Intron Biotechnology (Seoul, Korea). A Dual-Glo™ Luciferase Assay System was from Promega (Madison, WI). Protease inhibitor cocktail tablets (Complete) were from Roche (Basel, Switzerland). Anti-Runx2, anti-actin, and HRP-conjugated IgG antibodies were from Santa Cruz Biotechnology (Santa Cruz, CA). Anti-fibronectin and anti-vitronectin antibodies were from Chemicon (Temecula, CA).

VI.2.2. Preparation of matrices

Collagen matrix was prepared by pouring 1, 3, or 5 mg/ml type I collagen in PBS (pH 7.4) into a culture dish and was solidified in an incubator at 37℃. Fibrin matrix was prepared by mixing fibrinogen and thrombin solutions, which contained 1, 3, or 5 mg/ml fibrinogen in PBS (pH 7.4), 1 U/ml thrombin, 50 μg/ml aminocaproic acid, and 1 mM of $CaCl_2$, and pouring the solution into a culture dish.

VI.2.3. Scanning electron microscopy (SEM)

The matrices were rinsed in PBS and fixed using 2.5% (v/v) glutaraldehyde in a 0.1 M cacodylate buffer (pH 7.4). After freeze-drying, the specimen was dehydrated by dipping it in increasing concentrations of ethanol and then by critical point drying. After drying, the specimens were sputter-coated with gold-paladium and observed under an SEM at 12 kV (FESEM Hitachi S-4700, Japan).

VI.2.4. Protein adsorption

Binding of serum proteins to matrices was examined as described in a previous report with some modifications (15). In brief, matrices were incubated in the presence of 10% (v/v) mouse serum at 37℃. After the 4 h of incubation, serum solution was removed from the matrices. The matrices were washed with PBS under gentle agitation for 20 min. The washing solution was then discarded and fresh PBS was replaced to wash again. A total of three washings were conducted to remove free and loosely adsorbed proteins (there was a negligible amount of proteins in the third washing solution). The remaining proteins (adsorbed) to the matrices were recovered by incubation in 1% (w/v) SDS solution after homogenization. Amounts of proteins were determined by MicroBCA™ assay. The recovered serum protein samples were subject to 8% (w/v) SDS-PAGE and followed by Western blot analysis.

VI.2.5. Cell culture

MC3T3-E1 pre-osteoblasts were seeded on both matrices at densities of 5×10^3 cells/cm^2 and 2.5×10^4 cells/cm^2 for a proliferation test and at a density of 2.5×10^4 cells/cm^2 for differentiation ones. About 12 h after cell seeding, the cells were cultured in α-MEM supplemented with 10% (v/v) FBS, 50 μg/ml ascorbic acid, and 5 mM β-glycerophosphate.

VI.2.6. Cell proliferation

After 1, 3, 5, and 7 days of culture, 100 μl of Mg^{2+} Lysis/Wash buffer was added and then 10 μl of PicoGreen® reagent was added to each sample according to the manufacturer's instructions. After the incubation, the fluorescence was measured using FLUOstar OPTIMA (BMG Labtech Gmbh, Ortenberg, Germany).

VI.2.7. Determination of calcium contents

The matrices on which the cells were cultured for 7 days were examined for calcium deposition by use of a calcium assay kit (Sigma). The cultures were placed in 0.5 N HCl and incubated for 24 h. Then calcium reagent working solution was added to each sample according to manufacturer's instruction. The absorbance was measured at 575 nm.

VI.2.8. Alkaline phosphatase (ALP) assay

ALP activity was measured using spectrophotometry with p-nitrophenyl phosphate (p-NPP) as a substrate. After either 3 or 7 days of culture, cells were collected and homogenized in 0.5 ml of distilled water using a sonicator and then centrifuged. Cell homogenate aliquots were incubated with 15 mM p-NPP in 0.1 M glycine-NaOH (pH 10.3) at 37℃ for 30 min. The reaction was stopped with 0.25 M NaOH, and absorbance was measured at 410 nm.

VI.2.9. Luciferase assay

Either 2 μg of the Runx2 activity reporter vector (6XOSE2-Luc) or 2 μg of the

empty vector pcDNA3.1 was transfected into MC3T3-E1 cells. The cells were maintained in ascorbic acid-free α-MEM, and then they were trypsinized and collected in a tube. Transient transfections were performed using the microporator MP-100 (Digital Bio Technology, Suwon, Korea). Then, the cells were seeded and cultured as described above. One day after culturing in the differentiation medium, luciferase activity was measured using the Dual-Glo™ Luciferase Assay System. Renilla luciferase activity was used for normalization.

VI.2.10. Western blot assay

Cell lysates were prepared using a buffer of 10 mM Tris-Cl, pH 7.5, 150 mM NaCl, 1 mM EDTA, pH 8.0, 1% (v/v) Triton X-100, 0.5% (w/v) sodium deoxycholate, 0.1% (w/v) SDS, 1 mM PMSF, and a complete protease inhibitor cocktail tablet. Samples containing equal amounts of protein were subjected to SDS-PAGE and subsequently transferred onto a polyvinylidene difluoride membrane. The membrane was blocked with 3% (w/v) bovine serum albumin and incubated with each antibody followed by incubation with HRP-conjugated secondary antibody. Luminescence was detected with an LAS-1000 (Fuji, Tokyo, Japan).

VI.2.11. Statistical analysis

All of the results are expressed as the means ± S.D. (n=4). All experiments were repeated three times. Significant differences were analyzed using ANOVA. P values < 0.05 were considered to indicate a statistically significant difference.

VI.3. Results

VI.3.1. Matrix morphology

Both matrices were prepared using the same concentrations (1 or 3 mg/ml) of collagen and fibrinogen. The morphology of the collagen and fibrin matrix was examined using SEM (Fig. III-1). The fiber thickness of collagen and fibrin was 74.0 ± 22.9 nm (number of counted fibers, n = 409) and 67.6 ± 20.2 nm (n = 416), respectively. In repeated experiments, significant difference in the thickness of collagen and fibrin were not observed.

VI.3.2. Protein adsorption

Protein adsorption to the matrices was also assessed. As shown in Fig. III-2, the level of total serum protein adsorption to fibrin was similar to that of collagen. Considering their similar fiber thicknesses, the total surface area of collagen and fibrin should be similar. Thus, the observed similarities in protein absorption reflected their similar total surface areas. Serum fibronectin and vitronectin bound to both matrices were measured using the band intensities in Western blot analyses. Statistical analysis from three independent experiments showed that the adsorption of serum vitronectin to fibrin and collagen was not significantly different. However, fibrin adsorbed approximately 6.7 times more serum fibronectin than collagen. Fibronectin belongs to a family of high molecular weight glycoproteins that are present on cell surfaces, in extracellular fluids, and in connective tissues.

VI.3.3. Osteoblast proliferation

We determined the cell proliferation on both matrices at low (5×10^3 cells/cm^2) and high densities (2.5×10^4 cells/cm^2) of cell seeding. At both cell densities, fibrin supported cell proliferation at greater levels than collagen at all of the time points (Fig. III-3, ANOVA, $P < 0.05$). The supportive effect of fibrin was more evident at a low cell density than a high cell density. After 7 days of culture, the cell proliferation of fibrin was 7.3 times greater than that of collagen at a low cell density and approximately 1.2 times greater at a high density.

VI.3.4. Osteoblast differentiation

To examine the effects of collagen and fibrin on osteoblast differentiation, we evaluated the expression and transcriptional activity of Runx2, ALP activity, and calcium deposition on the matrices. Both the collagen and fibrin matrices significantly promoted the differentiation and maturation of osteoblasts compared to that of the tissue culture dish (TCD). After 2 days of culture, the cells on fibrin expressed Runx2 transcripts at a greater level than those on collagen, and the level of Runx2 protein was approximately 2.5 times greater in cells grown on fibrin than those on collagen (Fig. III-4A). The transcriptional activity of Runx2 was also higher on fibrin (Fig. III-4A), consistent with the expression levels of Runx2. After 7 days of culture, the cells grown on fibrin showed approximately 2.7 times greater ALP activity than those on collagen (Fig. III-4B). Calcium deposition on both collagen and fibrin was significantly increased compared to those on TCD. However, calcium deposition on fibrin showed similar levels compared to those on collagen (Fig. III-4C).

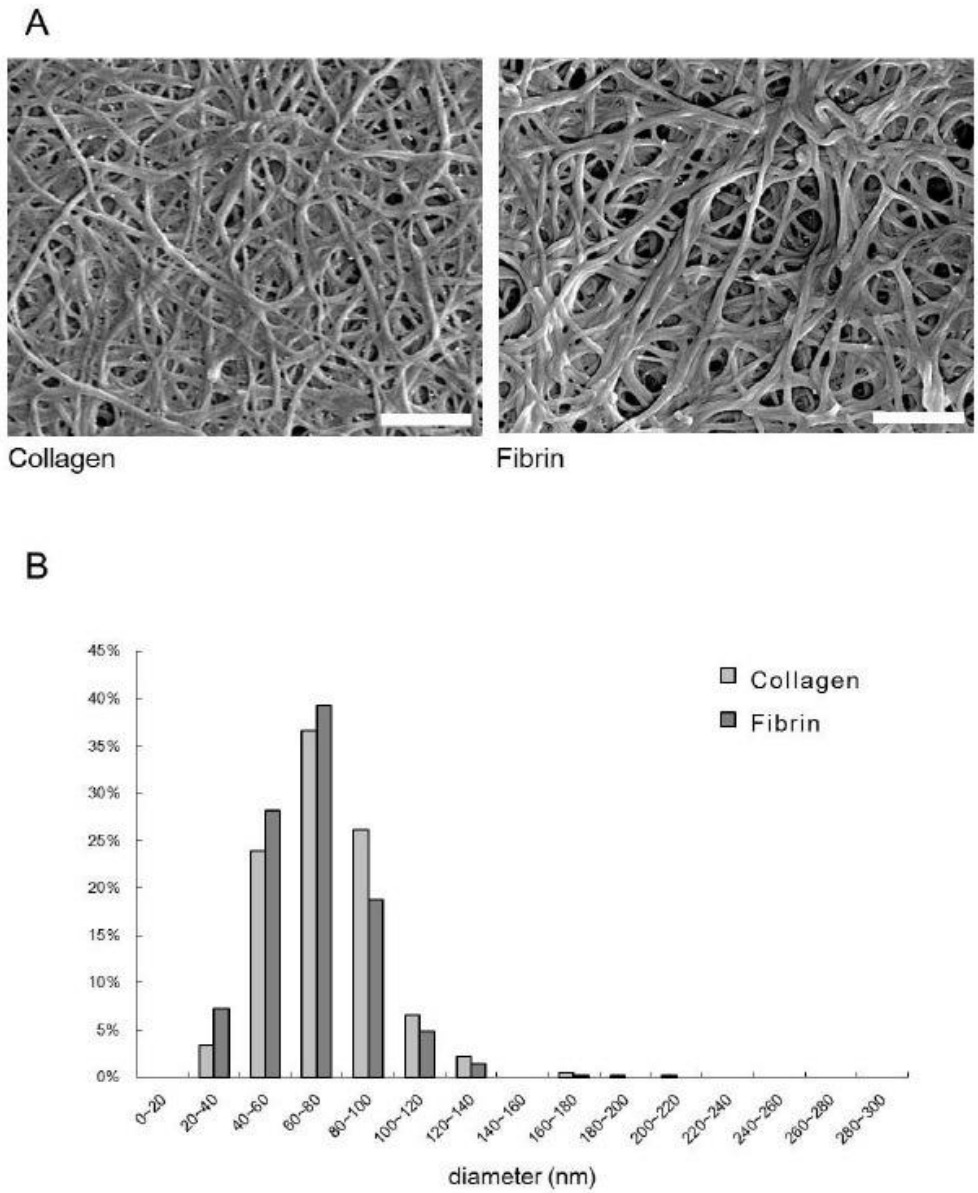

Figure III-1. Scanning electron microscopic images of the collagen and fibrin matrices (A). The fiber thickness (B) was measured using scanning electron microscopic images at a magnification of 20,000×. Bar length: 1 μm.

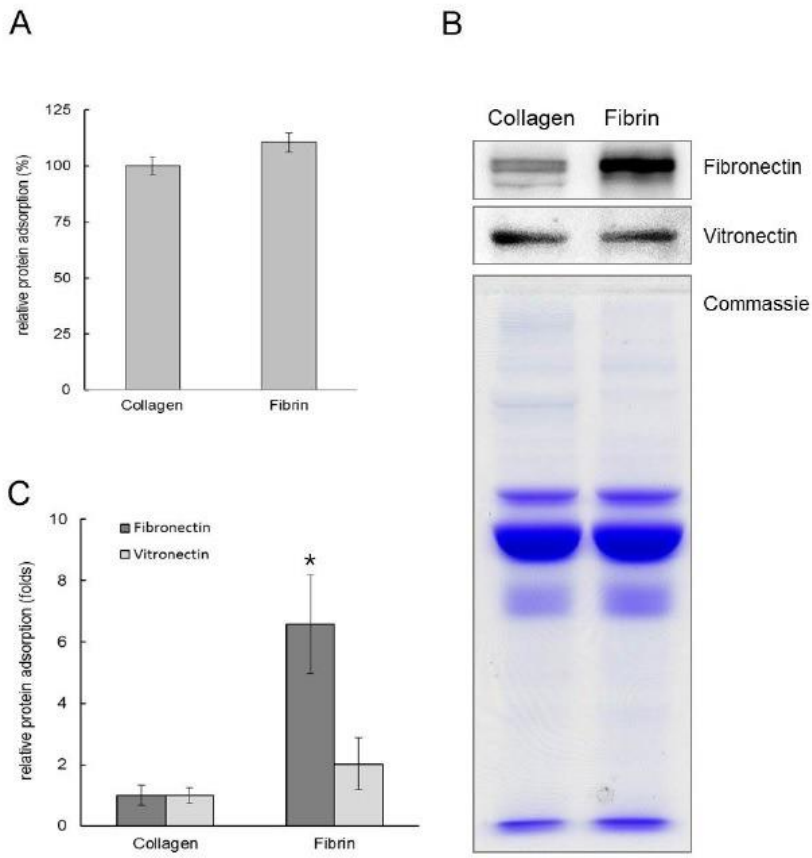

Figure III-2. Profiles on the binding of serum proteins to collagen and fibrin. (A) The amount of total serum protein binding to collagen and fibrin matrices was determined by MicroBCA™ assay. (B) Western blots for fibronectin and vitronectin adsorbed to collagen and fibrin matrices from serum. Recovered serum proteins adsorbed to the matrices were separated via SDS–PAGE. (C) Serum fibronectin and vitronectin bound to fibrin was measured using the band intensities in Western blot analyses. *Serum fibronectin adsorbed to fibrin was significantly different from that of collagen (ANOVA, $P < 0.05$).

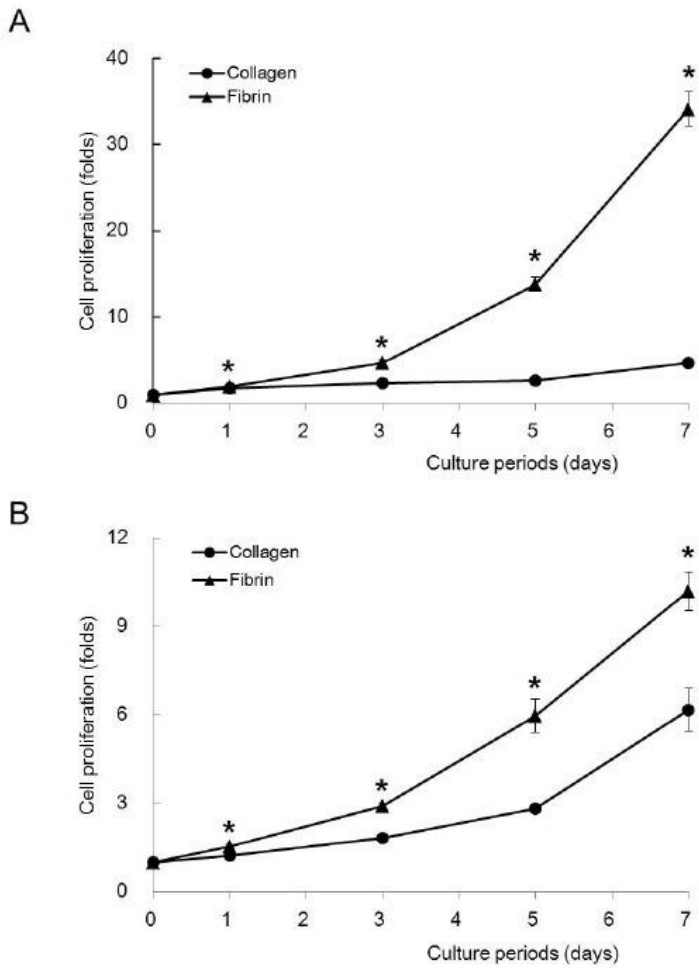

Figure III-3. Osteoblast proliferation. MC3T3-E1 cells were seeded on collagen and fibrin at densities of 5×10^3 cells per cm^2 (A) and 2.5×10^4 cells per cm^2 (B). *Significantly different from collagen (ANOVA, $P < 0.05$).

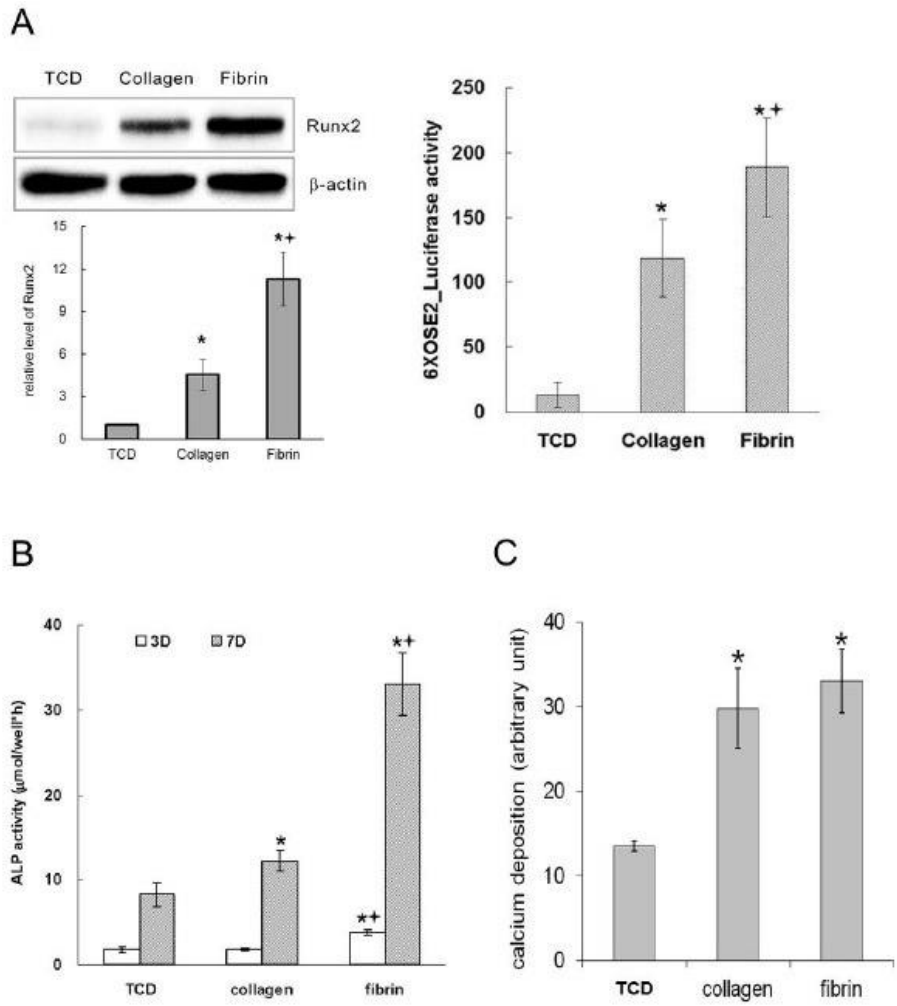

Figure III-4. Osteoblast differentiation. MC3T3-E1 cells were seeded at a density of 2.5×10^4 cells per cm^2 and cultured for 2 days (A) or 7 days (B, C). (A) Expression (left) and transcriptional activity (right) of Runx2. (B) Alkaline phosphatase activity. (C) Calcium deposition on the matrices. *Significantly different from TCD. †Significantly different from collagen (ANOVA, $P < 0.05$).

VI.4. Discussion

Fibronectin belongs to a family of high molecular weight glycoproteins that are present on cell surfaces, in extracellular fluids, and in connective tissues. Fibronectin interacts with other extracellular matrix proteins and cellular ligands, such as collagen, fibrin, and integrins. Fibronectin regulates the adhesion, proliferation, and differentiation of osteoblasts [Wilson et al. 2005; Marie 2013]. The protein adsorption results obtained in the present study indicate that the fibronectin binding capacity of fibrin was significantly greater than that of collagen, which contributed to the favorable cell response for regeneration. (Fig. III-2)

The high fibronectin binding capacity of fibrin may provide a favorable environment for cell proliferation. (Fig. III-3) In addition, thrombin, a component of fibrin, may induce osteoblast differentiation, as previously reported [Song et al. 2005a]. Cells used in tissue engineering are limited in number and are difficult to propagate. With respect to tissue regeneration, the capacity of fibrin to support cell proliferation provides a significant advantage over collagen.

Repeated experiments confirmed that the enhancement of osteoblast differentiation by fibrin was significantly greater than that of collagen. In addition, our results on osteoblast differentiation were also consistent. (Fig. III-4) Given that Runx2 is a transcription factor that switches on the expression of osteoblast phenotypes [Komori et al. 1997; Xiao et al. 2002; Phillips et al. 2006], these results suggest that Runx2 is a suitable molecular marker for the evaluation of biomaterials that support bone regeneration.

VI.5. Conclusion

The results obtained in the present study consistently indicate that fibrin is a better biopolymer than collagen in terms of protein adsorption, osteoblast proliferation, and osteoblast differentiation. These findings suggest that fibrin is superior to collagen as a component of composite scaffolds for enhancing the biological performance of synthetic polymer scaffolds or as a sole material in various bone regenerative applications. Furthermore, fibrin can be prepared from autologous blood products, which highlights its importance in clinical applications [Bensaïd et al. 2003; Flanagan et al. 2007]. Because scaffolds for bone tissue regeneration require adequate mechanical strength and timely degradation properties, further studies on the modification of these properties due to fibrin must be performed.

VII. PART IV.

The effects of the modulation of the fibronectin-binding capacity of fibrin by thrombin on osteoblast differentiation

This part was already published in Biomaterials 33, no. 16 (Jun 2012): 4089-99. doi: 10.1016/j.biomaterials.2012.02.028

VII.1. Introduction

Fibrin is a fibrillar biopolymer that is naturally formed during blood clotting. Hemostasis is a primary role of fibrin, but fibrin also functions as a provisional matrix during wound healing [Laurens et al. 2006; Mosesson 2005; Wolberg 2007]. Fibrin possess the properties suitable for its use in regenerative medicine. For instance, fibrin is capable of conveying matrix proteins such as fibronectin (FN) and growth factors [Makogonenko et al. 2002; Erickson and Fowler 1983; Rybarczyk et al. 2003]. Given these features, fibrin has been widely studied in biomedical research for its ability to repair hard and soft tissues [Ahmed et al. 2008; Breen et al. 2009; Nair et al. 2009; Davis et al. 2011; Proulx et al. 2011; Flanagan et al. 2007; Falanga et al. 2007]. Fibrin is typically prepared by mixing fibrinogen and thrombin solutions. A serine protease thrombin exposes cryptic sites that function cooperatively in fibrin polymerization, and soluble fibrinogen is transformed into insoluble fibrin. Commercially available fibrins have been shown to be effective in promoting soft tissue healing [Amrani et al. 2001]. Fibrin sealants combined with bones or bone substitutes promoted new bone formation in several studies, of which outcomes appeared to be largely dependent on the compositions of fibrin and its related structures [Lucht et al. 1986; Karp et al. 2004; Brittberg et al. 1997].

The structure of the fibrin matrix affects its biological functions [Laurens et al. 2006; Mosesson 2005; Wolberg 2007], of which mechanism still remains unclear. A number of variables can influence the structure of fibrin, including the local pH, ionic strength, and the concentrations of calcium and thrombin. The concentration of thrombin present at the time of gelation has important influences on fibrin clot structure. The low thrombin concentrations produce fibrin clots that are turbid and composed of thick, loosely-woven fibrin strands. Higher concentrations of thrombin

produce fibrin clots that are composed of relatively thinner, more tightly packed fibrin strands [Wolberg 2007; Collet et al. 2000]. In addition to the role of thrombin in formation and modulation of the fibrin structure that can affect its biological function, thrombin can also affect cells directly. The cellular effects of thrombin are seen via protease-activated receptors (PARs). Different PARs are known to be expressed by several cell types, such as osteoblasts, monocytes, platelets, endothelial cells, vascular smooth muscle cells, and fibroblasts. PAR signaling is known to mediate a variety of processes such as hemostasis, thrombosis, inflammation, cancer, and embryonic development. During the early stages of bone repair, thrombin is believed to contribute to the PAR1-mediated proliferation of osteoblasts [Song et al. 2005a; Song et al. 2005b]. However, there is disagreement regarding its effect on osteoblasts differentiation. Thrombin has been reported to stimulate proliferation but to inhibit alkaline phosphatase (ALP) through activation of PAR1, for which experiments conventional tissue culture dishes were used as a substrate in cultures [Song et al. 2005a; Song et al. 2005b]. On the other hand, thrombin- or fibrin-coated ceramics has been shown to enhance the expressions of ALP [Bluteau et al. 2006; Breen et al. 2009]. Based on these previous reports, we hypothesized that osteoblast differentiation is not caused by a direct cell response to thrombin via PAR1 but by a response caused by thrombin-induced alterations in fibrin structures.

Runx2 has been widely accepted as an early osteogenic transcription factor that can switch on to osteoblast differentiation [Komori et al. 1997; Prince et al. 2000; Lee et al. 1999; Xiao et al. 2002; Phillips et al. 2006]. Runx2-knockout mice display complete bone loss due to arrested osteoblast maturation, and Runx2 plays a critical role in osteoblast marker gene expression including ALP, osteocalcin, and bone sialoprotein [Komori et al. 1997; Prince et al. 2000]. Most osteogenic factors, such

as BMPs, can induce the expression of Runx2 and various extracellular signals can affect the transcriptional activity of Runx2 [Lee et al. 1999; Xiao et al. 2002]. Therefore, Runx2 is mostly used in gene therapy for bone regeneration [Phillips et al. 2006]. Thus, Runx2 is one of key regulatory factors that may be suitable for evaluating biomaterials that support bone regeneration and for studying the mechanisms of this process.

In this study, the fibrin matrices were prepared by using concentrations of thrombin, we confirmed effects of thrombin on fibrin-promoted osteoblast differentiation by checking extents of calcium deposition, alkaline phosphatase (ALP) activity, and level of Runx2. We studied its mode of action on osteoblast differentiation using PAR1-activating, integrin-blocking, and fibronectin-binding blocking peptides by examining levels of Runx2 and phosphorylated integrins. Furthermore, it was assessed the effects of thrombin on the fibronectin-binding to fibrin and the consequent alteration in levels of Runx2.

VII.2. Materials and methods

VII.2.1. Materials and reagents

Bovine fibrinogen, thrombin, aminocaproic acid, l-ascorbic acid and glycerol 2-phosphate were purchased from Sigma (St. Louis, MO). Fetal bovine serum (FBS), HEPES buffer solution and penicillin–streptomycin solution were from GibcoBRL (Carlsbad, CA). Ascorbic acid-free α-MEM was from WelGene (Daegu, Korea). Alexafluor 546-conjugated phalloidin was from Molecular probes (Eugene, OR). West-Zol™ was from Intron Biotechnology (Seoul, Korea). Protease inhibitor cocktail tablets (Complete) were purchased from Roche (Basel, Switzerland). PAR1 agonist peptide (SFLLR–NH2), RGDS, and RGES were synthesized by Peptron (Daejeon, Korea). A fibronectin-binding blocking peptide HHLGGAKQAGDV was purchased from Sigma. Anti-Runx2, anti-Integrin β_1, anti-Integrin β_3, anti-actin, and HRP-conjugated IgG antibodies were purchased from Santa Cruz Biotechnology (Santa Cruz, CA). Anti-FN and anti-vitronectin (VTN) antibodies were purchased from Chemicon (Temecula, CA). Anti-phospho-Integrin β_1 and anti-phospho-Integrin β_3 antibodies were from Sigma.

VII.2.2. Preparation of matrices

Fibrin matrices were prepared by mixing fibrinogen and thrombin solutions, which contained 5 mg/ml of fibrinogen in PBS (pH 7.4), 0.25–4 U/ml of thrombin, 50 μg/ml of aminocaproic acid and 1 mm of $CaCl_2$. Total 6 ml of the mixed solution was poured into the 60-mm culture dishes and solidified in an incubator at 37 °C.

VII.2.3. Cell culture

MC3T3-E1 clone 4 (MC4) pre-osteoblasts were seeded on fibrin matrices at a density of 5.25×10^5 cells per 60 mm dish. Approximately 12 h after cell seeding, the cells were cultured in α-MEM supplemented with 10% FBS, 50 μg/ml of ascorbic acid and 5 mm of β-glycerophosphate. For the experiments to examine the effect of RGDS, the cells in a tube were pre-treated with the peptide for 10 min, seeded on fibrin matrices, and cultured in the presence of the peptide for a day. To evaluate the cell response to HHLGGAKQAGDV peptide, cells were seeded on the fibrin matrices and cultured in the presence of the peptide for a day.

VII.2.4. Scanning electron microscopy (SEM)

The matrices or the cell-seeded matrices after a day of culture were rinsed in PBS and fixed using 2.5% glutaraldehyde in a 0.1 M cacodylate buffer (pH 7.4). After freeze-drying, the specimen was dehydrated by dipping it in increasing concentrations of ethanol and then by critical point drying. After drying, the specimens were sputter-coated with gold-paladium and observed under an SEM at 12 kV (FE-SEM Hitachi S-4700, Japan).

VII.2.5. Determination of calcium contents

The matrices on which the cells were cultured for 7 days were examined for calcium deposition by use of a calcium assay kit (Sigma). The cultures were placed in 0.5 N HCl solution and incubated for 24 h. Then calcium reagent working solution was added to each sample according to manufacturer's instruction. The absorbance

was measured at 575 nm.

VII.2.6. ALP activity

ALP activity was measured using spectrophotometry with p-nitrophenyl phosphate (p-NPP). After 7 days of culture, cells were collected and homogenized in 0.5 ml of distilled water using a sonicator and then centrifuged. Cell homogenate aliquots were incubated with 15 mM p-NPP in 0.1 M glycine-NaOH (pH 10.3) at 37 °C for 30 min. The reaction was stopped with 0.25 M NaOH and absorbance was measured at 410 nm.

VII.2.7. Western blot analysis

Cell lysates were prepared using a buffer of 10 mm Tris–Cl (pH7.5), 150 mM NaCl, 1 mM EDTA (pH 8.0), 1% Triton X-100, 1 mM phenylmethylsulfonyl fluoride, 50 mM NaF, 0.2 mM Na_3VO_4, phosphatase inhibitor, and complete protease inhibitor cocktail tablet. The samples were subjected to 8–10% SDS-PAGE and then they were transferred onto a polyvinylidene difluoride (PVDF) membrane. The membrane was blocked by 3% bovine serum albumin and incubated with each primary antibody. This procedure was followed by incubation with an HRP-conjugated secondary antibody. Luminescence was detected by Fujifilm LAS-1000 (Fuji, Tokyo, Japan). β-actin was used as a loading control.

VII.2.8. Binding of serum FN and VTN to fibrin

Binding of serum FN and VTN to fibrin was examined by Western blot analyses as described in a previous report with some modifications [Woo et al. 2003]. In brief,

the fibrin matrices were incubated in the presence of 10% mouse serum at 37 °C. After the 4 h of incubation, serum solution was removed from the matrices. The fibrin matrices were washed with PBS under gentle agitation for 20 min. The washing solution was then discarded and fresh PBS was replaced to wash again. A total of three washings were conducted to remove free and loosely adsorbed proteins (there was a negligible amount of proteins in the third washing solution). The remaining proteins (adsorbed) to the fibrin were recovered by incubation in 1% SDS solution after homogenization. The recovered serum protein samples were subject to 8% SDS-PAGE and followed by western blot analysis as described above.

VII.2.9. Statistical analysis

Data from the repeated experiments are presented as the mean and standard deviation. Statistical analyses were performed using analysis of variance (ANOVA). Differences were considered significant if the p value was <0.05.

VII.3. Results

VII.3.1. Morphology

The morphology of the fibrin matrices formed by different concentrations of thrombin was examined using SEM (Fig. IV-1). The fiber thickness was measured from SEM images. The thickness of fiber was 213.4 ± 80.5 nm at 0.25 U/ml of thrombin (number of counted fibers, n = 202), 199.0 ± 69.9 nm at 1 U/ml (n = 218) and 180.6 ± 52.2 nm at 4 U/ml (n = 202). The distribution of fiber thickness seemed more uniform in the fibrin that was prepared by higher concentrations of thrombin. These features indicate that thrombin significantly decreased the thickness of fibrin fiber.

We also observed the morphology of the cells grown on these matrices using SEM, a day after cell seeding. The MC4 pre-osteoblasts seeded on a tissue culture dish (TCD) were flattened and showed few long slender cell processes (Fig. IV-2A). In contrast, cells on a fibrin matrix (5 mg/ml of fibrinogen and 1 U/ml of thrombin) formed abundant long slender cell processes, which were intermingled with the fibrin fibers (Fig. IV-2A) Distribution of actin cytoskeleton was matched well with SEM images (Fig. IV-2B), appearing slender cells were connected to the neighboring cells by the long cell processes. These morphology and cytoskeletal distribution of the cells on fibrin matrices looked different from those to TCD. However, the morphology of the cells on a fibrin matrix was hardly distinguished from that on the other fibrin matrices with different concentrations of thrombin (data not shown).

VII.3.2. Osteoblast differentiation

To examine the effects of the fibrins prepared by various concentrations of thrombin on osteoblast differentiation, we evaluated calcium deposition on the matrices, ALP activity, and Runx2 expression. After 7 days of culture, the cells grown on fibrin containing 0.25 U/ml thrombin showed 3.1-fold and 3.8-fold greater calcium deposition and ALP activity, respectively, than those on TCD (Fig. IV-3A and B). The level of Runx2 that was checked after 1-day culture showed 5.4-fold higher in the cells grown on fibrin 0.25 U/ml thrombin with than those on TCD (Fig. IV-3C). It was also obvious that thrombin embedded in fibrin matrices enhanced the calcium deposition, ALP activity, and level of Runx2 in a dose-dependent manner. Repeated experiments confirmed that the thrombin enhancement of osteoblast differentiation in the cells cultured on fibrin is statistically significant. Compared with the fibrin containing 0.25 U/ml thrombin, the fibrin matrix containing 4 U/ml of thrombin-enhanced 2.1-fold greater Runx2 expression, while the fibrin with 4 U/ml thrombin supported 1.4-fold and 1.2-fold higher calcium deposition and ALP activity, respectively. Given that Runx2 is a transcription factor that switches on the expressions of osteoblast phenotype, these results suggest that Runx2 would be a molecular marker suitable for evaluating the effect of thrombin on fibrin-accelerated osteoblast differentiation and for investigating the mechanisms.

VII.3.3. Effect of a PAR1 agonist on Runx2

We examined the effect of a PAR1 activating peptide on Runx2 expression to confirm our hypothesis that osteoblast differentiation is not caused by a direct cell response to thrombin via PAR1 but by a response caused by thrombin-induced alterations in fibrin structures. Neither in the cells grown on fibrin nor in the cells grown on TCD, the PAR1 activating peptide produced any significant increase of

Runx2 expression (Fig. IV-4A and B). The levels of Runx2 in cells grown on plastic also were not altered by thrombin treatment (Fig. IV-4C). These results suggest that thrombin can modulate fibrin-induced Runx2 expression in a PAR1-independent manner and that the biological properties of fibrin can be altered by thrombin.

VII.3.4. Effect of thrombin on fibrin-induced phosphorylation of integrins

To depict how thrombin as a component of fibrin can increase Runx2 expression, we checked the expression of integrins and their levels of phosphorylation. Cells can bind to fibrin through integrin receptors directly or indirectly via fibronectin-mediation and trigger signal transduction cascades [Laurens et al. 2006; Mosesson 2005; Savage et al. 1995; Plow et al. 1985]. Integrins have been reported to play an essential role in the regulation of osteoblast differentiation [Xiao et al. 2002; Moursi et al. 1997; Jikko et al. 1999]. In our study, integrins β_1 and β_3 were detected at higher levels in the cells grown on fibrin than in those grown on TCD, and these levels were sustained but not altered by thrombin (Fig. IV-5). Interestingly, it was obvious that thrombin dose-dependently increased the phosphorylation of integrins β_1 and β_3. Repeated experiments verified that the thrombin enhancement of integrin phosphrylations in the cells cultured on fibrin is statistically significant. To confirm the relation between the phosphorylation of integrins and Runx2 expression, we treated the cells grown on fibrin with RGDS peptide, which inhibits the binding of matrix ligands such as fibronectin to integrin receptors. The blocking peptide significantly inhibited fibrin-induced Runx2 expression in a dose-dependent manner, whereas the RGES non-functional control peptide did not result in any significant changes (Fig. IV-6A). In Fig. IV-6B, it was consistently demonstrated that the RGDS

blocking peptide attenuated the thrombin-promoted phosphorylation of integrins and Runx2 expression. It was also noticeable that the more potent inhibitions occurred when the higher dose of thrombin was engaged. These results indicate that thrombin dose-dependently increased integrin phosphorylation in osteoblasts grown on fibrin, which contributed to Runx2 expression.

VII.3.5. Effect of thrombin on the fibronectin-binding capacity of fibrin

It was finally assessed whether thrombin increases the fibronectin-binding capacity of fibrin and whether increased fibronectin-binding to fibrin results in thrombin-enhanced Runx2 expression. Western blot analyses showed that thrombin greatly increased the amount of serum fibronectin that adsorbed to the fibrin matrices in a dose-dependent manner (Fig. IV-7). Compared with the fibrin containing 0.25 U/ml thrombin, the fibrin matrix containing 4 U/ml of thrombin adsorbed 6.2-fold and 3.1-fold greater amounts of serum fibronectin and serum vitronectin, respectively, while total serum protein adsorbed only 1.4-fold more to the fibrin with 4 U/ml thrombin. Ponceau S staining following SDS-PAGE confirmed that greater amounts of serum proteins adsorbed to the fibrin with high concentration of thrombin. The profile of adsorbed serum proteins to 4 U/ml thrombin-containing fibrin appeared different from that to 0.25 U/ml thrombin-containing fibrin. These findings consistently indicate that thrombin can modulate the binding capacity of fibronectin to fibrin and suggest that fibrin with 4 U/ml thrombin may have certain features to enhance the binding of specific proteins such as fibronectin.

To study the effect of fibronectin-binding to fibrin on Runx2 expression, we used a fibronectin-binding blocking peptide HHLGGAKQAGDV [Makogonenko et al. 2002; Erickson and Fowler 1983; Plow et al. 1984]. First, it was confirmed whether

the HHLGGAKQAGDV peptide inhibits fibronectin-binding to fibrin. The inhibitory effect of the peptide was evident for the fibrin prepared with 4 U/ml thrombin, although the peptide did not show significant difference in the fibrin with 0.25 U/ml thrombin. Fibronectin-binding to fibrin was dose-dependently decreased by the HHLGGAKQAGDV peptide (Fig. IV-8A). Also the HHLGGAKQAGDV peptide inhibited the fibrin-induced Runx2 expression in a dose-dependent manner (Fig. IV-8B). These inhibitory effects of the peptide were significant. As shown in Fig. IV-8C, it was consistently demonstrated that the HHLGGAKQAGDV blocking peptide attenuated the thrombin-promoted phosphorylation of integrins and Runx2 expression. The more potent inhibitions occurred when the higher dose of thrombin was engaged, just like the RGDS peptide did. These results indicate that thrombin dose-dependently increased the fibronectin-binding to fibrin, which contributed to integrin phosphorylation and Runx2 expression in osteoblasts grown on fibrin.

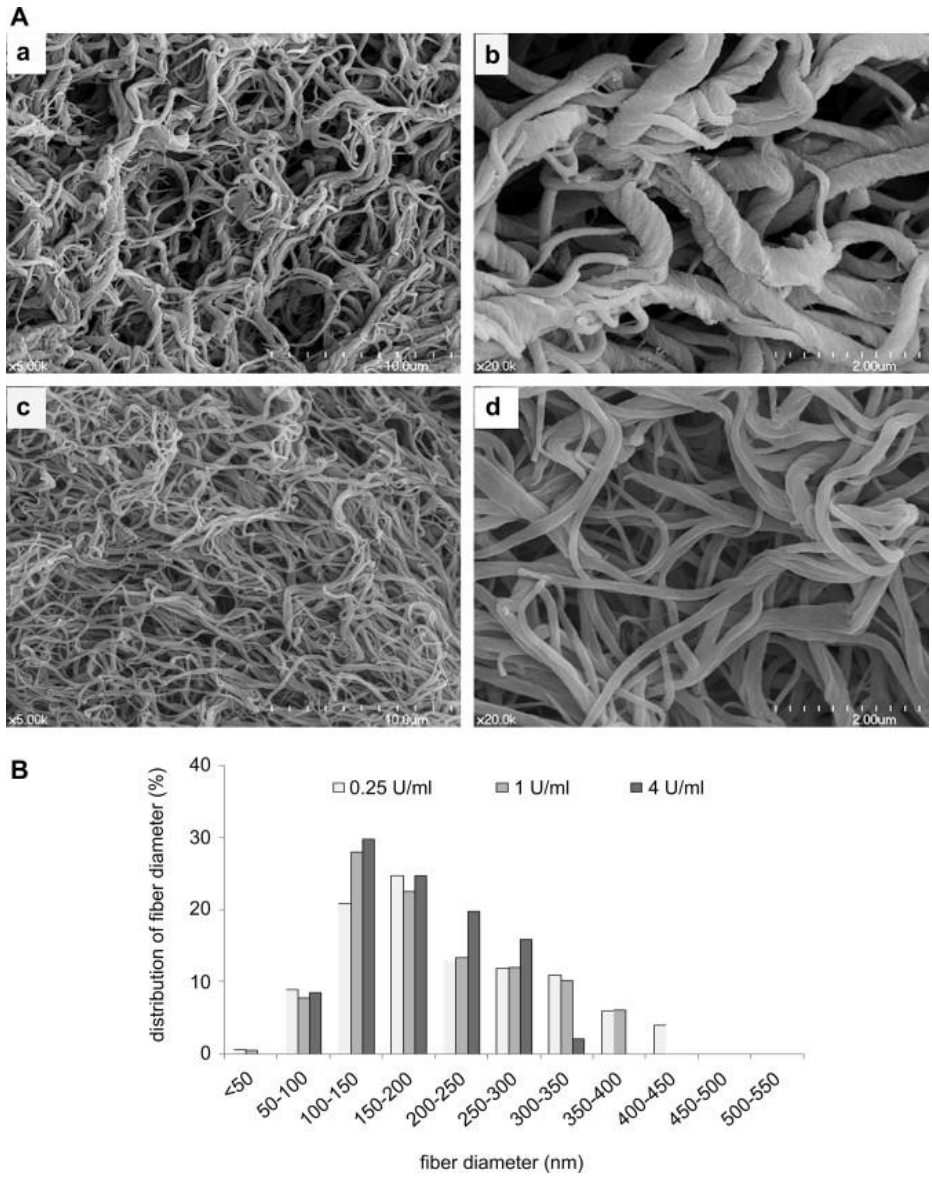

Figure IV-1. (A) Scanning electron microscopic views of fibrin matrices with different concentrations of thrombin (a and b - 0.25 U/ml; c and d - 4 U/ml). (B) Fiber thickness was measured on scanning electron microscopic images with a magnification of 20,000×. Thrombin significantly decreased the fiber thickness (ANOVA, $p < 0.05$).

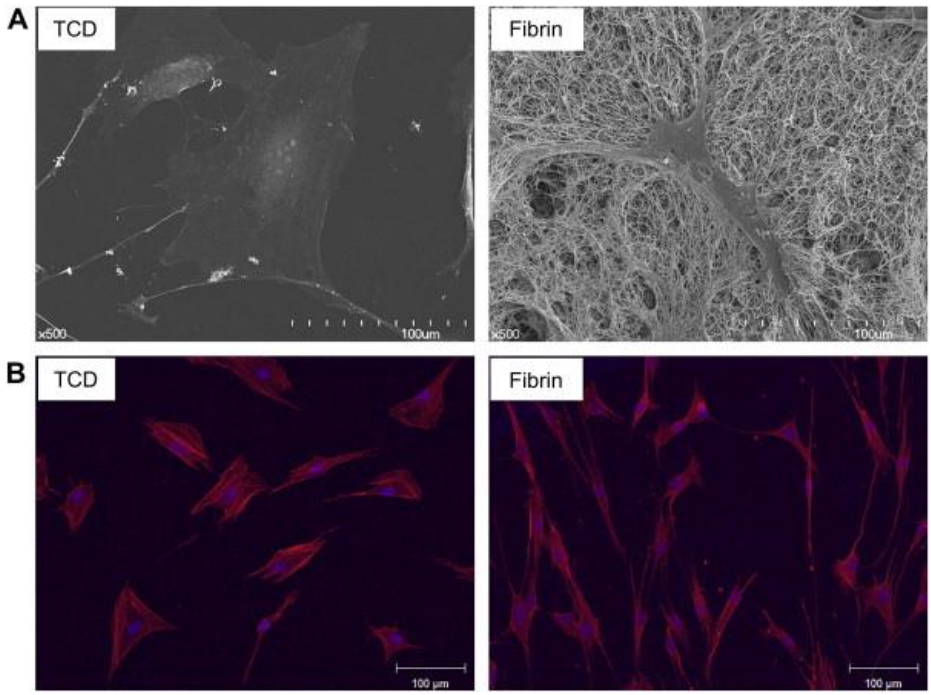

Figure IV-2. (A) Scanning electron microscopic views of MC4 cells grown on TCD and on a fibrin matrix. (B) Actin-staining images of cells grown on TCD and on a fibrin matrix with a fluorescence-conjugated phalloidin. Magnification was 100×.

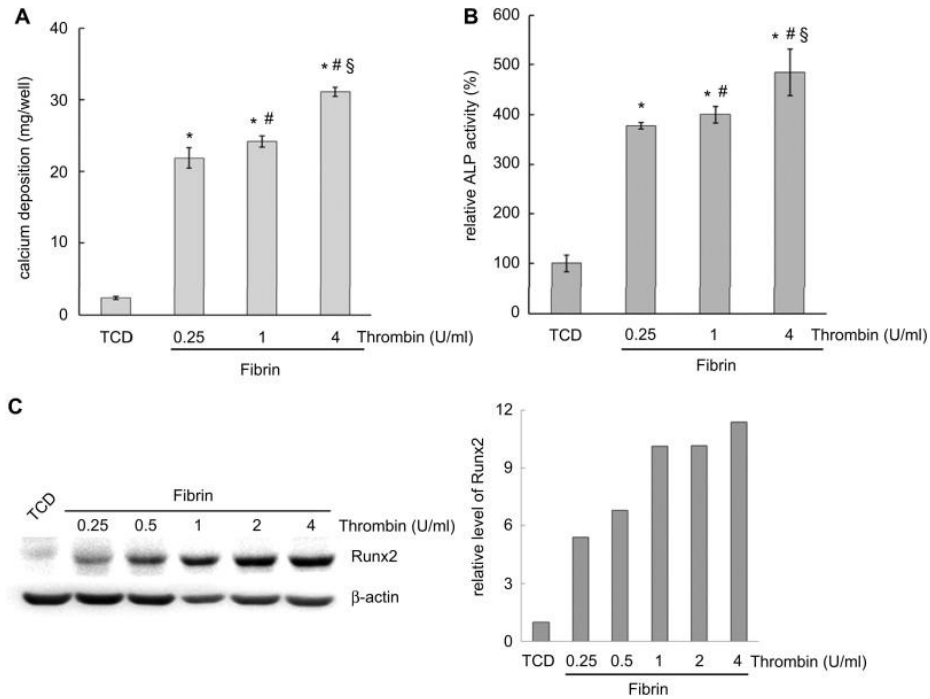

Figure IV-3. Effects of thrombin on the fibrin-induced osteoblasts differentiation. Quantifications of calcium contents in the matrices (A) and alkaline phosphatase activities (B). The MC4 cells were cultured for seven days. Data are presented as averages ± SDs (n = 4). * Significantly different from TCD, # significantly different from 0.25 U/ml of thrombin, and § significantly different from 1 U/ml of thrombin (ANOVA, $p < 0.05$). (C) Western blot analysis for Runx2. MC4 cells were cultured for a day on the matrices. The intensities of Runx2 protein were measured and normalized by β-actin. Similar results were obtained from three independent experiments. Representative result is shown. Thrombin significantly increased the level of Runx2 (ANOVA, $p < 0.05$).

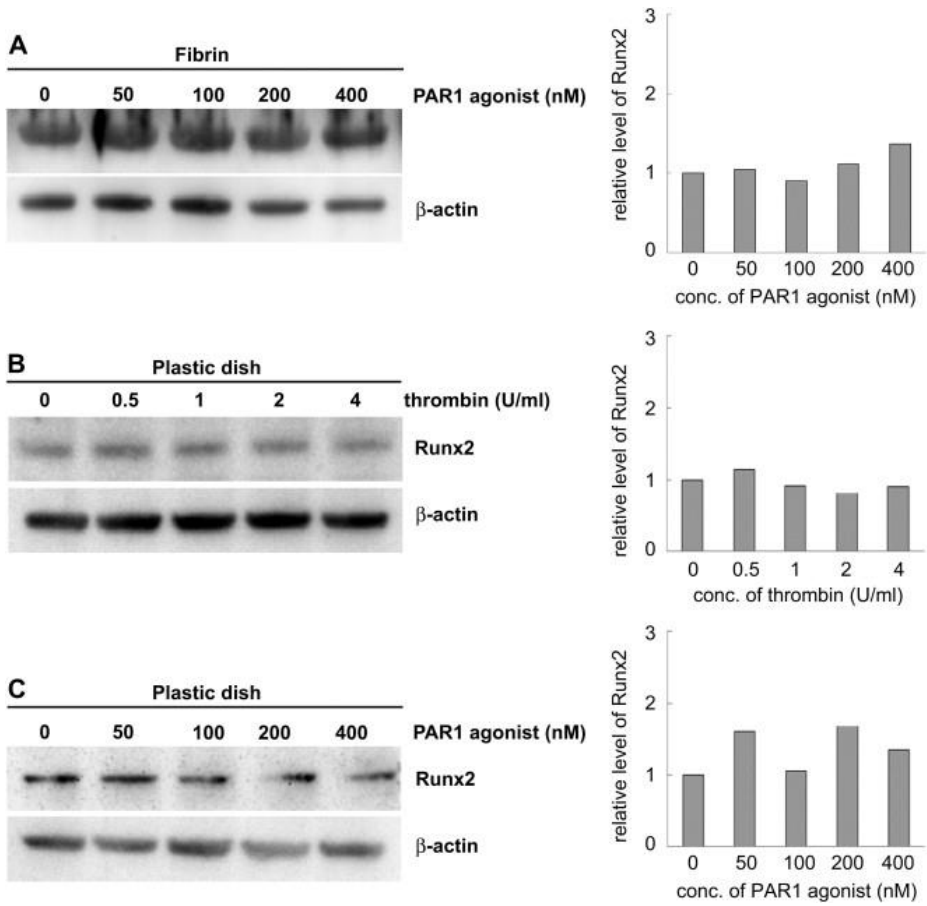

Figure IV-4. Effect of a protease-activated receptor 1 (PAR1) on Runx2. Western blot analyses were performed for detection of Runx2. The MC4 cells were cultured for a day on a fibrin matrix (prepared by mixing 5 mg/ml of fibrinogen and 1 U/ml of thrombin) in the culture medium containing a PAR1 agonist (A), cultured on TCD in the culture medium containing thrombin (B), and cultured on TCD in the culture medium containing a PAR1 agonist (C). The intensities of Runx2 protein were measured and normalized by β-actin. Similar results were obtained from three independent experiments. Representative results are shown.

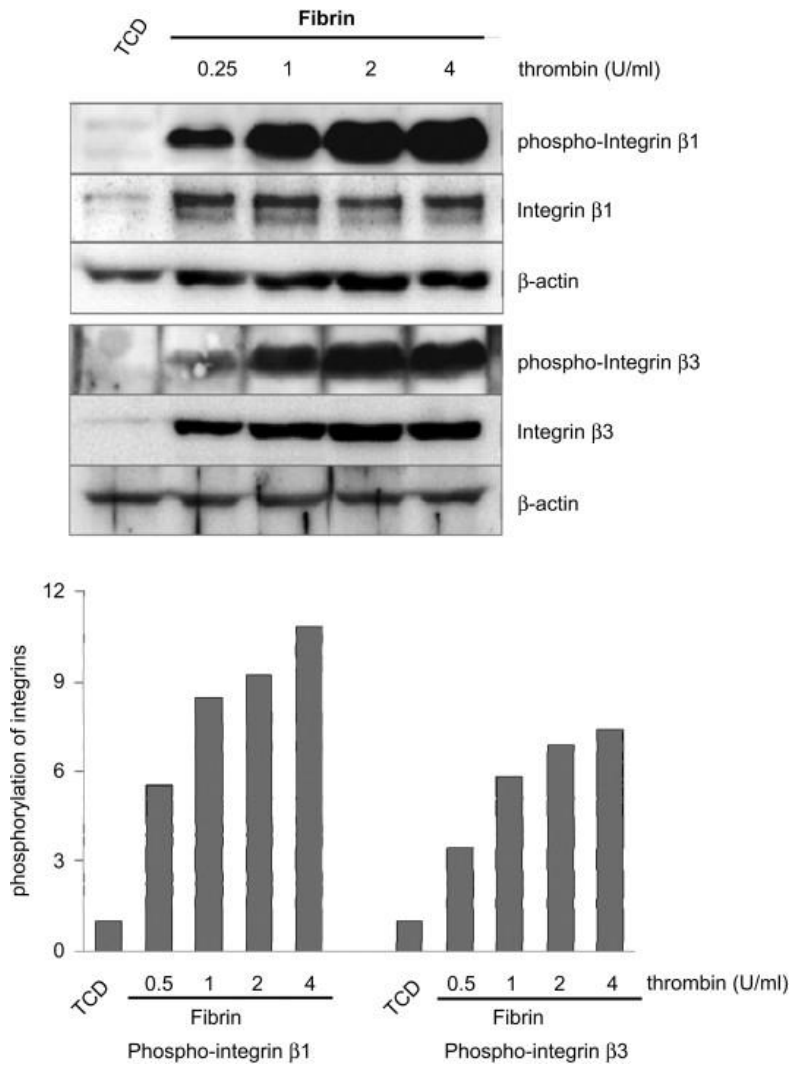

Figure IV-5. Effects of thrombin engaged in fibrin on phosphorylation of integrins. MC4 cells were cultured for a day on the matrices. The intensities of phospho-integrins β_1 and β_3 were measured and normalized by β-actin. Similar results were obtained from three independent experiments. Representative result is shown. Thrombin significantly increased the phosphorylations of integrins β_1 and β_3 (ANOVA, $p < 0.05$).

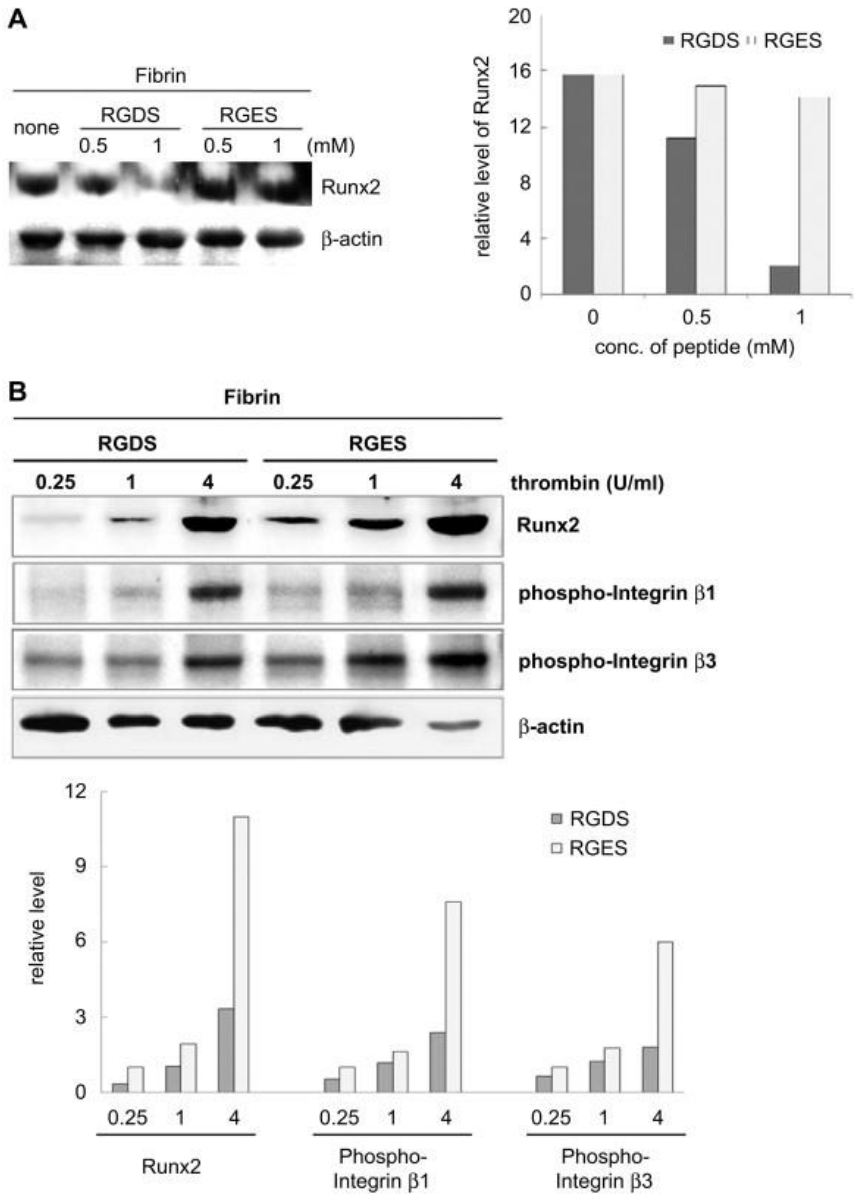

Figure IV-6. (A) Effect of an integrin-blocking peptide RGDS on the level of Runx2. The matrices were pre-treated with a blocking peptide RGDS or a control non-functional peptide RGES, and MC4 cells were cultured on these matrices for a day.

The intensities of Runx2 protein were measured and normalized by β-actin. Similar results were obtained from three independent experiments. Representative result is shown. RGDS significantly decreased the level of Runx2 (ANOVA, $p < 0.05$). (B) Effect of an integrin-blocking peptide on the thrombin-promoted Runx2 in MC4 cells grown on a fibrin matrix. The cells were pre-treated with a blocking peptide RGDS or a control peptide RGES and cultured on the matrices for a day. The intensities of Runx2 and phospho-integrins β_1 and β_3 were measured and normalized by β-actin. Similar results were obtained from three independent experiments. Representative result is shown. RGDS significantly reduced thrombin-enhanced Runx2 and integrin phosphorylation (ANOVA, $p < 0.05$).

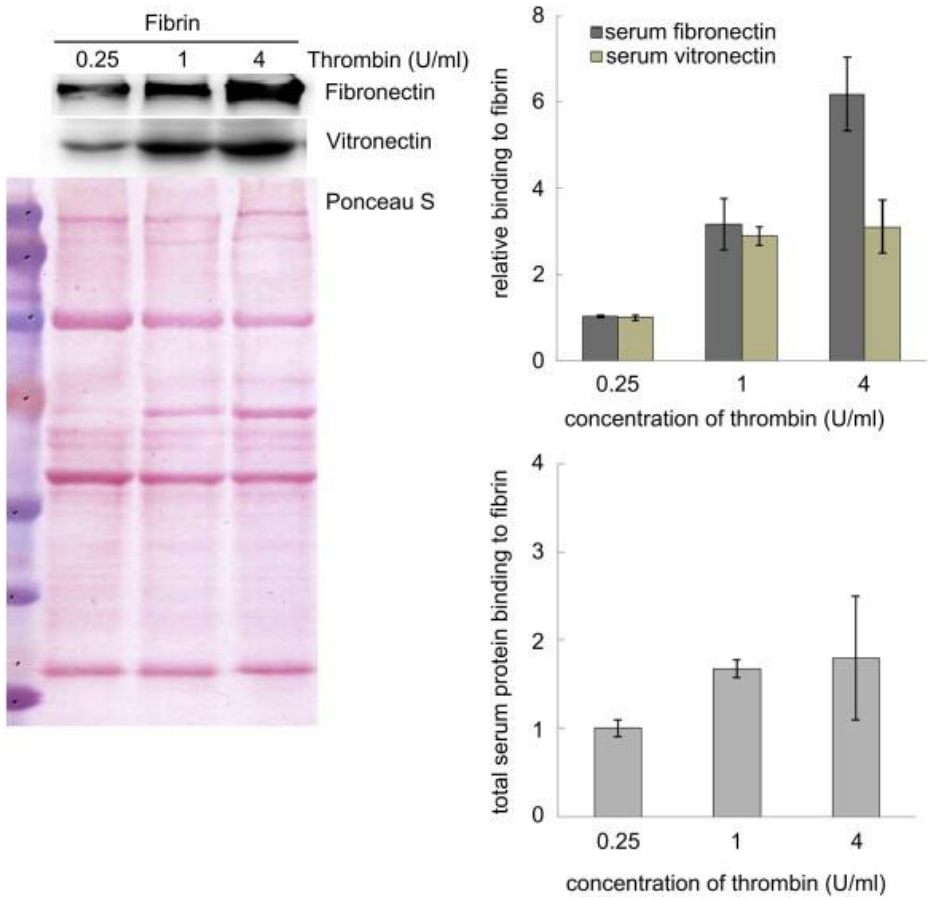

Figure IV-7. Effect of thrombin on the binding of serum proteins to fibrin matrix. Western blots for fibronectin and vitronectin adsorbed to the fibrin matrices from serum. The recovered serum proteins adsorbed to the fibrins were separated in SDS-PAGE. Serum fibronectin and vitronectin bound to fibrin was measured by the band intensities in Western blot analyses. The amount of total serum protein binding to fibrin was determined by Micro BCA assay. Similar results were obtained from three independent experiments. Representative result is shown. Thrombin significantly increased serum fibronectin-, serum vitronectin-, and total serum proteins-binding to fibrin (ANOVA, $p < 0.05$).

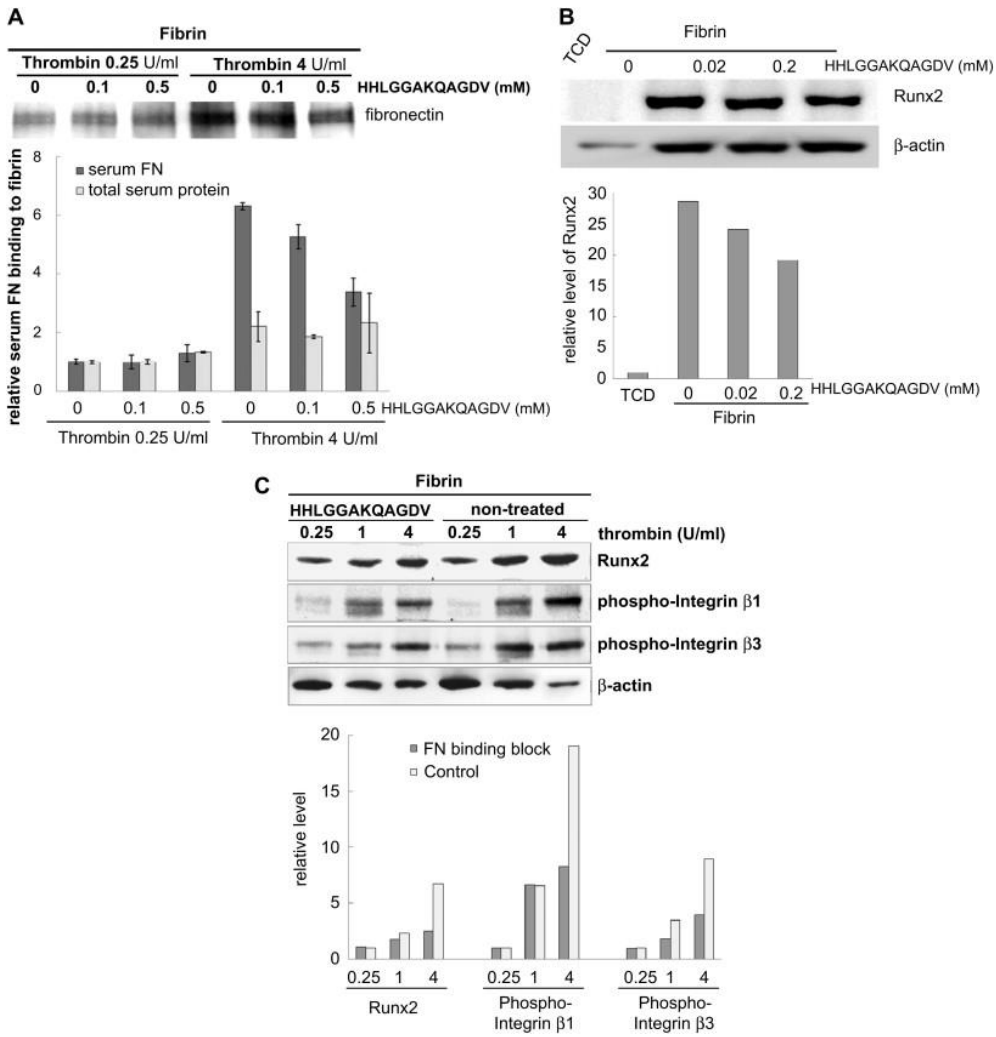

Figure IV-8. (A) Effect of a fibronectin-binding block peptide HHLGGAKQAGDV on the adsorption of fibronectin to fibrin. HHLGGAKQAGDV significantly decreased the fibronectin-binding to fibrin formed with 4 U/ml thrombin (ANOVA, $p < 0.05$). (B) Effect of HHLGGAKQAGDV peptide on the level of Runx2. MC4 cells were cultured on the fibrin matrices in the culture medium containing HHLGGAKQAGDV peptide for a day. The intensities of Runx2 protein were

measured and normalized by β-actin. Similar results were obtained from three independent experiments. Representative result is shown. HHLGGAKQAGDV significantly decreased the level of Runx2 (ANOVA, $p < 0.05$). (C) Effect of HHLGGAKQAGDV peptide on the thrombin-promoted Runx2 and integrin phosphorylation in MC4 cells grown on a fibrin matrix. MC4 cells were cultured on the fibrin matrices in the culture medium containing HHLGGAKQAGDV peptide for a day. The intensities of Runx2 and phospho-integrins β_1 and β_3 were measured and normalized by β-actin. Similar results were obtained from three independent experiments. Representative result is shown. RGDS significantly reduced thrombin-enhanced Runx2 and integrin phosphorylation (ANOVA, $p < 0.05$).

VII.4. Discussion

We demonstrated that the thrombin that is engaged in fibrin accelerates osteoblast differentiation, as confirmed by extent of calcium deposition, ALP activity, and level of Runx2. It was also shown that thrombin enhancement of Runx2 in the cells grown on fibrin is directed via integrins but not via PAR1, by performing experiments using a PAR1 agonist and an integrin-blocking RGDS peptide. Furthermore, we provided evidence that thrombin modulates the fibronectin-binding capacity of fibrin and that this modulation of thrombin contributes to integrin phosphorylation and Runx2 expression in the cells. These results suggest that high contents of thrombin alter the fibrin structure that provide better microenvironments for osteoblast differentiation through enhancing the fibronectin-binding capacity of fibrin.

In this study, the thrombin engaged in fibrin-promoted fibrin-enhanced Runx2 expression dose-dependently. Interestingly, the thrombin that was added to a culture medium for the culture of cells grown on plastic, in which thrombin acts as an activator of PAR1, did not increase Runx2. A PAR1-activating peptide treatment to the culture of cells grown on fibrin and on plastic showed no significant alteration of Runx2 expression. Thus, it can be concluded that thrombin affects cells indirectly by altering the fibrin structure. The structure of the fibrin matrix affects its biological functions [Laurens et al. 2006; Mosesson 2005; Wolberg 2007]. It is well known that a high concentration of thrombin forms the fibrin gel with relatively thinner and more tightly packed fibrin strands [Wolberg 2007; Collet et al. 2000], which was also confirmed in this study. The large surface area provided by a nanofibrous scaffolding allows for the greater adsorption of serum proteins [Woo et al. 2003], and this can contribute to osteoblast differentiation [Woo et al. 2007]. Similarly, the thinner and more tightly packed fibrin matrix formed by higher content of thrombin would

increase the total surface area that is available for serum proteins including fibronectin to adsorb. We showed that amount of the serum proteins that adsorbed to fibrin was increased along with the contents of thrombin engaged in fibrin. Considering the diameters of the fibrin matrices containing concentrations of thrombin, the amount of serum proteins that adsorbed to fibrin seems related to the surface area. However, we revealed that the thrombin enhancement of fibronectin adsorption profoundly exceeded that of total serum proteins. Thus, it is plausible that thrombin specifically increased the fibronectin-binding capacity of fibrin beyond a variable of surface area. Previously it has been shown that thrombin exposed the cryptic fibronectin-binding sites in fibrinogen and that fibronectin mostly bound to polymerized fibrin but rarely bound to fibrinogen [Makogonenko et al. 2002; Erickson and Fowler 1983]. These reports support our results. Furthermore, we provide evidence that thrombin-enhanced fibronectin-binding to fibrin consequently promotes integrin phosphorylation and Runx2 expression in the cells grown on fibrin, by presenting that inhibition of fibronectin-binding to fibrin profoundly attenuated the thrombin enhancement of integrin phosphorylation and Runx2 expression.

There are more than 20 different types of integrins, which are composed of noncovalent αß heterodimers. Fibrinogen interacts with $\alpha_v\beta_3$ that is widely expressed in kinds of cells via RGD recognition specificity [Laurens et al. 2006; Mosesson 2005; Savage et al. 1995]. Fibronectin, which can bind to fibrinogen, interacts with integrins $\alpha_4\beta_1$, $\alpha_5\beta_1$ and $\alpha_v\beta_3$ via the RGD motif [Makogonenko et al. 2002; Plow et al. 1985; Moursi et al. 1997]. Integrins β_1 and β_3, which can bind to fibrinogen or fibronectin with specific α subunits, are phosphorylated and capable of transducing signals to the inside of the cells. Our results showed that the phosphorylation of integrins β_1 and β_3 was dose-dependently increased in the cells grown on fibrin

matrices along with thrombin engagement. RGDS, an integrin-blocking peptide, caused a decrease in the level of Runx2 protein produced by fibrin, which was not likely controlled by a non-functional peptide RGES. There are several reports that have shown that integrin-mediated signaling contributes to osteoblast differentiation. α_vß integrins were co-localized with BMP-2 receptors, and the intact function of α_vß was essential in BMP-2 activity [Lai and Cheng 2005]. Fibronectin regulated calvarial osteoblast differentiation, which was caused by RGD motif in fibronectin [Moursi et al. 1997]. A functional blocking monoclonal antibody to the â1 integrin subunit significantly diminished osteoblastic differentiation [Gronthos et al. 2001]. The α_1ß$_1$ and α_2ß$_1$ complexes regulate early osteoblast differentiation, which is induced by BMP-2 [Xiao et al. 2002]. Our results and those of other researchers indicate that an integrin-mediated signal is up-regulated in osteoblasts grown on fibrin and leads to the enhancement of Runx2 expression.

VII.5. Conclusion

This study examined the effect of thrombin that is engaged in fibrin on osteoblast differentiation and its mode of action, under the hypothesis that osteoblast differentiation is not caused by a direct cell response to thrombin via PAR1 but by a response caused by thrombin-induced alterations in fibrin structures. Thrombin-promoted fibrin-enhanced osteoblasts differentiation in a dose-dependent manner, as confirmed by extent of calcium deposition, ALP activity, and level of Runx2. A synthetic activating peptide of PAR1 did not alter the level of Runx2. Instead, thrombin that was engaged in fibrin dose-dependently increased the phosphorylation of integrins β_1 and β_3. The integrin-blocking peptide RGDS reduced thrombin-enhanced Runx2 in the cells grown on fibrin, whereas the non-functional peptide RGES did not change the level of Runx2. Furthermore, thrombin dose-dependently increased the fibronectin-binding to fibrin. Inhibition of fibronectin-binding to fibrin using a blocking peptide attenuated the thrombin-induced integrin phosphorylations and Runx2 expression. These results in this study provide evidence that thrombin engaged in fibrin accelerates osteoblasts differentiation via integrins but not via PAR1 through modulating the fibronectin-binding capacity of fibrin, and this suggests that high contents of thrombin alter the fibrin structure that provide better microenvironments for osteoblast differentiation through enhancing the fibronectin-binding capacity of fibrin.

VIII. Conclusion

In this study, the importance of the morphological features of the ECM on osteoblast differentiation was confirmed, considering that the same mechanism can be obtained even when the appearance of collagen is relatively simply simulated through electrospinning using a synthetic polymer. In addition, this phenomenon was also verified by using exogenous Runx2. These results suggest that the morphological characteristics of the ECM represented by collagen, is one of the key elements in hard tissue regeneration.

The one practical example was presented by applying a nanofibrous engineered matrix on the pulp capping procedure in a beagle experimental model, using electrospun PCL which is well-known as a biocompatible synthetic material. The PCL fiber mesh (PCL-F) provided the nanofibrous matrix, allowing the cells to induce differentiation and protected the cytotoxicity from the early stage of MTA hydration. The PCL-f group showed excellent dentin bridge formation and health pulp condition, regarding the pulp capping procedure in the beagle experiment model.

Fibrin was investigated as a natural polymer material to mimic the fibrous morphological features of collagen. Fibrin has great advantages in terms of cost and immunity, for tissue engineering and clinical approaches. In this study, fibrin formed a similar morphology to collagen, had superior osteoblast differentiation ability and showed a higher selective adsorption for fibronectin and vitronectin, which have positive effects on osteogenic differentiation and bone regeneration. The MC3T3-E1 cells had a higher proliferation rate and differentiation on fibrin than collagen. Next, it was certified that this ability of osteogenic differentiation, was dependent on the

concentration of thrombin used in the polymerization of fibrin. Integrins β_1 and β_3 bind on fibrin and fibronectin, thereby, promoting the osteogenic differentiation. The selective fibronectin absorption and integrin β_1, β_3 binding was increased depending on the concentration of thrombin used in preparing the fibrin matrix. This finding appears to provide important guidance, regarding the use of fibrin in biomedical applications.

The abovementioned results of this study strongly suggest the necessity to study the molecular biological mechanism of the structural elements of the ECM, on cell differentiation and tissue regeneration. Also, from a tissue engineering perspective, the need to explore effective artificial ECM structures for each target organization that should be regenerated, is strongly advocated.

IX. References

Accorinte, M. D L. R., Holland, R., Reis, A., Bortoluzzi, M. C., Murata, S. S., Dezan Jr, E., Souza, V. AND Alessandro, L. D. 2008. Evaluation of Mineral Trioxide Aggregate and Calcium Hydroxide Cement as Pulp-capping Agents in Human Teeth. Journal of Endodontics 34: 1-6.

Addi, C., Murschel, F. AND De Crescenzo, G. 2016. Design and Use of Chimeric Proteins Containing a Collagen-Binding Domain for Wound Healing and Bone Regeneration. Tissue Eng Part B Rev.

Aeinehchi, M., Eslami, B., Ghanbariha, M. AND Saffar, A. S. 2003. Mineral trioxide aggregate (MTA) and calcium hydroxide as pulp-capping agents in human teeth: A preliminary report. International Endodontic Journal 36: 225-231.

Agrafioti, Anastasia, Taraslia, Vasiliki, Chrepa, Vanessa, Lymperi, Stefania, Panopoulos, Panos, Anastasiadou, Ema AND Kontakiotis, Evangelos G. 2016. Interaction of dental pulp stem cells with Biodentine and MTA after exposure to different environments. Journal of Applied Oral Science 24: 481-486.

Ahmed, T. A. E., Dare, E. V. AND Hincke, M. 2008. Fibrin: A versatile scaffold for tissue engineering applications. Tissue Engineering - Part B: Reviews 14: 199-215.

Alves, L. B., Mariguela, V. C., Grisi, M. F., Souza, S. L., Novaes Junior, A. B., Taba Junior, M., Oliveira, P. T. AND Palioto, D. B. 2015. Expression of osteoblastic phenotype in periodontal ligament fibroblasts cultured in three-dimensional collagen gel. J Appl Oral Sci 23: 206-214.

Amrani, D. L., Diorio, J. P. AND Delmotte, Y. 2001. Wound healing: Role of commercial fibrin sealants. Annals of the New York Academy of Sciences, p. 566-579.

Arnold, M., Cavalcanti-Adam, E. A., Glass, R., Blümmel, J., Eck, W., Kantlehner, M., Kessler, H. AND Spatz, J. P. 2004. Activation of integrin function by nanopatterned adhesive interfaces. Chemphyschem 5: 383-388.

Aruna, S. T., Balaji, L. S., Kumar, S. Senthil AND Prakash, B. Shri. 2017. Electrospinning in solid oxide fuel cells – A review. Renewable and Sustainable Energy Reviews 67: 673-682.

Asghari, Fatemeh, Samiei, Mohammad, Adibkia, Khosro, Akbarzadeh, Abolfazl AND Davaran, Soodabeh. 2017. Biodegradable and biocompatible polymers for tissue engineering application: a review. Artif Cells Nanomed Biotechnol 45: 185-192.

Babitha, S., Rachita, Lakra, Karthikeyan, K., Shoba, Ekambaram, Janani, Indrakumar, Poornima, Balan AND Purna Sai, K. 2017. Electrospun protein nanofibers in

healthcare: A review. International Journal of Pharmaceutics 523: 52-90.

Balto, H. A. 2004. Attachment and morphological behavior of human periodontal ligament fibroblasts to mineral trioxide aggregate: A scanning electron microscope study. Journal of Endodontics 30: 25-29.

Baraba, Anja, Pezelj-Ribaric, Sonja, Roguljić, Marija AND Miletic, Ivana. 2016. Cytotoxicity of Two Bioactive Root Canal Sealers. Acta Stomatologica Croatica 50: 8-13.

Beniash, E., Hartgerink, J. D., Storrie, H., Stendahl, J. C. AND Stupp, S. I. 2005. Self-assembling peptide amphiphile nanofiber matrices for cell entrapment. Acta Biomaterialia 1: 387-397.

Bensaïd, W., Triffitt, J. T., Blanchat, C., Oudina, K., Sedel, L. AND Petite, H. 2003. A biodegradable fibrin scaffold for mesenchymal stem cell transplantation. Biomaterials 24: 2497-2502.

Black, Cameron R. M., Goriainov, Vitali, Gibbs, David, Kanczler, Janos, Tare, Rahul S. AND Oreffo, Richard O. C. 2015. Bone Tissue Engineering. Current Molecular Biology Reports 1: 132-140.

Bluteau, G., Pilet, P., Bourges, X., Bilban, M., Spaethe, R., Daculsi, G. AND Guicheux, J. 2006. The modulation of gene expression in osteoblasts by thrombin coated on biphasic calcium phosphate ceramic. Biomaterials 27: 2934-2943.

Bonson, S., Jeansonne, B. G. AND Lallier, T. E. 2004. Root-end filling materials alter fibroblast differentiation. Journal of Dental Research 83: 408-413.

Bortoluzzi, E. A., Broon, N. J., Bramante, C. M., Consolaro, A., Garcia, R. B., De Moraes, I. G. AND Bernadineli, N. 2008. Mineral Trioxide Aggregate with or without Calcium Chloride in Pulpotomy. Journal of Endodontics 34: 172-175.

Breen, A., O'brien, T. AND Pandit, A. 2009. Fibrin as a delivery system for therapeutic drugs and biomolecules. Tissue Engineering - Part B: Reviews 15: 201-214.

Brittberg, M., Sjögren-Jansson, E., Lindahl, A. AND Peterson, L. 1997. Influence of fibrin sealant (Tisseel®) on osteochondral defect repair in the rabbit knee. Biomaterials 18: 235-242.

Bruderer, M, Richards, Rg, Alini, M AND Stoddart, Mj. 2014. Role and regulation of RUNX2 in osteogenesis. Eur Cell Mater 28: 269-286.

Chen, V. J. AND Ma, P. X. 2004. Nano-fibrous poly(L-lactic acid) scaffolds with interconnected spherical macropores. Biomaterials 25: 2065-2073.

Chiti, M. C., Dolmans, M. M., Donnez, J. AND Amorim, C. A. 2017. Fibrin in Reproductive Tissue Engineering: A Review on Its Application as a Biomaterial for Fertility Preservation. Annals of Biomedical Engineering: 1-14.

Chong, E. J., Phan, T. T., Lim, I. J., Zhang, Y. Z., Bay, B. H., Ramakrishna, S. AND Lim, C. T. 2007. Evaluation of electrospun PCL/gelatin nanofibrous scaffold for wound healing and layered dermal reconstitution. Acta Biomaterialia 3: 321-330.

Collet, J. P., Park, D., Lesty, C., Soria, J., Soria, C., Montalescot, G. AND Weisel, J. W. 2000. Influence of fibrin network conformation and fibrin diameter on fibrinolysis speed: Dynamic and structural approaches by confocal microscopy. Arteriosclerosis, Thrombosis, and Vascular Biology 20: 1354-1361.

Craig, A. S., Birtles, M. J., Conway, J. F. AND Parry, D. A. 1989. An estimate of the mean length of collagen fibrils in rat tail-tendon as a function of age. Connective Tissue Research 19: 51-62.

Cui, Wenguo, Zhou, Yue AND Chang, Jiang. 2010. Electrospun nanofibrous materials for tissue engineering and drug delivery. Science and Technology of Advanced Materials 11: 014108.

D'antò, V., Di Caprio, M. P., Ametrano, G., Simeone, M., Rengo, S. AND Spagnuolo, G. 2010. Effect of mineral trioxide aggregate on mesenchymal stem cells. Journal of Endodontics 36: 1839-1843.

Davis, H. E., Miller, S. L., Case, E. M. AND Leach, J. K. 2011. Supplementation of fibrin gels with sodium chloride enhances physical properties and ensuing osteogenic response. Acta Biomaterialia 7: 691-699.

De Souza Costa, C. A., Duarte, P. T., De Souza, P. P. C., Giro, E. M. A. AND Hebling, J. 2008. Cytotoxic effects and pulpal response caused by a mineral trioxide aggregate formulation and calcium hydroxide. American Journal of Dentistry 21: 255-261.

Dominguez, M. S., Witherspoon, D. E., Gutmann, J. L. AND Opperman, L. A. 2003. Histological and scanning electron microscopy assessment of various vital pulp-therapy materials. Journal of Endodontics 29: 324-333.

Erickson, H. P. AND Fowler, W. E. 1983. Electron microscopy of fibrinogen, its plasmic fragments and small polymers. Annals of the New York Academy of Sciences Vol. 408: 146-163.

Exposito, Jean-Yves, Valcourt, Ulrich, Cluzel, Caroline AND Lethias, Claire. 2010. The fibrillar collagen family. International Journal of Molecular Sciences 11: 407-426.

Falanga, V., Iwamoto, S., Chartier, M., Yufit, T., Butmarc, J., Kouttab, N., Shrayer, D. AND Carson, P. 2007. Autologous bone marrow-derived cultured mesenchymal stem cells delivered in a fibrin spray accelerate healing in murine and human cutaneous wounds. Tissue Engineering 13: 1299-1312.

Fernandes, Hugo, Moroni, Lorenzo, Van Blitterswijk, Clemens AND De Boer, Jan. 2009.

Extracellular matrix and tissue engineering applications. Journal of Materials Chemistry 19: 5474-5484.

Flanagan, T. C., Cornelissen, C., Koch, S., Tschoeke, B., Sachweh, J. S., Schmitz-Rode, T. AND Jockenhoevel, S. 2007. The in vitro development of autologous fibrin-based tissue-engineered heart valves through optimised dynamic conditioning. Biomaterials 28: 3388-3397.

Fliefel, Riham, Kühnisch, Jan, Ehrenfeld, Michael AND Otto, Sven. 2017. Gene Therapy for Bone Defects in Oral and Maxillofacial Surgery: A Systematic Review and Meta-Analysis of Animal Studies. Stem Cells and Development 26: 215-230.

Franceschi, R. T., Xiao, G., Jiang, D., Gopalakrishnan, R., Yang, S. AND Reith, E. 2003. Multiple signaling pathways converge on the Cbfa1/Runx2 transcription factor to regulate osteoblast differentiation. Connective Tissue Research 44: 109-116.

Frenot, Audrey AND Chronakis, Ioannis S. 2003. Polymer nanofibers assembled by electrospinning. Current opinion in colloid & interface science 8: 64-75.

Fridland, M. AND Rosado, R. 2003. Mineral trioxide aggregate (MTA) solubility and porosity with different water-to-powder ratios. Journal of Endodontics 29: 814-817.

Fridland, M. AND Rosado, R. 2005. MTA solubility: A long term study. Journal of Endodontics 31: 376-379.

Goldberg, F., Massone, E. J. AND Spielberg, C. 1984. Evaluation of the dentinal bridge after pulpotomy andcalcium hydroxide dressing. Journal of Endodontics 10: 318-320.

Goldberg, M. AND Smith, A. J. 2004. Cells and extracellular matrices of dentin and pulp: A biological basis for repair and tissue engineering. Critical Reviews in Oral Biology and Medicine 15: 13-27.

Gronthos, S., Mankani, M., Brahim, J., Robey, P. G. AND Shi, S. 2000. Postnatal human dental pulp stem cells (DPSCs) in vitro and in vivo. Proceedings of the National Academy of Sciences of the United States of America 97: 13625-13630.

Gronthos, S., Simmons, P. J., Graves, S. E. AND G. Robey, P. 2001. Integrin-mediated interactions between human bone marrow stromal precursor cells and the extracellular matrix. Bone 28: 174-181.

Guilak, F., Cohen, D. M., Estes, B. T., Gimble, J. M., Liedtke, W. AND Chen, C. S. 2009. Control of Stem Cell Fate by Physical Interactions with the Extracellular Matrix. Cell Stem Cell 5: 17-26.

Haglund, R., He, J., Jarvis, J., Safavi, K. E., Spångberg, L. S. W. AND Zhu, Q. 2003. Effects of root-end filling materials on fibroblasts and macrophages in vitro. Oral Surgery, Oral Medicine, Oral Pathology, Oral Radiology, and Endodontics 95: 739-745.

Hamidi, Hellyeh AND Ivaska, Johanna. 2017. Vascular Morphogenesis: An Integrin and Fibronectin Highway. Current Biology 27: R158-R161.

Hanks, C. T., Sun, Z. L., Fang, D. N., Edwards, C. A., Wataha, J. C., Ritchie, H. H. AND Butler, W. T. 1998. Cloned 3T6 cell line from CD-1 mouse fetal molar dental papillae. Connective Tissue Research 37: 233-249.

Heino, Jyrki. 2007. The collagen family members as cell adhesion proteins. Bioessays 29: 1001-1010.

Hsieh, Jessica Y., Smith, Tim D., Meli, Vijaykumar S., Tran, Thi N., Botvinick, Elliot L. AND Liu, Wendy F. 2017. Differential regulation of macrophage inflammatory activation by fibrin and fibrinogen. Acta Biomaterialia 47: 14-24.

Huber, Robert J. AND O'day, Danton H. 2017. Extracellular matrix dynamics and functions in the social amoeba Dictyostelium: A critical review. Biochimica et Biophysica Acta (BBA) - General Subjects 1861: 2971-2980.

Jeon, E. J. ET AL. 2006. Bone morphogenetic protein-2 stimulates Runx2 acetylation. Journal of Biological Chemistry 281: 16502-16511.

Jikko, A., Harris, S. E., Chen, D., Mendrick, D. L. AND Damsky, C. H. 1999. Collagen integrin receptors regulate early osteoblast differentiation induced by BMP-2. Journal of Bone and Mineral Research 14: 1075-1083.

Jun, J. H., Yoon, W. J., Seo, S. B., Woo, K. M., Kim, G. S., Ryoo, H. M. AND Baek, J. H. 2010. BMP2-activated Erk/MAP kinase stabilizes runx2 by increasing p300 levels and histone acetyltransferase activity. Journal of Biological Chemistry 285: 36410-36419.

Kapp, Tobias G, Rechenmacher, Florian, Neubauer, Stefanie, Maltsev, Oleg V, Cavalcanti-Adam, Elisabetta A, Zarka, Revital, Reuning, Ute, Notni, Johannes, Wester, Hans-Jürgen AND Mas-Moruno, Carlos. 2017. A Comprehensive Evaluation of the Activity and Selectivity Profile of Ligands for RGD-binding Integrins. Scientific Reports 7: 39805.

Karp, J. M., Sarraf, F., Shoichet, M. S. AND Davies, J. E. 2004. Fibrin-filled scaffolds for bone-tissue engineering: An in vivo study. Journal of Biomedical Materials Research - Part A 71: 162-171.

Karsenty, G. 2008. Transcriptional control of skeletogenesis. Annual Review of Genomics and Human Genetics, p. 183-196.

Kim, Youhwan, Ko, Hyojin, Kwon, Ik Keun AND Shin, Kwanwoo. 2016. Extracellular Matrix Revisited: Roles in Tissue Engineering. International Neurourology Journal 20: S23-29.

Knight, C. G., Morton, L. F., Peachey, A. R., Tuckwell, D. S., Farndale, R. W. AND Barnes, M. J. 2000. The collagen-binding a-domains of integrins α1/β1 and α2/β1 recognize the same specific amino acid sequence, GFOGER, in native (triple- helical) collagens. Journal of Biological Chemistry 275: 35-40.

Komori, T. ET AL. 1997. Targeted disruption of Cbfa1 results in a complete lack of bone formation owing to maturational arrest of osteoblasts. Cell 89: 755-764.

Lai, C. F. AND Cheng, S. L. 2005. αvβ integrins play an essential role in BMP-2 induction of osteoblast differentiation. Journal of Bone and Mineral Research 20: 330-340.

Lam, C. X. F., Savalani, M. M., Teoh, S. H. AND Hutmacher, D. W. 2008. Dynamics of in vitro polymer degradation of polycaprolactone-based scaffolds: Accelerated versus simulated physiological conditions. Biomedical Materials 3.

Laurens, N., Koolwijk, P. AND De Maat, M. P. 2006. Fibrin structure and wound healing. Journal of thrombosis and haemostasis : JTH 4: 932-939.

Lee, M. H. ET AL. 1999. Transient upregulation of CBFA1 in response to bone morphogenetic protein-2 and transforming growth factor β1 in C2C12 myogenic cells coincides with suppression of the myogenic phenotype but is not sufficient for osteoblast differentiation. Journal of Cellular Biochemistry 73: 114-125.

Lee, M. H., Kim, Y. J., Kim, H. J., Park, H. D., Kang, A. R., Kyung, H. M., Sung, J. H., Wozney, J. M., Kim, H. J. AND Ryoo, H. M. 2003. BMP-2-induced Runx2 Expression Is Mediated by Dlx5, and TGF-β1 Opposes the BMP-2-induced Osteoblast Differentiation by Suppression of Dlx5 Expression. Journal of Biological Chemistry 278: 34387-34394.

Li, Dan AND Xia, Younan. 2004. Electrospinning of nanofibers: reinventing the wheel? Advanced Materials 16: 1151-1170.

Li, W. J., Danielson, K. G., Alexander, P. G. AND Tuan, R. S. 2003. Biological response of chondrocytes cultured in three-dimensional nanofibrous poly(ε-caprolactone) scaffolds. Journal of Biomedical Materials Research - Part A 67: 1105-1114.

Li, W. J., Laurencin, C. T., Caterson, E. J., Tuan, R. S. AND Ko, F. K. 2002. Electrospun nanofibrous structure: A novel scaffold for tissue engineering. Journal of Biomedical Materials Research 60: 613-621.

Lucht, U., Bünger, C., Møller, J. T., Joyce, F. AND Plenk, H. 1986. Fibrin sealant in bone transplantation: No effects on blood flow and bone formation in dogs. Acta Orthopaedica 57: 19-24.

Lucke, Jayne C., Herbert, Danielle, Partridge, Brad AND Hall, Wayne D. 2010. Anticipating the use of life extension technologies. EMBO Reports 11: 334-338.

Luo, Z., Zhao, X. AND Zhang, S. 2008. Self-organization of a chiral D-EAK16 designer

peptide into a 3D nanofiber scaffold. Macromolecular Bioscience 8: 785-791.

Lynch, M. P., Stein, J. L., Stein, G. S. AND Lian, J. B. 1995. The influence of type I collagen on the development and maintenance of the osteoblast phenotype in primary and passaged rat calvarial osteoblasts: Modification of expression of genes supporting cell growth, adhesion, and extracellular matrix mineralization. Experimental Cell Research 216: 35-45.

Ma, P. X. 2008. Biomimetic materials for tissue engineering. Advanced Drug Delivery Reviews 60: 184-198.

Macdiarmid, Ag, Jones, We, Norris, Id, Gao, J, Johnson, At, Pinto, Nj, Hone, J, Han, B, Ko, Fk AND Okuzaki, H. 2001. Electrostatically-generated nanofibers of electronic polymers. Synthetic Metals 119: 27-30.

Makogonenko, E., Tsurupa, G., Ingham, K. AND Medved, L. 2002. Interaction of fibrin(ogen) with fibronectin: Further characterization and localization of the fibronectin-binding site. Biochemistry 41: 7907-7913.

Marie, P. J. 2013. Targeting integrins to promote bone formation and repair. Nature Reviews Endocrinology 9: 288-295.

Marini, J. C. ET AL. 2007. Consortium for osteogenesis imperfecta mutations in the helical domain of type I collagen: Regions rich in lethal mutations align with collagen binding sites for integrins and proteoglycans. Human Mutation 28: 209-221.

Mcbeath, R., Pirone, D. M., Nelson, C. M., Bhadriraju, K. AND Chen, C. S. 2004. Cell shape, cytoskeletal tension, and RhoA regulate stem cell lineage commitment. Developmental Cell 6: 483-495.

Mcconnel, Charles AND Turner, Leigh. 2005. Medicine, ageing and human longevity. EMBO Reports 6: S59-S62.

Miura, M., Gronthos, S., Zhao, M., Lu, B., Fisher, L. W., Robey, P. G. AND Shi, S. 2003. SHED: Stem cells from human exfoliated deciduous teeth. Proceedings of the National Academy of Sciences of the United States of America 100: 5807-5812.

Mizuno, M., Fujisawa, R. AND Kuboki, Y. 2000. Type I collagen-induced osteoblastic differentiation of bone-marrow cells mediated by collagen-α2β1 integrin interaction. Journal of Cellular Physiology 184: 207-213.

Moll, Cwi, Schmiedinger, T, Moll, Ma, Seppi, T, Pfaller, K, Hess, Mw, Gutleben, K, Lindtner, Ra, Blauth, M AND Krumschnabel, G. 2017. Extracellular matrix mimicking scaffold promotes osteogenic stem cell differentiation: A new approach in osteoporosis research. Bio-Medical Materials and Engineering 28: 87-103.

Mosesson, M. W. 2005. Fibrinogen and fibrin structure and functions. Journal of Thrombosis

and Haemostasis 3: 1894-1904.

Moursi, A. M., Globus, R. K. AND Damsky, C. H. 1997. Interactions between integrin receptors and fibronectin are required for calvarial osteoblast differentiation in vitro. Journal of Cell Science 110: 2187-2196.

Murray, P. E. AND García-Godoy, F. 2006. The incidence of pulp healing defects with direct capping materials. American Journal of Dentistry 19: 171-177.

Nair, M. B., Varma, H. K. AND John, A. 2009. Platelet-rich plasma and fibrin glue-coated bioactive ceramics enhance growth and differentiation of goat bone marrow-derived stem cells. Tissue Engineering - Part A 15: 1619-1631.

Nakashima, K., Zhou, X., Kunkel, G., Zhang, Z., Deng, J. M., Behringer, R. R. AND De Crombrugghe, B. 2002. The novel zinc finger-containing transcription factor Osterix is required for osteoblast differentiation and bone formation. Cell 108: 17-29.

Norman, James J. AND Desai, Tejal A. 2006. Methods for Fabrication of Nanoscale Topography for Tissue Engineering Scaffolds. Annals of Biomedical Engineering 34: 89-101.

Oh, J. H., Kim, H. J., Kim, T. I., Baek, J. H., Ryoo, H. M. AND Woo, K. M. 2012. The effects of the modulation of the fibronectin-binding capacity of fibrin by thrombin on osteoblast differentiation. Biomaterials 33: 4089-4099.

Oh, J. H., Seo, J., Yoon, W. J., Cho, J. Y., Baek, J. H., Ryoo, H. M. AND Woo, K. M. 2011. Suppression of Runx2 protein degradation by fibrous engineered matrix. Biomaterials 32: 5826-5836.

Okiji, T. AND Yoshiba, K. 2009. Reparative dentinogenesis induced by mineral trioxide aggregate: A review from the biological and physicochemical points of view. Int J Dent 2009.

Osathanon, T., Linnes, M. L., Rajachar, R. M., Ratner, B. D., Somerman, M. J. AND Giachelli, C. M. 2008. Microporous nanofibrous fibrin-based scaffolds for bone tissue engineering. Biomaterials 29: 4091-4099.

Otto, F. ET AL. 1997. Cbfa1, a candidate gene for cleidocranial dysplasia syndrome, is essential for osteoblast differentiation and bone development. Cell 89: 765-771.

Pagel, Charles N, De Niese, Michael R, Abraham, Linda A, Chinni, Carla, Song, Shu-Jun, Pike, Robert N AND Mackie, Eleanor J. 2003. Inhibition of osteoblast apoptosis by thrombin. Bone 33: 733-743.

Paranjpe, A., Zhang, H. AND Johnson, J. D. 2010. Effects of mineral trioxide aggregate on human dental pulp cells after pulp-capping procedures. Journal of Endodontics

36: 1042-1047.

Park, O. J., Kim, H. J., Woo, K. M., Baek, J. H. AND Ryoo, H. M. 2010. FGF2-activated ERK mitogen-activated protein kinase enhances Runx2 acetylation and stabilization. Journal of Biological Chemistry 285: 3568-3574.

Pektok, E., Nottelet, B., Tille, J. C., Gurny, R., Kalangos, A., Moeller, M. AND Walpoth, B. H. 2008. Degradation and healing characteristics of small-diameter poly(ε-caprolactone) vascular grafts in the rat systemic arterial circulation. Circulation 118: 2563-2570.

Pelliccioni, G. A., Ciapetti, G., Cenni, E., Granchi, D., Nanni, M., Pagani, S. AND Giunti, A. 2004. Evaluation of osteoblast-like cell response to Proroot™ MTA (mineral trioxide aggregate) cement. Journal of Materials Science: Materials in Medicine 15: 167-173.

Phillips, J. E., Hutmacher, D. W., Guldberg, R. E. AND García, A. J. 2006. Mineralization capacity of Runx2/Cbfa1-genetically engineered fibroblasts is scaffold dependent. Biomaterials 27: 5535-5545.

Pitt Ford, T. R., Torabinejad, M., Abedi, H. R., Bakland, L. K. AND Kariyawasam, S. P. 1996. Using mineral trioxide aggregate: As a pulp-capping material. Journal of the American Dental Association 127: 1491-1494.

Plow, E. F., Marguerie, G. A. AND Ginsberg, M. H. 1985. Fibronectin binding to thrombin-stimulated platelets: Evidence for fibrin(ogen) independent and dependent pathways. Blood 66: 26-32.

Plow, E. F., Srouji, A. H., Meyer, D., Marguerie, G. AND Ginsberg, M. H. 1984. Evidence that three adhesive proteins interact with a common recognition site on activated platelets. Journal of Biological Chemistry 259: 5388-5391.

Prince, M., Banerjee, C., Javed, A., Green, J., Lian, J. B., Stein, G. S., Bodine, P. V. N. AND Komm, B. S. 2000. Expression and regulation of RUNX2/Cbfa1 and osteoblast phenotypic markers during the growth and differentiation of human osteoblasts. Journal of Cellular Biochemistry 80: 424-440.

Proulx, M. K. ET AL. 2011. Fibrin microthreads support mesenchymal stem cell growth while maintaining differentiation potential. Journal of Biomedical Materials Research - Part A 96 A: 301-312.

Qin, C., Baba, O. AND Butler, W. T. 2004. Post-translational modifications of SIBLING proteins and their roles in osteogenesis and dentinogenesis. Critical Reviews in Oral Biology and Medicine 15: 126-136.

Ramakrishna, Seeram 2005. An introduction to electrospinning and nanofibers. World

Scientific.

Ramakrishna, Seeram, Fujihara, Kazutoshi, Teo, Wee-Eong, Yong, Thomas, Ma, Zuwei AND Ramaseshan, Ramakrishna. 2006. Electrospun nanofibers: solving global issues. Materials Today 9: 40-50.

Reneker, Darrell H. AND Yarin, Alexander L. 2008. Electrospinning jets and polymer nanofibers. Polymer 49: 2387-2425.

Ricard-Blum, Sylvie. 2011. The collagen family. Cold Spring Harbor Perspectives in Biology 3: a004978.

Rybarczyk, B. J., Lawrence, S. O. AND Simpson-Haidaris, P. J. 2003. Matrix-fibrinogen enhances wound closure by increasing both cell proliferation and migration. Blood 102: 4035-4043.

Savage, B., Bottini, E. AND Ruggeri, Z. M. 1995. Interaction of integrin αIIbβ3with multiple fibrinogen domains during platelet adhesion. Journal of Biological Chemistry 270: 28812-28817.

Schnell, E., Klinkhammer, K., Balzer, S., Brook, G., Klee, D., Dalton, P. AND Mey, J. 2007. Guidance of glial cell migration and axonal growth on electrospun nanofibers of poly(ε-caprolactone) and a collagen/poly(ε-caprolactone) blend. Biomaterials 28: 3012-3025.

Schröder, U. 1985. Effects of calcium hydroxide-containing pulp-capping agents on pulp cell migration, proliferation, and differentiation. Journal of Dental Research 64 Spec No: 541-548.

Shahi, Maryam, Peymani, Amir AND Sahmani, Mehdi. 2017. Regulation of Bone Metabolism. Reports of Biochemistry and Molecular Biology 5: 73-82.

Shin, M., Yoshimoto, H. AND Vacanti, J. P. 2004. In Vivo Bone Tissue Engineering Using Mesenchymal Stem Cells on a Novel Electrospun Nanofibrous Scaffold. Tissue Engineering 10: 33-41.

Shoulders, Matthew D. AND Raines, Ronald T. 2009. COLLAGEN STRUCTURE AND STABILITY. Annual Review of Biochemistry 78: 929-958.

Sionkowska, Alina, Skrzyński, Sławomir, Śmiechowski, Krzysztof AND Kołodziejczak, Agata. 2017. The review of versatile application of collagen. Polymers for Advanced Technologies 28: 4-9.

Song, Minju, Yu, Bo, Kim, Sol, Hayashi, Marc, Smith, Colby, Sohn, Suhjin, Kim, Euiseong, Lim, James, Stevenson, Richard G. AND Kim, Reuben H. 2017. Clinical and Molecular Perspectives of Reparative Dentin Formation: Lessons Learned from Pulp-Capping Materials and the Emerging Roles of Calcium. Dental Clinics of

North America 61: 93-110.

Song, S. J., Pagel, C. N., Campbell, T. M., Pike, R. N. AND Mackie, E. J. 2005a. The role of protease-activated receptor-1 in bone healing. American Journal of Pathology 166: 857-868.

Song, S. J., Pagel, C. N., Pike, R. N. AND Mackie, E. J. 2005b. Studies on the receptors mediating responses of osteoblasts to thrombin. International Journal of Biochemistry and Cell Biology 37: 206-213.

Subbiah, Thandavamoorthy, Bhat, Gs, Tock, Rw, Parameswaran, S AND Ramkumar, Ss. 2005. Electrospinning of nanofibers. Journal of Applied Polymer Science 96: 557-569.

Tamura, Y., Takeuchi, Y., Suzawa, M., Fukumoto, S., Kato, M., Miyazono, K. AND Fujita, T. 2001. Focal adhesion kinase activity is required for bone morphogenetic protein - Smad1 signaling and osteoblastic differentiation in murine MC3T3-E1 cells. Journal of Bone and Mineral Research 16: 1772-1779.

Thompson, C. J., Chase, G. G., Yarin, A. L. AND Reneker, D. H. 2007. Effects of parameters on nanofiber diameter determined from electrospinning model. Polymer 48: 6913-6922.

Tzaphlidou, M. 2005. The role of collagen in bone structure: an image processing approach. Micron 36: 593-601.

Viguet-Carrin, S., Garnero, P. AND Delmas, P. D. 2006. The role of collagen in bone strength. Osteoporosis International 17: 319-336.

Wallace, J. M., Orr, B. G., Marini, J. C. AND Holl, M. M. B. 2011. Nanoscale morphology of Type I collagen is altered in the Brtl mouse model of Osteogenesis Imperfecta. Journal of Structural Biology 173: 146-152.

Wang, J., Ma, H., Jin, X., Hu, J., Liu, X., Ni, L. AND Ma, P. X. 2011. The effect of scaffold architecture on odontogenic differentiation of human dental pulp stem cells. Biomaterials 32: 7822-7830.

Wang, Lingyun, Pan, Di, Yan, Qi AND Song, Yuhua. 2017a. Activation Mechanisms of αVβ3 Integrin by Binding to Fibronectin: A Computational Study. Protein Science.

Wang, Yunlong, He, Hong, Cao, Zhengguo, Fang, Yi, Du, Mingyuan AND Liu, Zhijian. 2017b. Regulatory effects of bone morphogenetic protein-4 on tumour necrosis factor-α -suppressed Runx2 and osteoprotegerin expression in cementoblasts. Cell Proliferation.

Wilson, C. J., Clegg, R. E., Leavesley, D. I. AND Pearcy, M. J. 2005. Mediation of biomaterial-cell interactions by adsorbed proteins: A review. Tissue Engineering 11: 1-18.

Wnek, G. E., Carr, M. E., Simpson, D. G. AND Bowlin, G. L. 2003. Electrospinning of nanofiber

fibrinogen structures. Nano Letters 3: 213-216.

Wolberg, A. S. 2007. Thrombin generation and fibrin clot structure. Blood Reviews 21: 131-142.

Woo, K. M., Chen, V. J., Jung, H. M., Kim, T. I., Shin, H. I., Baek, J. H., Ryoo, H. M. AND Ma, P. X. 2009. Comparative evaluation of nanofibrous scaffolding for bone regeneration in critical-size calvarial defects. Tissue Engineering - Part A 15: 2155-2162.

Woo, K. M., Chen, V. J. AND Ma, P. X. 2003. Nano-fibrous scaffolding architecture selectively enhances protein adsorption contributing to cell attachment. Journal of Biomedical Materials Research - Part A 67: 531-537.

Woo, K. M., Jun, J. H., Chen, V. J., Seo, J., Baek, J. H., Ryoo, H. M., Kim, G. S., Somerman, M. J. AND Ma, P. X. 2007. Nano-fibrous scaffolding promotes osteoblast differentiation and biomineralization. Biomaterials 28: 335-343.

Woodruff, M. A. AND Hutmacher, D. W. 2010. The return of a forgotten polymer - Poly(ε-caprolactone) in the 21st century. Progress in Polymer Science (Oxford) 35: 1217-1256.

Xiao, G., Gopalakrishnan, R., Jiang, D., Reith, E., Benson, M. D. AND Franceschi, R. T. 2002. Bone morphogenetic proteins, extracellular matrix, and mitogen-activated protein kinase signaling pathways are required for osteoblast-specific gene expression and differentiation in MC3T3-E1 cells. Journal of Bone and Mineral Research 17: 101-110.

Xu, L., Anderson, A. L., Lu, Q. AND Wang, J. 2007. Role of fibrillar structure of collagenous carrier in bone sialoprotein-mediated matrix mineralization and osteoblast differentiation. Biomaterials 28: 750-761.

Yamashita, M., Ying, S. X., Zhang, G. M., Li, C., Cheng, S. Y., Deng, C. X. AND Zhang, Y. E. 2005. Ubiquitin ligase Smurf1 controls osteoblast activity and bone homeostasis by targeting MEKK2 for degradation. Cell 121: 101-113.

Yang, X., Yang, F., Walboomers, X. F., Bian, Z., Fan, M. AND Jansen, J. A. 2010. The performance of dental pulp stem cells on nanofibrous PCL/gelatin/nHA scaffolds. Journal of Biomedical Materials Research - Part A 93: 247-257.

Yoo, H. S., Kim, T. G. AND Park, T. G. 2009. Surface-functionalized electrospun nanofibers for tissue engineering and drug delivery. Advanced Drug Delivery Reviews 61: 1033-1042.

Yoshimoto, H., Shin, Y. M., Terai, H. AND Vacanti, J. P. 2003. A biodegradable nanofiber scaffold by electrospinning and its potential for bone tissue engineering.

Biomaterials 24: 2077-2082.

Zeltz, C. AND Gullberg, D. 2016. The integrin-collagen connection--a glue for tissue repair? Journal of Cell Science 129: 653-664.

Zhao, M., Qiao, M., Harris, S. E., Oyajobi, B. O., Mundy, G. R. AND Chen, D. 2004. Smurf1 Inhibits Osteoblast Differentiation and Bone Formation in Vitro and in Vivo. Journal of Biological Chemistry 279: 12854-12859.

Zhao, Z., Zhao, M., Xiao, G. AND Franceschi, R. T. 2005. Gene transfer of the Runx2 transcription factor enhances osteogenic activity of bone marrow stromal cells in vitro and in vivo. Molecular Therapy 12: 247-253.

서지혜. 2007. 교원섬유기질에 의한 Runx2 단백질의 안정화 기전 = Type I Collagen Inhibits Degradation of Runx2 Protein through Down-regulation of Smurf1 in MC4 Cells. 서울대학교 치과대학원 석사학위논문.

요약(국문초록)

본 연구는 나노섬유구조를 가진 세포외기질의 형태학적 특징이 골모세포 및 상아모세포의 분화에 미치는 영향을 알아보고 골재생 및 상아질재생에 나노섬유 지지체의 적용 가능성을 탐색하고자 하였다. 아교질(collagen)은 경조직 세포외기질 단백질의 대부분을 차지하는 섬유단백질이며, 골모세포 분화 및 경조직 재생에 우수한 효과를 가지고 있다고 보고되어 왔다. 선행연구에서 아교질의 섬유구조가 골모세포 분화 유도 핵심 전사인자인 Runx2 단백질의 안정화를 유도함이 관찰된 바 있다. 이에, 본 연구에서는 아교질의 형태학적 특징을 모사할 합성 고분자 물질로서 시험관내 실험에서는 세포배양접시의 재료인 폴리스티렌(polystyrene)을, 동물 실험에 적용하기 위해서는 생체적합성이 높다고 알려진 폴리엡실론카프로락톤(poly-ε-caprolactone)을 선택하여 전기방사를 통해 아교질과 유사한 형태학적 섬유 구조를 가진 섬유기질을 제작하였고, 천연 고분자 물질로는 환자 자신의 몸에서 획득 가능한 섬유소(fibrin)로 섬유기질을 제작하여 세포 분화 및 재생에 미치는 영향을 평가하였다. 폴리스티렌을 이용한 시험관내 시험에서 Runx2 단백질은 아교질에서와 마찬가지로 전기방사된 폴리스티렌 섬유기질 위에서 분해가 억제되었으며, 이는 MC3T3-E1 골모세포 및

Runx2 유전자 이식된 C2C12 근모세포 모두에서 확인되었다. 비글견을 이용한 치수복조술(pulp capping) 모형 실험에서는 섬유구조의 폴리엡실론카프로락톤 막을 적용한 경우 우수한 상아질다리(dentin bridge) 형성과 건강한 치수의 유지를 확인할 수 있었다. 폴리엡실론카프록톤 막은 섬유 형태의 세포외기질을 제공할 뿐 아니라 치수복조술에 사용된 mineral trioxide aggregate가 처치 직후 수화단계에서 발생시키는 세포독성을 차단하는 효과를 가지고 있음을 MDPC-23 상아모세포를 이용한 시험관내 실험을 통해 확인하였다. 섬유소는 아교질과 형태학적으로 유사하도록 제조될 수 있었으며, 골재생을 촉진시킨다고 알려진 섬유결합소(fibronectin)의 선택흡착(selective adsorption)이 아교질보다 더 우수함을 확인하였다. 뿐만 아니라, MC3T3-E1 골모세포의 세포증식률, Runx2 단백질량 및 전사 활성도, 알칼리성 인산분해효소 활성이 아교질보다 섬유소 위에서 더 높게 나타나 골분화 및 재생에 보다 유리한 특성을 보였다. 이러한 섬유소의 특성은 섬유소원(fibrinogen)으로부터 섬유소를 제조할 때 처리되는 트롬빈의 농도가 증가할수록 더 크게 나타났다. 처리된 트롬빈의 농도 증가에 따라 선택 흡착된 섬유결합소의 수준이 증가하였으며, 기질에 선택 흡착된 섬유결합소가 증가할수록 MC3T3-E1 골모세포의 Runx2 단백질 수준이 증가하였고, 골모세포의 분화와 관련되어 있다고 알려진

인테그린 베타1과 베타3의 활성도가 증가함을 확인하였다. 이상의 연구 결과는 천연 및 합성 고분자 재료를 이용하여 세포외기질의 섬유모양 형태적 특징을 모방함으로써 골모세포와 상아모세포의 분화를 촉진하고 재생을 도모할 수 있음을 제시하였으며, 임상적 목적에 따라 적절한 재료를 선택하여 재생이 필요한 경조직의 세포외기질 형태를 인공적으로 제공하면 아교질을 적용하였을 때와 유사하거나 보다 우수한 효과를 기대할 수 있을 것이라는 점을 시사한다.

주요어: 나노섬유, 조직재생, 전기방사, 골모세포, 상아모세포

학 번: 2010-22022